

2

WHOI-93-33
UOP Report 93-4

AD-A271 175



**The Marine Light – Mixed Layer Experiment
Cruise and Data Report**

R/V Endeavor

**Cruise EN-224, Mooring Deployment, 27 April-1 May 1991
Cruise EN-227, Mooring Recovery, 5-23 September 1991**

Albert J. Plueddemann
Robert A. Weller
Thomas D. Dickey
John Marra
George H. Tupper
Bryan S. Way
William M. Ostrom
Paul R. Bouchard
Andrea L. Oien
Nancy R. Galbraith

**Upper Ocean Processes Group
Woods Hole Oceanographic Institution
Woods Hole, Massachusetts 02543**

DTIC
ELECTE
OCT 21 1993
S B D

May 1993

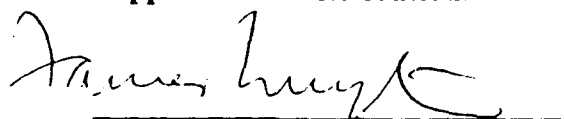
Technical Report

Funding was provided by the Office of Naval Research under Contract N00014-89-J-1683.

Reproduction in whole or in part is permitted for any purpose of the
United States Government. This report should be cited as:
Woods Hole Oceanog. Inst. Tech. Rept., WHOI-93-33.

Approved for publication; distribution unlimited.

Approved for Distribution:



James Luyten, Chair
Department of Physical Oceanography

93-25323



93 10 20 067

**WHOI-93-33
UOP Report 93-4**

**The Marine Light – Mixed Layer Experiment
Cruise and Data Report**

R/V Endeavor

**Cruise EN-224, Mooring Deployment, 27 April-1 May 1991
Cruise EN-227, Mooring Recovery, 5-23 September 1991**

Albert J. Plueddemann
Robert A. Weller
Thomas D. Dickey
John Marra
George H. Tupper
Bryan S. Way
William M. Ostrom
Paul R. Bouchard
Andrea L. Oien
Nancy R. Galbraith

**Upper Ocean Processes Group
Woods Hole Oceanographic Institution
Woods Hole, Massachusetts 02543**

May 1993


Technical Report

Funding was provided by the Office of Naval Research under Contract N00014-89-J-1683.

Reproduction in whole or in part is permitted for any purpose of the
United States Government. This report should be cited as:
Woods Hole Oceanog. Inst. Tech. Rept., WHOI-93-33.

Approved for publication; distribution unlimited.

Approved for Distribution:


James Luyten, Chair
Department of Physical Oceanography

Abstract

The Marine Light-Mixed Layer experiment took place in the sub-Arctic North Atlantic ocean, approximately 275 miles south of Reykjavik, Iceland. The field program included a central surface mooring to document the temporal evolution of physical, biological and optical properties. The surface mooring was deployed at approximately 59°N, 21°W on 29 April 1991 and recovered on 6 September 1991. The Upper Ocean Processes Group of the Woods Hole Oceanographic Institution was responsible for design, preparation, deployment, and recovery of the mooring. The Group's contribution to the field measurements included four different types of sensors: a meteorological observation package on the surface buoy, a string of 15 temperature sensors along the mooring line, an acoustic Doppler current profiler, and four instruments for measuring mooring tension and accelerations. The observations obtained from the mooring are sufficient to describe the air-sea fluxes and the local physical response to surface forcing. The objective in the analysis phase will be to determine the factors controlling this physical response and to work towards an understanding of the links among physical, biological, and optical processes. This report describes the deployment and recovery of the mooring, the meteorological data, and the subsurface temperature and current data.

DTIC QUALITY INSPECTED 2

Accession For	
NTIS GRA&I	<input checked="" type="checkbox"/>
DTIC TAB	<input type="checkbox"/>
Unannounced	<input type="checkbox"/>
Justification	
By _____	
Distribution/	
Availability Codes	
Dist	Avail and/or Special
A-1	

Table of Contents

Abstract	i
List of Tables and Figures	iii
1 Introduction	1
2 Mooring Deployment and Recovery	3
2.1 The MLML Mooring	3
2.2 Instrumentation	6
2.3 Deployment	13
2.4 Recovery	18
3 Data Presentation	21
3.1 Meteorological Variables	21
3.2 Air-Sea Fluxes	26
3.3 Upper-Ocean Temperature	28
3.4 Upper-Ocean Currents	31
Acknowledgments	107
References	108
Appendix 1: Cruise Participants	110
Appendix 2: Chronological Log	111

List of Figures

1	The MLML mooring site	4
2	The 1991 MLML mooring	5
3	The buoy tower	10
4	Pre-deployment CTD cast	14
5	Mooring anchor survey	16
6	Surface buoy positions in May	17
7	Pre-recovery CTD cast	19
8	Meteorological variables from the two VAWRs	35
9	Differences between meteorological variables	39
10	Best available meteorological variables	43
11	Air-sea fluxes from bulk formulae	52
12	Eight-hour mean temperatures versus depth	61
13	Sub-surface temperature time series	62
14	Contours of sub-surface temperature	71
15	Velocity time series, East component	80
16	Velocity time series, North component	89
17	Sub-surface velocity vectors at selected depths	98
18	Pre-deployment buoy spin	116

List of Tables

1	VAWR sensor specifications	8
2	VAWR sensor positions	9
3	Statistics of VAWR differences	22
4	STL data recovery	28
5	Calibration Adjustments	31
6	Temperature and current depth grid	32

1 Introduction

The Marine Light-Mixed Layer (MLML) field program was conceived as a part of the Marine Bioluminescence and Upper Ocean Physics Accelerated Research Initiative sponsored by the Office of Naval Research, and was predicated on the concept that temporal and spatial variability in the marine ecosystem are intimately related to physical processes. The Upper Ocean Processes Group (UOPG) at WHOI took responsibility for the design, deployment, and recovery of an instrumented surface mooring which served as the focal point for the field program. The long-term goal of our work in the MLML program is to develop an improved understanding of upper ocean physical processes and the links among physical, biological, and optical processes. In particular, we are interested in the horizontal and vertical structure of density and velocity in the upper ocean and the response of those fields to heat and momentum fluxes at the sea surface.

From the MLML mooring we have obtained observations sufficient to describe the air-sea fluxes and the local physical response to surface forcing. During the analysis phase, effort will be concentrated on determination of the factors controlling this physical response and consideration of the links between the physical, and bio-optical components of the seasonal cycle in the high-latitude North Atlantic. The primary objectives of this work are: (1) to document the upper ocean response to surface forcing and determine the controlling factors in the restratification and mixed layer deepening processes, (2) to assess the relationship between physical forcing and the bio-optical properties of the water column, in particular the relationship between the onset of restratification and the spring bloom of phytoplankton, and (3) to determine the extent to which bio-optical properties can be predicted given knowledge of the physical forcing and to consider the feedback between physical and bio-optical properties in the development of a mixed layer

model. These objectives will be addressed in close collaboration with the other MLML principal investigators.

In order to understand the link between physical forcing and bio-optical variability we must first know the surface forcing. This forcing consists of wind stress and the sensible, latent, and radiative heat fluxes, which can be computed from the meteorological variables recorded on the mooring using bulk aerodynamic formulae. Given this record of surface forcing, we wish to document the upper ocean response and determine the controlling factors in the restratification and deepening processes. The deep winter mixed layer at the MLML site (Robinson *et al.*, 1979; Levitus, 1982) results from convective mixing due to surface heat loss combined with strong wind forcing. Of particular interest is the spring restratification process, presumably driven by net heating during periods of weak wind forcing. Several studies have been devoted to the seasonal evolution of temperature and current structures in the upper ocean at temperate latitudes (e.g., Briscoe and Weller, 1984, as part of the LOnG Term Upper Ocean Study experiment, and Dickey *et al.*, 1991, as part of the Biowatt experiment). However, there have been few intensive studies of the springtime transition of the mixed layer and restratification of the upper water column and even fewer comparable observational programs at latitudes higher than 45°N. The temperature and velocity measurements from the MLML mooring document the upper ocean response at a high latitude site with unprecedented vertical (20 m intervals over the upper 300 m) and temporal (1–15 min) resolution.

This report describes the deployment and recovery of the mooring, the meteorological data, and the subsurface temperature and current data.

2 Mooring Deployment and Recovery

2.1 The MLML Mooring

The MLML experimental site (Figure 1) is in a region characterized by high winds, large waves, and strong currents. This severe environment represented a challenge to our ability to make detailed measurements of local atmospheric forcing and the biological, optical, and physical variability of the upper ocean. The process of meeting this challenge began in 1989 with the design and deployment of the MLML pilot mooring. The pilot mooring remained on station for 10 weeks, after which the failure of a component in the mooring line (a pear-ring link) caused the surface buoy to go adrift and the mooring line to sink to the bottom. The surface buoy was recovered soon afterwards and the sub-surface portion of the mooring was recovered in July of 1990. Analysis of data from the buoy and consideration of the mooring design indicated that both the static tension and cyclic loading on the mooring hardware were higher than anticipated, resulting in the component failure. The 1991 mooring was designed both to minimize the static tension along the mooring line and to survive peak tensions in excess of those observed on the pilot mooring.

Benefiting from extensive evaluation of the performance of the pilot mooring, the 1991 MLML mooring (Figure 2) proved to be a reliable severe-environment platform from which 131 days of surface and sub-surface data were collected between 29 April and 6 September of 1991. The critical design elements of the 1991 mooring included upgraded hardware designed to survive cyclic loading, an increase in scope (the ratio of the slack length of the mooring to the water depth) to minimize static tension, and a compliant element which allowed the mooring to be "tuned" so that the resonant frequency was outside of the surface wave band. The 1991

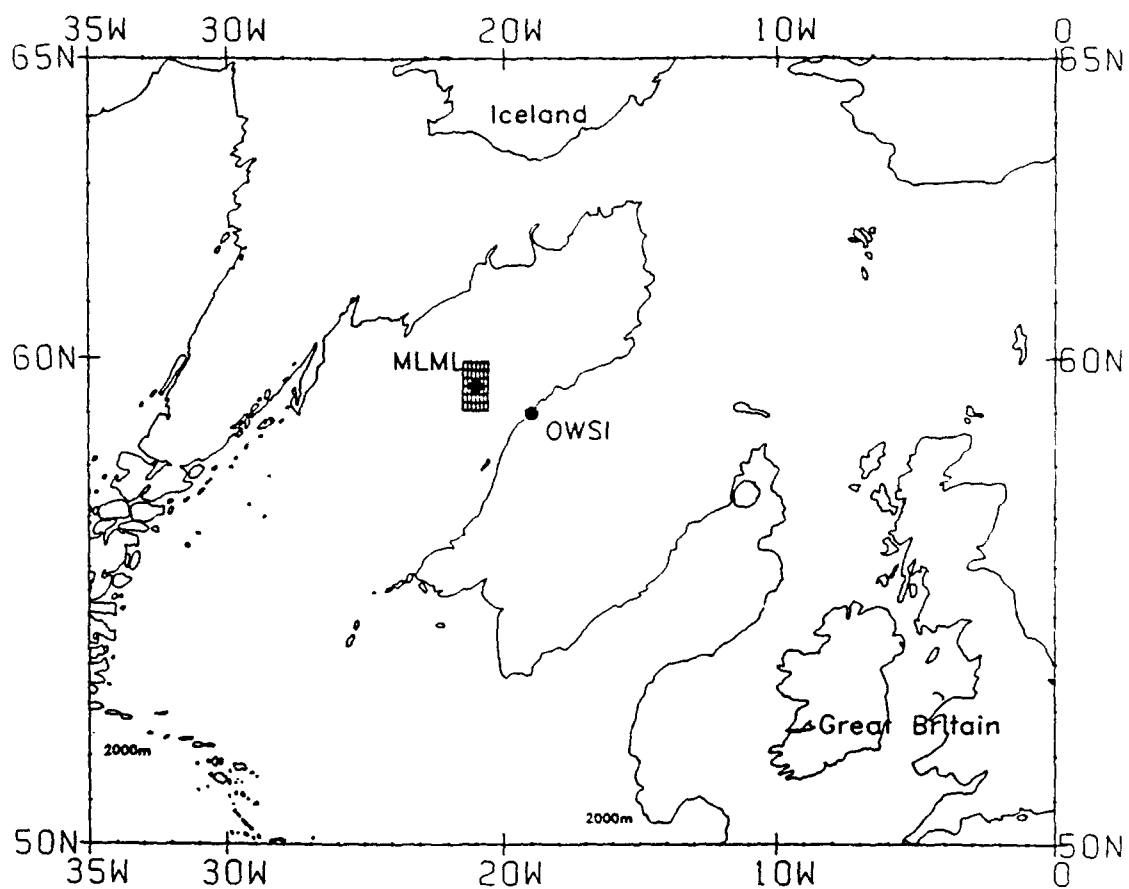


Figure 1: The MLML mooring site at 59.5°N, 21°W is shown along with a grid representing the shipboard survey region. The site at 59°N, 19°W is Ocean Weather Station India (OSWI) where the data of Lambert and Hebenstreit (1985) were collected.

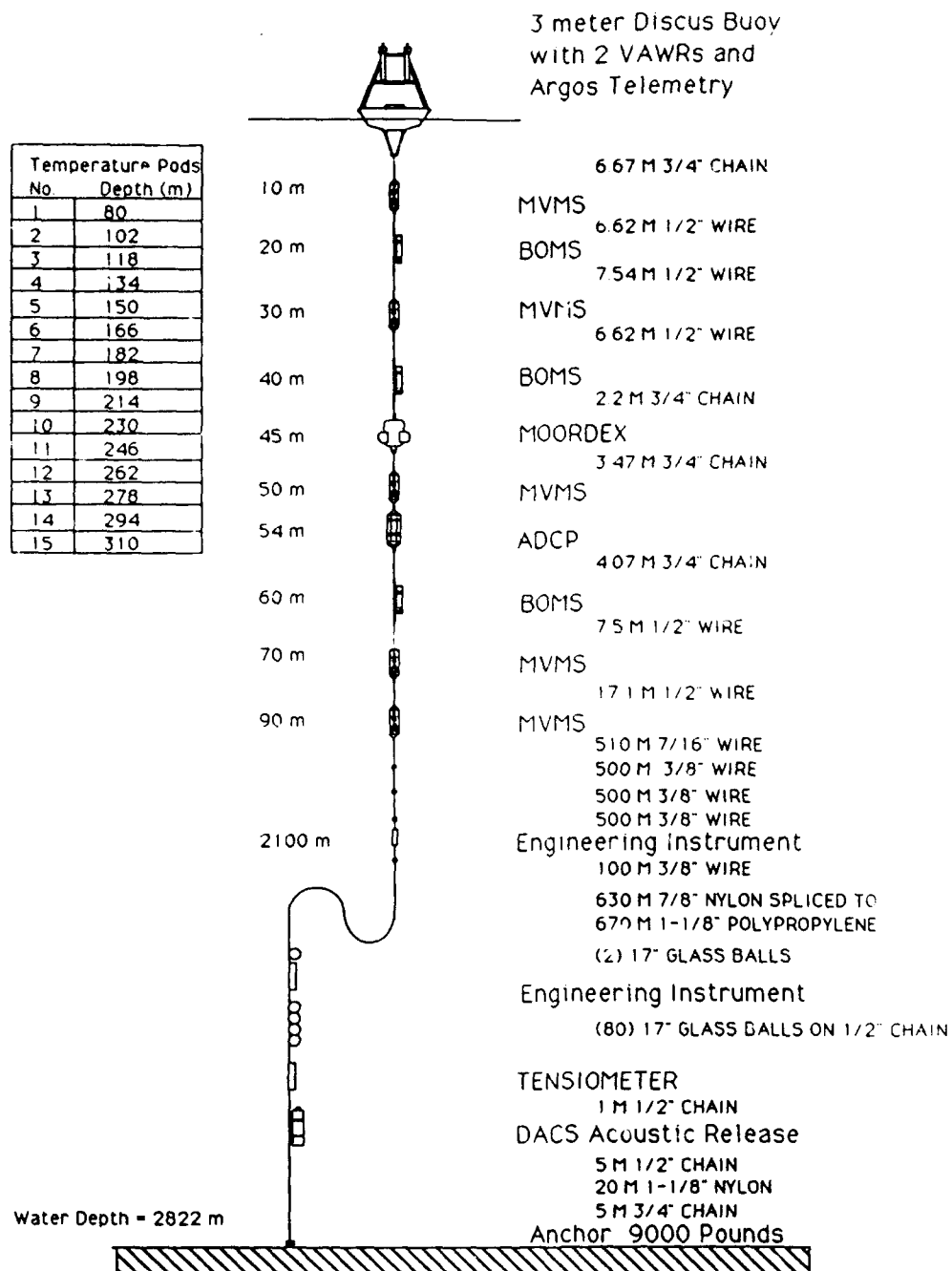


Figure 2: Schematic diagram of the 1991 MLML surface mooring. Instrument acronyms are described in the text.

mooring was of compound (wire, nylon, and polypropylene) construction, using a 10 foot diameter discus as a surface float. The scope of the mooring was 1.25. The mooring used the so-called "inverse catenary" design, wherein a section of negatively buoyant nylon is spliced to a section of positively buoyant polypropylene just above the flotation balls. At low current speeds, the nylon/polypro section takes on an "S" shape (Figure 2). This allows scopes significantly greater than one while eliminating the possible tangling problem of slack line hanging down and fouling lower components in low currents.

2.2 Instrumentation

Our responsibility for instrumentation on the mooring included the meteorological measurements and the current and temperature measurements below about 100 m depth. Instrumentation prepared by the UOPG included two Vector Averaging Wind Recorders (VAWR), 15 Submersible Temperature Loggers (STL), an Acoustic Doppler Current Profiler (ADCP), three engineering instruments, and a tensiometer.

Complementary instrumentation in the upper 100 m deployed by other MLML investigators included five Multi-Variable Moored Systems (MVMSs; T. Dickey, University of Southern California (USC) and J. Marra, Lamont-Doherty Geological Observatory (LDGO)), three Bio-Optical Moored Systems (BOMS; R. Smith, University of California, Santa Barbara (UCSB)), and a moored bioluminescence sensor (MOORDEX; J. Case, UCSB). The MVMSs provide point measurements of horizontal velocity and temperature in addition to bio-optical variables, and we include those velocity and temperature measurements in this report. No other data from the USC, LDGO, or UCSB instruments are included.

Instrumentation on the surface buoy included two VAWRs, an engineering instrument for sampling tension and vertical acceleration, a BOMS, and a dissolved oxygen sensor. A communications module was included to allow the VAWR to transmit meteorological data via ARGOS satellite. Two ARGOS antennas were mounted on the buoy tower. Each transmitted data from one of the VAWRs and also provided buoy position data. Another ARGOS transmitter in the buoy well was connected to a flat, deck-mounted antenna. Besides telemetering instantaneous values of buoy tension and battery voltage, this transmitter system was meant to be the backup buoy location device if heavy seas broke off the tower-mounted antennas. An additional backup ARGOS transmitter was mounted on one leg of the three-legged bridle below the buoy. It was mounted upside down and activated by a mercury switch in the event that the mooring broke at or near the bridle and the buoy turned upside down.

Two engineering instruments were placed on the mooring, one at a position 100 meters above the wire/nylon interface and the other just above the glass ball section. They measured tension, inclination, temperature and depth. One chart-recording tensiometer was placed between the glass balls and the release.

One VAWR was scheduled for deployment on the MLML buoy by Marra. To ensure that surface forcing data was collected successfully, we proposed a second VAWR for installation on the buoy. In addition to the ARGOS telemetry, the VAWRs recorded data internally at 15 min intervals. Both VAWRs were outfitted with sensors for the measurement of wind speed (WS), wind direction (WD), sea-surface temperature (SST), air temperature (AT), incoming shortwave radiation (SW), barometric pressure (BP), relative humidity (RH), and incoming longwave radiation (LW). The sensor specifications for the VAWR are given in Table 1.

Parameter	Sensor	Range	Comments
Wind Speed	Gill 3-cup Anemometer R.M. Young Model 12170C 100 cm/rev	0.2-50 m/s	Vector-averaging
Wind Direction	Integral Vane w/ Vane follower WHOI / EG&G	0-360°	Vector-averaging
Short wave Radiation	Pyranometer Eppley Model: 8-48	0-1400 watts/m ²	Average system
Long wave Radiation	Pyrgeometer Model: PIR	0-700 watts/m ²	Average system
Relative Humidity	Variable Dielectric Conductor Vaisala Humicap	0-100%	3.5 sec sample
Barometric Pressure	Quartz Crystal Digiquartz Paroscientific Model: 215	0-1034 mb	2.5 sec sample (Burst taken midway through avg. period)
Sea Temperature	Thermistor Thermometrics 4K @ 25° C	-5 to +30°C	1/2 time average Measured during first half of avg. period.
Air Temperature	Thermistor Yellow Springs #44034 5K @ 25°C	-10 to +35° C	1/2 time average Measured during 2nd half of avg. period.

Table 1: Sensor specifications for the Vector Averaging Wind Recorder (VAWR).

sensor	height (m)	separation (m)
SW/LW	3.6	0.1
WS	3.5	1.1
WD	3.2	1.1
AT/RH	2.8	0.2
BP	2.5	0.6
SST (SN 184)	-1.0	-
SST (SN 706)	-2.0	-

Table 2: Height above the buoy waterline is shown for sensors on the two MLML VAWRs. Horizontal separation is given for sensors at the same height on both VAWRs.

All of the VAWR sensors, except SST, were attached to the discus buoy tower. The two SST sensors were attached to the buoy bridle at depths of approximately 1 m and 2 m. The buoy tower was a tripod design, with the distance between legs tapering from about 2.5 m at the buoy deck to 0.6 m at the upper platform (Figure 3).

The two VAWR pressure housings were supported by an intermediate platform at about 1.5 m height, and the sensors were clustered around the upper platform at about 3 m height. Sensor positions with respect to the water line are given in Table 2.

All of the meteorological sensors were calibrated both before and after the experiment and "ground truth" measurements were made prior to deployment and recovery of the buoy. The calibrations are discussed in Section 3 and the chronology of the ground truth testing is given in Appendix 2.

Through the efforts of other MLML investigators, the upper 100 meters of the mooring was instrumented with five MVMSs, three BOMS, and the MOORDEX

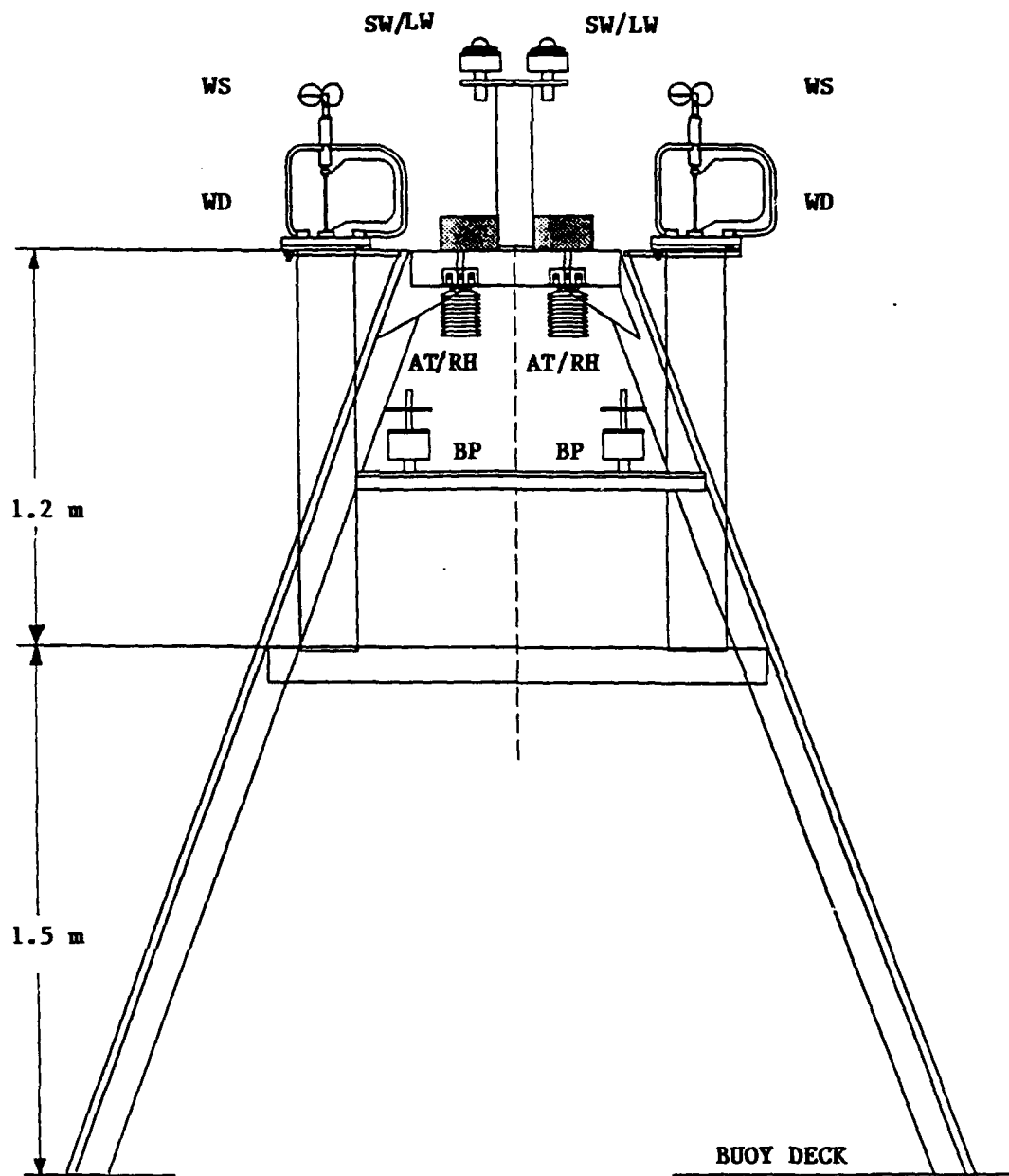


Figure 3: Schematic diagram of the meteorological sensor tower on the 1991 MLML buoy. The buoy deck is approximately 0.4 m above the water line. Sensor acronyms are described in the text.

(Figure 2). The MVMSs were deployed at 10 m, 30 m, 50 m, 70 m and 90 m depth and the BOMS at 20 m, 40 m and 60 m depth. These instruments provided temperature data at 10 m intervals (except at 80 m) and currents at 20 m intervals between 10 m and 90 m depth. UOPG instrumentation (15 temperature loggers and an ADCP) was deployed to supplement these measurements and extend the range of current and temperature observations to cover the full range of expected mixed layer depths.

The fifteen Submersible Temperature Loggers (STLs) were acquired from Richard Brancker Research Ltd. in Canada. These are *self-contained* instruments which record internally to solid state memory. Ten of the loggers were Model XL-100 and five were Model XX-105. The two models differ in their temperature precision and pressure case design. The XX-105 has increased precision compared to the XL-100, but over a reduced temperature range. The XL-100 pressure case is rated to 1000 m and uses an externally mounted thermistor, while the XX-105 pressure case is rated to 7500 m and has the thermistor mounted internally. We worked with the manufacturer to modify the XL-100 and XX-105 units to have similar temperature range and precision. For the XL-100, the original YSI 44203 thermistor was replaced by a YSI 44033, resulting in a precision of 0.012°C over a range of -5 to 30°C . The resistors of the XX-105 bridge circuit were chosen to give a nominal precision of 0.004°C over a range of 3.5 to 33°C (the actual precision varies slightly with temperature from 0.002° at the low end to 0.007° at the high end). The stated accuracy of the STLs is 0.01°C . During calibration tests at WHOI we found the XL-100 units met this specification, while the XX-105 units typically performed somewhat better (e.g. 0.005°C).

The STLs were attached to the mooring wire using a hinge-type clamp which was tightened around the wire. One STL was placed at 80 m depth to continue the 10 m temperature spacing down to 90 m. The remaining 14 sensors were placed at

16 m intervals between 102 m and 310 m depth to match the center points of the averaged ADCP depth cells (see explanation below).

The ADCP was a 150 kHz, self-contained unit manufactured by RD Instruments in San Diego. Outfitted with pendulum tilt sensors, a flux gate compass, and 20 Mbytes of solid state memory, the instrument was clamped to a load cage with the transducers pointing downwards from a depth of 54 m. Four transducers transmitted acoustic energy along narrow beams (approximately 4° half-power beam width) insonifying a volume of fluid determined by the beam width, the duration of the acoustic pulse, and the distance from the transducers. Backscattered energy from the insonified volume arrives at the transducers with a Doppler shift proportional to the average speed of the scatterers in the volume. To the extent that the scatterers are advected with the fluid, Doppler shifts estimated at successive times after transmission provide a profile of water velocity as a function of distance along the beam.

For MLML, the ADCP was configured to send out pulsed transmissions at one second intervals for a period of 60 s. This sequence of 60 transmissions, called an ensemble, was repeated at 15 min intervals. Values of velocity in earth coordinates, echo amplitude, and data quality parameters for each beam, along with heading, tilt, and temperature data were averaged for each ensemble and recorded to memory. The precision of velocity estimates from ADCPs depends principally on the operating frequency and the pulse length. For MLML the estimated precision of the 15 min average horizontal velocities is about 2 cm/s.

The backscattered signal from each transmission is processed over equally spaced time intervals corresponding to successively deeper insonified volumes known as depth cells (the depth cell length is the vertical component of the insonified volume). For MLML, data were processed over time intervals corresponding to a 8 m

depth cell, while the nominal depth resolution of the transmitted pulse was 16 m. Thus, the data were oversampled in depth and successive depth cells are not independent. Forty depth cells were recorded for each transmission, giving a profiling interval of 320 m. The first depth cell recorded was centered at a depth of 66 m and the center of the last cell was at a depth of 378 m. Prior to analysis, the data is usually averaged over two depth cells so that the sampling interval matches the 16 m depth resolution. Considering the two-cell average ADCP data we see that the 102 m STL is at the center of the third averaged cell, the 118 m STL at the center of the fourth averaged cell, etc., down to the 310 m STL which is at the center of the 16th averaged cell.

2.3 Deployment

The ship used for the deployment cruise was the R/V ENDEAVOR, operated by the University of Rhode Island, which sailed out of Reykjavik, Iceland for the MLML experiment. The UOPG scientific party arrived in Reykjavik on 22 April 1991 to begin cruise preparations. The ENDEAVOR sailed at mid-day on Saturday, 27 April 1991, arriving at the launch site approximately 275 miles south of Reykjavik at 0420 Z, 29 April. Winds were out of the northeast at 15 gusting to 25 knots. The sea state was 5, with an 8-foot swell, as estimated by the bridge. A CTD was taken to 275 meters at 0500 Z to document pre-deployment vertical structure (Figure 4). The acoustic release lowering was done to 750 meters.

The mooring launch commenced after breakfast on 29 April, with the entire launch operation taking just under eight hours to complete. The anchor went over the side at 1542:30 Z and hit bottom at 1603:52, giving an average descent rate of 132 meters per minute. At the time of anchor launch, GPS was down, so we elected to do the acoustic survey of anchor position using Loran-C. Later, when

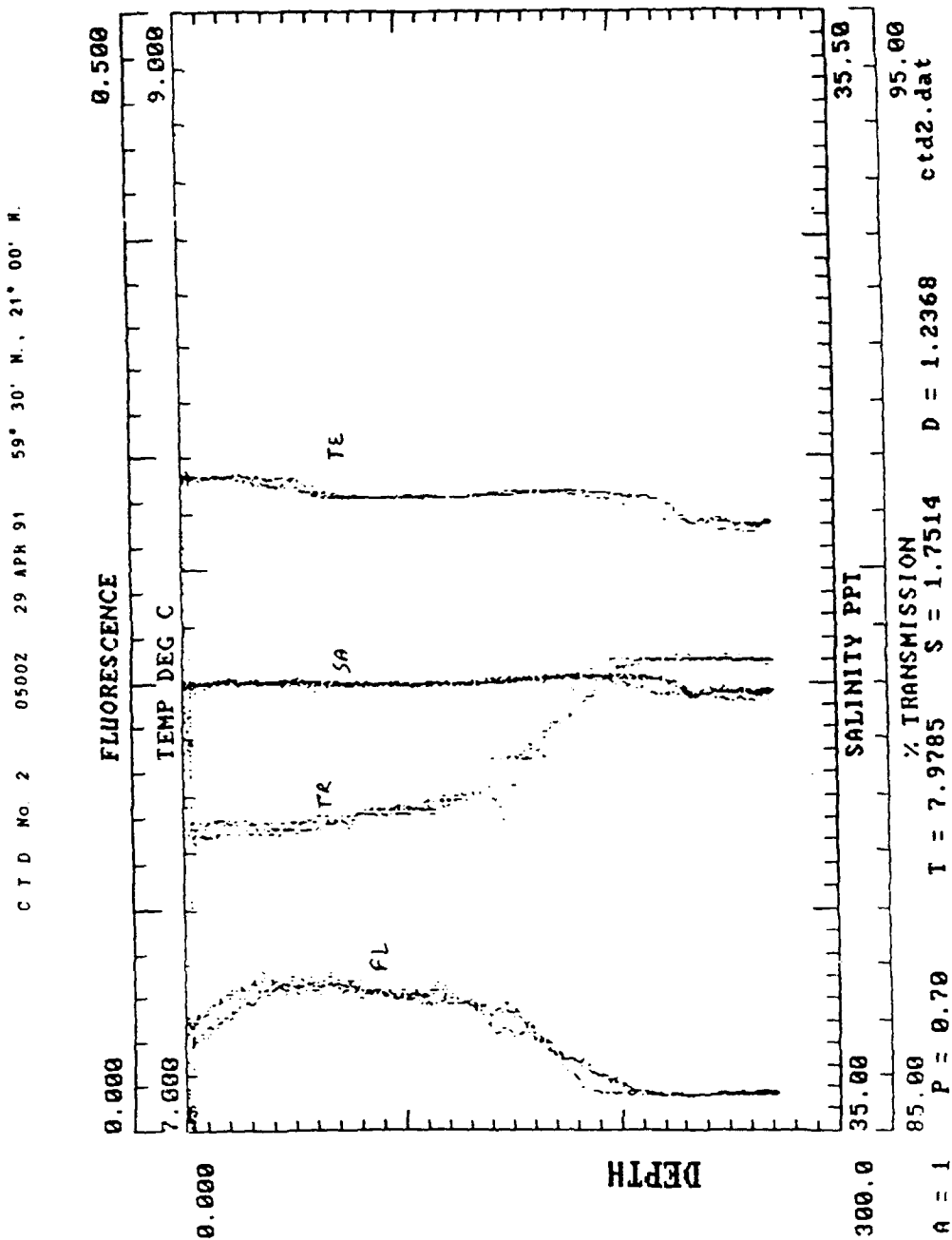


Figure 4: CTD cast taken from R/V ENDEAVOR on 29 April 1992, just prior to deployment of the MLML mooring

GPS was back up, we calculated the offset between GPS and Loran-C. The Loran-C position was 0.44 Nautical miles away and bearing 006° from GPS position. The final position of the anchor was calculated using this offset (Figure 5), giving 59° 35.61'N latitude, 20° 57.85'W longitude. The water depth at the anchor site was determined to be 2822 m. After the anchor survey, the ship approached the surface buoy to log its position and take some video footage. The Buoy position was about 1.2 miles northeast of the anchor.

At 1758 Z on 29 April we launched a Metocean drifter buoy number 14314, given to us by the U. S. Navy (Naval Oceanographic Command) at Keflavik, Iceland. Position of the drifter launch was 59° 34.6'N, 20° 57.2'W. Having completed deployment operations, the ENDEAVOR left the MLML site and returned to Reykjavik on 1 May 1991.

There was interest in documenting the watch circle of the large-scope MLML mooring, which would also aid in determining the safe approach distance to the anchor position for ships working in the area. From the water depth and a scope of 1.25 the horizontal excursion for the buoy is estimated at 2.1 km (1.1 n-mi). However, since the scope is defined using the slack length of the mooring, we must account for the stretch of the synthetic components under load. Assuming that the 1300 m of nylon and polypropylene stretches 15% gives a maximum horizontal excursion to 4.7 km (2.5 n-mi). Buoy positions determined from ARGOS telemetry for the period 1-9 May are shown in Figure 6. These positions have accuracy of about 350 m (0.2 n-mi). The plot shows that the buoy is typically found between the slack-length excursion and the maximum excursion.

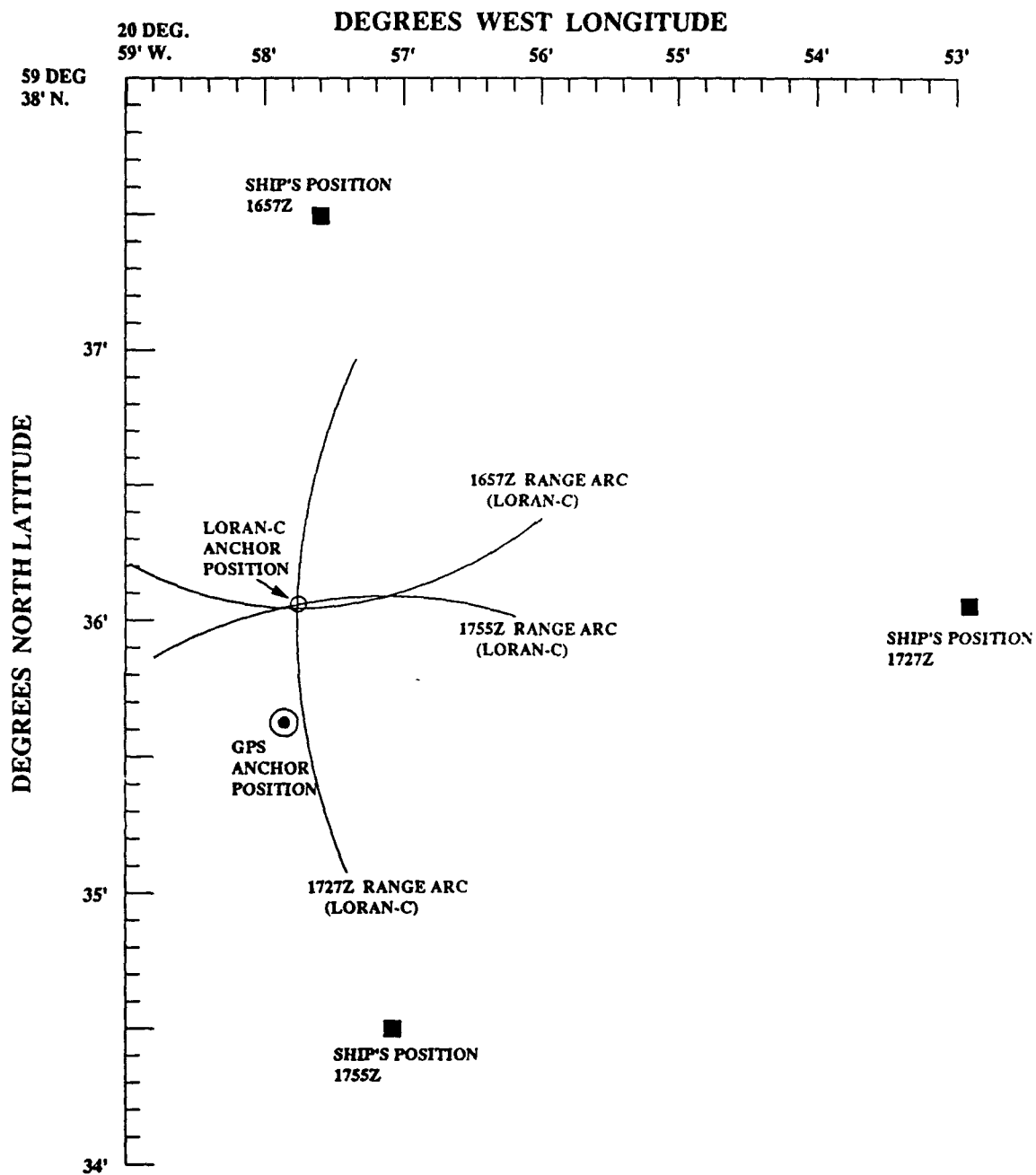


Figure 5: The MLML-91 mooring anchor position, determined from Loran-C fixes while GPS was down, and later adjusted using GPS (see text). The position of the anchor was determined to be 59° 35.61'N, 20° 57.85'W.

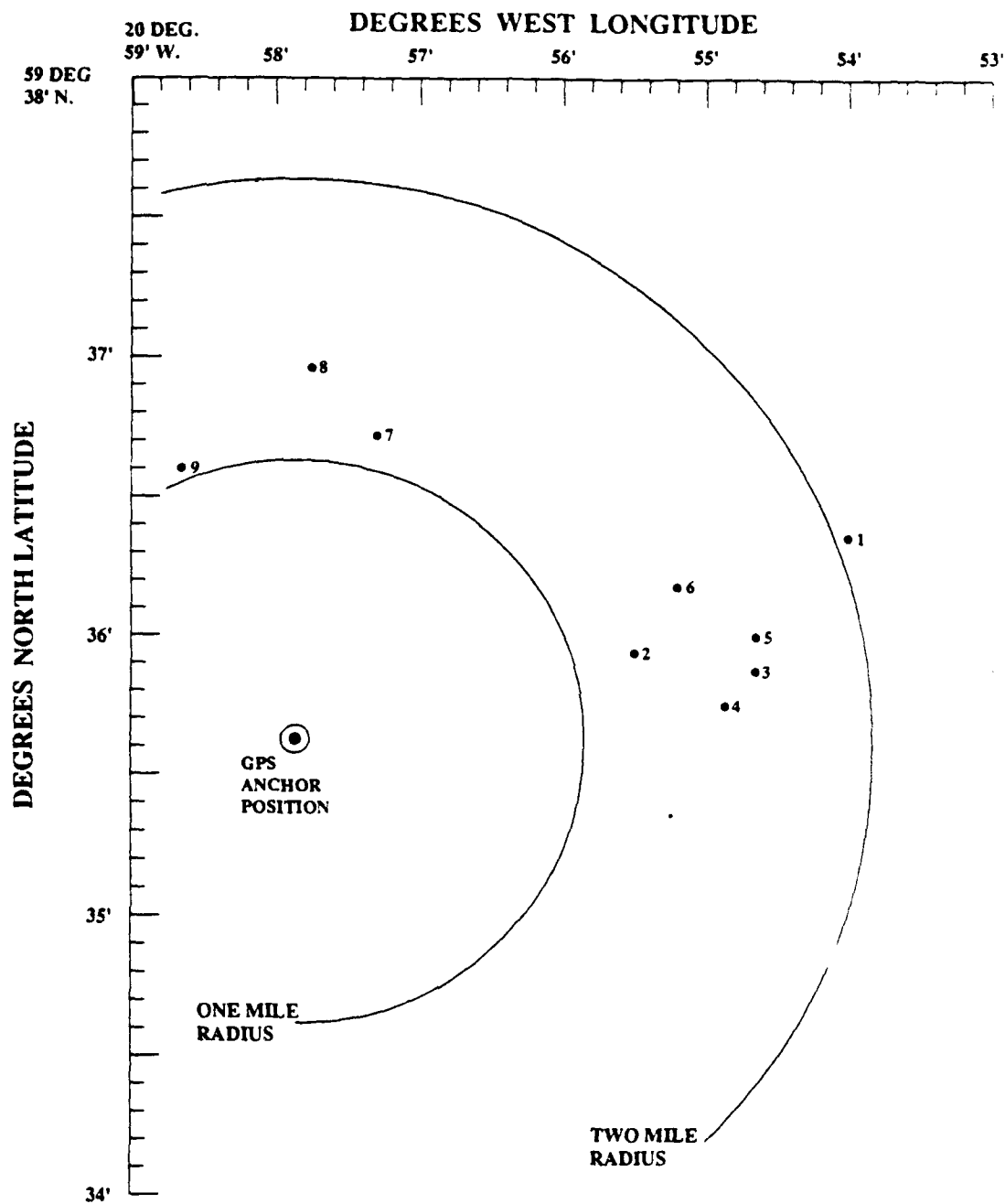


Figure 6: MLML-91 buoy positions from ARGOS for the period 1-9 May relative to the estimated anchor position.

2.4 Recovery

The R/V ENDEAVOR sailed from Reykjavik, Iceland for the mooring recovery at 1030 Z, 5 September 1991. The weather forecast called for flat seas for several days, an unusual occurrence at the MLML site, but very good news for the mooring recovery team. A call was made to WHOI just before the ship sailed to check the VAWR ARGOS telemetry data from the mooring, confirming that the highest barometric pressure and lowest wind speeds of the entire experimental record were being observed.

On the morning of 6 September ENDEAVOR arrived at the mooring site. En-route to the mooring in calm seas (sea state 1), the buoy was seen on radar at a distance of six miles. At 1100 Z, the buoy was sighted visually at three miles. The ENDEAVOR hove-to 1/4 mile downwind of the buoy for a half-hour of meteorological ground truth measurements. These data appear in Appendix 2. At least a hundred seagulls were seen around the buoy, mostly swimming, but some perched on the deck with one sitting on top of the BOMS sensor. The deck of the buoy was covered with a greenish algae/weed growth, indicating it had been awash a good bit. Sensors appeared to be undamaged and looked like new. A CTD was taken to 400 meters before the mooring recovery (Figure 7).

The acoustic release was fired at 1250 Z on 6 September and the mooring began its ascent. The recovery went smoothly, with the mooring and all instruments aboard by 1800 Z. Recovery was slowed by the TSE winch not having enough drum capacity to hold all of the mooring; operations had to be stopped midway through to offspool wire so that the rest of the mooring could be hauled in.

The condition of all instruments on recovery was good, with two exceptions. The MVMS at 10 meters was covered with a black, oily fouling. The transmissometer of this instrument was missing, with broken cable hanging loose, and the MVMS

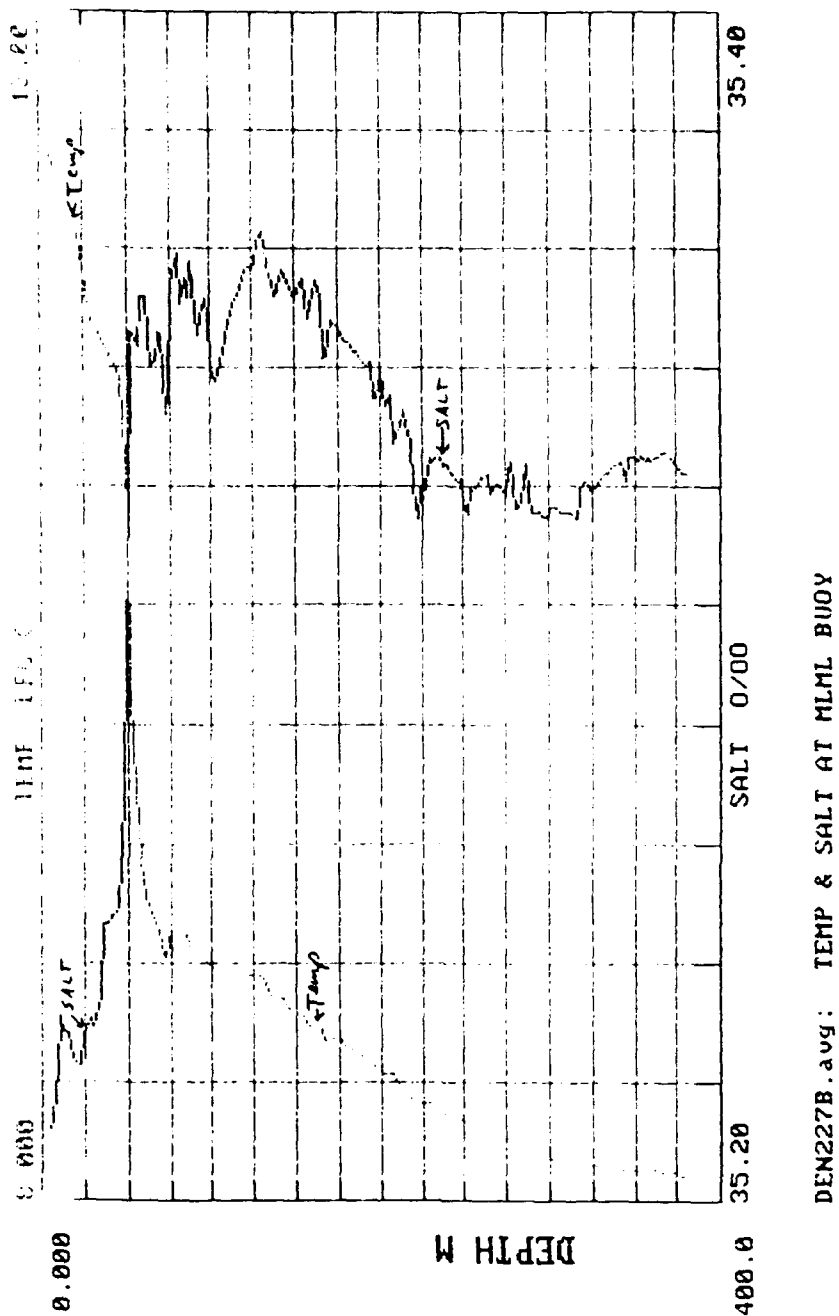


Figure 7: CTD cast taken from R/V ENDEAVOR on 6 September 1992, just prior to recovery of the MLML mooring

at 50 meters had a broken Oxygen probe. The Argos transmitter on the buoy bridle was severely corroded in the mid-section of its pressure case. It was hypothesized that this was due to the lack of a neoprene pad on the bottom mounting bracket base plate, allowing the aluminum case to directly touch the bracket. The mooring hardware and wire rope looked in good shape. None of the STL brackets showed any signs of slippage on the wire rope. The nylon had three small wuzzles all within 100 m of the nylon/polypro splice. The wuzzles may have been caused by the nylon going slack and then throwing a loop and tightening itself on the loop.

The ship left the MLML site after recovery operations were complete, arriving outside Reykjavik harbor early on 8 September. Personnel from LDGO and Mark Grosenbaugh from WHOI departed on the pilot boat, while the rest of the science party remained onboard, sailing south to track down and recover the surface float from the North-West mooring of the Subduction Experiment array which had gone adrift. After recovering the drifting portion of the Subduction mooring on 15 September, ENDEAVOR arrived at WHOI on 23 September, 1992.

3 Data Presentation

The surface meteorological variables, air-sea fluxes, upper ocean temperatures, and upper ocean currents observed from the MLML mooring are presented in this section. The observations come primarily from the UOPG instruments on the mooring (two VAWRs, the STLs, and the ADCP), but measurements of currents and temperature from the MVMSs are also included. The principal means of presentation is a series of figures and tables which are described in the text and presented at the end of the section.

3.1 Meteorological Variables

The VAWR data tapes were read for each instrument resulting in files containing time and eight meteorological variables: Wind speed (WS), wind direction (WD), sea-surface temperature (SST), air temperature (AT), incoming shortwave radiation (SW), barometric pressure (BP), relative humidity (RH), and incoming longwave radiation (LW). The longwave radiation measurements from MLML are discussed in Dickey *et al.* (1993) and will not be presented here.

A small number of obviously bad points (less than 0.2% of the samples) were edited out by hand and replaced by linearly interpolated values. In order to eliminate data from periods prior to deployment and after recovery of the mooring, a de-facto definition of MLML-91 start and end dates was made. The resulting files had 12384 15 min samples starting on 4/30/91 00:15 (yearday 120.0052) and ending on 9/05/91 23:45 (yearday 248.9948).

Time series of meteorological variables recorded by the two VAWRs on the MLML mooring are shown in four sections in Figure 8a-d. The data presented are at the 15 min intervals recorded by the instrument, with no additional averaging

variable	mean difference	std dev
WS (m/s)	-0.03 (0.4%)	0.21 (4.8%)
WD (°)	-4.60	3.74
SST_1 (°C)	+0.027	0.050
SST_2 (°C)	-0.036	0.467
AT (°C)	+0.002	0.083
SW (W/m ²)	-3.15 (1.8%)	5.16 (11%)
BP (mb)	-0.22	0.18
RH (%)	-1.11	0.81

Table 3: Statistics of the difference between measurements of like variables for the two VAWRs are shown. Statistics of the difference expressed as a percent of the two-sensor mean are also shown for some variables. SST_1 is the period of good performance, SST_2 the period of bad performance.

applied. Observations from VAWR Serial Number (SN) 184 are shown as a solid line, observations from SN 706 as a dashed line. The extent to which the two lines are indistinguishable is a first-order indication of the quality of the measurements. The only discrepancies discernible in these plots are in the relative humidity and the sea surface temperature.

Time series of the differences (SN 184 - SN 706) between variables observed by the two VAWRs are shown in four sections in Figure 9a-d. These time series, and their statistics (Table 3), allowed evaluation of VAWR performance. The best performing sensor for each variable was chosen to form the "best available" meteorological data from which to compute air-sea fluxes.

Estimates of the accuracy (difference between observed and true value), precision (repeatability of successive readings), and resolution (smallest change detectable by the sensor) for the VAWR are presented by Weller *et al.*, 1990. Values from their Table 3 are quoted in the discussion below. The sensors on the two

VAWRs were in close enough proximity that we expected experiment-long mean differences greater than the sensor accuracy to be indicative of calibration biases. The observed differences at 15 min intervals can be effected by true small-scale spatial variability in the measured quantity. Thus, it would be unlikely that the standard deviation of the differences would be as small as the sensor precision (the precision is the "best case" repeatability under controlled conditions). Still, we expected the standard deviation to be near the estimated sensor accuracy for most variables.

The wind speed difference had a mean of 0.03 m/s and a standard deviation of 0.2 m/s. The standard deviation of the difference expressed in terms of a percent of the wind speed was 5%. The wind direction difference had a mean of 5° and a standard deviation of 4°. This compares with an estimated accuracy of 2% for wind speed and 3° for wind direction. We concluded that the wind sensors were performing within tolerable bounds, although there was probably a small compass calibration bias resulting in the mean difference two degrees larger than the estimated accuracy. From the information available, it was not possible to know which sensor had the larger directional error. Instead we accepted a directional uncertainty of about 5° and chose SN 184 for wind speed and direction based on its more "reasonable" performance during the strong wind event on 20-21 May.

Sea surface temperature was the variable with the most obvious measurement problem. It can be seen from the plots that the difference is small up until about 21 May and after 1 August. During this "good" period, the mean and standard deviation of the difference are 0.03° and 0.05°, respectively. The pre and post deployment calibrations indicated both sensors to be accurate within 0.005° or less, quite reasonable given the estimated accuracy of 0.004°. The observed difference statistics about an order of magnitude larger than the estimated accuracy may be explained by the fact that the two sensors were separated by 1 m in the vertical.

The vertical variability of temperature near the sea surface presumably contributed to observed differences on the order of 0.01° .

During the "bad" period between 22 May and 31 July, the standard deviation of the difference increased to 0.5° and peak differences of up to 2° were observed. A sensor malfunction of some type is indicated, but the problem was transient in the data and did not show up the post deployment calibrations or electronics checks. Both SN 184 and 706 appeared to be effected. As a result it was not possible to determine the cause of the problem or to isolate the problem to a single sensor. Instead, we chose the SST from SN 706, which showed fewer sharp jumps than SN 184, and used the temperature from the MVMS at 10 m as a benchmark for correction.

It was found that with two ad-hoc adjustments to the SN 706 SST, we could get good agreement with the 10 m temperature. The first adjustment was made on day 151 where SST mysteriously jumps down by about a degree, and the second on day 168 where it jumps back up again. After several trials the final adjustments were $\Delta T_1 = +0.92^{\circ}$ between yearday 151.1927 and 151.3281, and $\Delta T_2 = -0.64$ between yearday = 168.3906 and 168.5990. These adjustments were done after the initial calibration adjustments (described in Section 3.3) were completed. This adjusted record from SN 706 was used for SST.

Air temperature showed a mean difference of 0.002°C and a standard deviation of 0.08°C . The observed mean difference indicates no biasing problems, given the estimated accuracy of 0.008°C . Similar to the situation for SST during its period of good performance, the standard deviation is significantly larger than the estimated accuracy. Simple regressions were used without success in an attempt to find a relationship between the air temperature difference, low wind speed, and high insolation. There was no evidence of electronics problems for either sensor, and the

pre and post deployment calibrations for both sensors were within the estimated accuracy. Under the assumption that the observed differences were the result of small-scale variability in the true air temperature, which we would like to average out, the mean value of AT from SN 184 and 706 was used.

Short wave radiation showed a mean difference of 3 W/m^2 (2%) and a standard deviation of 5 W/m^2 (11%). The mean difference is acceptable given the estimated accuracy of 3%. However, from the plots it appears that the large standard deviation is the result of an error in one (or both) of the sensors which is proportional to the magnitude of insolation. Calibration data showed that the SW sensor for VAWR SN 184 had a significant post deployment calibration error (about 4%) which could have accounted for the observed differences, while SN 706 performance was within specifications. Thus, we chose to use the SW data from SN 706.

Barometric pressure showed a mean difference and standard deviation both equal to 0.20 mb. This value is actually slightly less than the estimated accuracy of 0.26 mb. In addition, pre and post calibrations for both instruments indicated excellent performance. Since both sensors performed equally well, the choice of the "best" sensor is arbitrary. We chose to use the BP data from SN 706.

Relative humidity showed a mean difference and standard deviation both equal to 1%. This value is less than the estimated accuracy of 3%, and we can conclude that both instruments within their specifications. However, from the plots it can be seen that the observed difference is principally due to a high-humidity bias, with SN 706 reading approximately 2% higher than SN 184 for RH greater than 90%. It was found that SN 706 performed better than SN 184 in both pre and post calibration tests, particularly in the RH range between 80% and 95%. Thus, the RH measurements from SN 706 were chosen for the final data set.

The final meteorological data set, determined to be the best available observations from the two VAWRs in the manner described above, is shown in nine sections in Figure 10a-i. Note that the 14 day section intervals do not divide evenly into the 129 day experimental period. Rather than begin a tenth section, the last three days are not shown. The original 15 min data have been smoothed over four hours and plotted every two hours. The variables are the same as those shown in Figure 8, except here AT (solid) and SST (dashed) have been combined in one panel.

3.2 Air-Sea Fluxes

The fluxes of momentum, sensible heat, and latent heat for the MLML site were computed from the meteorological variables shown in Figure 10 using bulk aerodynamic formulae of Large and Pond (1981; 1982). Several steps were necessary to go from the raw meteorological variables to the momentum flux and total heat flux. The most involved of these is the estimation of outgoing longwave radiation from the sea surface, including a correction for cloud cover.

The outgoing longwave radiation can be estimated by assuming that the earth is nearly a black-body radiator and accounting for the presence of clouds. A review of several such approaches is given by Fung (1984). We used a formulation for LW as a function of SST, AT, and the mixing ratio from Clark *et al.* (1974). Corrections for slight departures from black-body behavior are included. Also included in this formulation is a cloud correction function $F(n)$, where n is the cloud fraction, a number between zero (no clouds) and one (complete cloud cover). We used the expression $F(n) = 1 - b * n^2$ where b is an empirical parameter which varies with latitude from about 0.5 at the equator to 0.8 at 80°N (see Fung, 1984). The difficulty is in determining the cloud fraction n .

The approach taken was to compute the clear sky shortwave radiation from astronomical theory (List, 1984) and estimate the cloud cover by comparing the computed clear sky value to the observations. The principal steps in this process are outlined below. The shortwave radiation record was corrected for a small night-time bias by subtracting a night-time mean of 5.49 W/m^2 from all data. A theoretical estimate of clear sky shortwave radiation for the MLML site was made using the formulations of List (1984). The theoretical values were "tuned" to be a good match to the sunniest days of the experiment by picking an albedo of 0.06 and an atmospheric transmission coefficient of 0.77. The cloud fraction was then estimated from the ratio of observed to theoretical shortwave radiation and checked for consistency, i.e., a sensible distribution between zero (sunniest day) and one (cloudiest day). This technique, of course, works only during the day. Night-time values of cloud cover were estimated by linear interpolation between the nearest two daytime values. After interpolation, the cloud fraction record was smoothed over 30 hours to reduce sensitivity to the day/night transitions.

The observed meteorological variables and the cloud fraction estimate are used as input to a flux computation routine. Output from the initial flux computation includes stability, wind stress, sensible and latent heat flux, and cloud corrected longwave radiation. Along with the observed shortwave radiation this forms a surface flux time series for MLML which is complete except for precipitation. As a final step, the heat flux components are combined to form the total heat flux.

The MLML bulk fluxes are presented in Figure 11a-i. The fluxes are computed from the 15 min meteorological variables, but have been smoothed over four hours prior to plotting. The five panels show (from top to bottom) sensible (solid) and latent (dashed) heat flux, shortwave (solid) and cloud corrected longwave (dashed) radiation, total heat flux, wind stress magnitude, and wind direction. The sign of

SN	model	depth	pre	post	data recovery
2535	XL-100	80	y	y	good data
2539	XL-100	102	y	y	good data
2538	XL-100	118	y	n	good data, failed during post-cal
2534	XL-100	134	y	n	no data, quit before deployment
2540	XL-100	150	y	y	good data
2533	XL-100	166	y	y	good data
3263	XX-105	182	y	y	good data
2536	XL-100	198	y	y	good data
2541	XL-100	214	y	y	good data
3299	XX-105	230	y	y	good data
3291	XX-105	246	y	y	good data
3301	XX-105	262	y	n	no data, water leak
2542	XL-100	278	y	n	no data, scrambled EPROM
3264	XX-105	294	y	n	partial record, water leak
2537	XL-100	310	y	y	good data

Table 4: Tabulation of instrument serial numbers, depth of deployment, and data recovery for the Brancker Submersible Temperature Loggers. Pre and post indicate pre-deployment and post-deployment calibrations, respectively.

sensible, latent and total heat fluxes as presented here are positive for a heat gain by the ocean.

3.3 Upper-Ocean Temperature

Complete records of high quality temperature data were obtained from 11 of the 15 STLs, a partial record was obtained from the 12th instrument, and no data were recovered from the remaining three (Table 4).

The three failures left gaps in the temperature record at 134 m depth and between 246 m and 310 m depth. Instrument SN 2538 failed during post calibration and was later repaired; good data were obtained during the deployment. SN 2534

and 2542 suffered from a ribbon cable chafing problem which was determined to be generic to the Model XL-100. This problem was corrected for XL-100s deployed after MLML. SN 3301 and 3264 were found to have small amounts of water (approximately one tablespoon) in the pressure case upon recovery. SN 3301 lost all data due to flooding, but a partial record (the first 90 days) was recovered from SN 3264.

The ten STLs which had post deployment calibrations were found to be extremely stable, i.e., the mean difference in observed temperature using the pre and post calibration constants was 0.005° or less, comparable to the instrument accuracy. This made the choice of pre or post deployment calibration coefficients for these units arbitrary. Due to the lack of post calibration for SN 2538 and 3264, the pre calibration coefficients were used for all instruments.

Temperature data were also obtained from the USC and Lamont MVMSs deployed between 10 m and 90 m. In order to be compatible with our STL sampling interval the USC raw data, originally sampled at 1 min intervals, were averaged to 15 min. Similarly, the Lamont data, originally sampled at 4 min, were averaged to 15 min intervals. Calibrations were not available for any of the USC or Lamont temperature sensors.

The USC records were complete, and no further processing was required. The Lamont temperature records at 30 m and 90 m had a gap between 27 July and 26 August. This segment was filled using linear interpolation between the nearest neighbors in the vertical, i.e., 30 m data were filled using USC MVMSs at 10 m and 50 m, 90 m data were filled using STLs at 80 m and 102 m. The Lamont 70 m temperature record stopped on 30 June. The missing 70 m data were also filled by interpolation, using the MVMS at 50 m and the STL at 80 m. During the processing of the Lamont temperature records, we took the opportunity to fill in

the missing data from the 294 m STL, interpolating between the STLs at 246 m and 310 m.

It was clear from the initial CTD cast (Figure 4) that the water column was fairly well mixed at the start of the deployment. The CTD temperatures were within about 0.1°C from the surface to 300 m, with a mean of about 8.130°C . The temperatures observed on the mooring were very stable immediately following deployment, after which significant surface warming began. Thus, we chose to compare mooring temperatures averaged over the first 8 hrs of 30 April to the expected values based on the CTD cast. Instruments with good pre and post deployment calibrations are shown in Figure 12 as circles, and are in good agreement with the CTD profile. Instruments without good calibrations are shown as crosses in the figure, and all but the Lamont 90 m MVMS appear suspect due to poor agreement with the CTD cast and the appearance of strong temperature inversions with depth.

As a first attempt at an ad-hoc "adjustment" of the temperature sensors with suspect calibrations, we forced their initial values to agree with the average of the STLs. The depth-mean from 80 m to 246 m of the STL 8 hr averages was 8.1304°C . The 8 hr averages for the other 7 sensors, and the adjustments used to bring their means into agreement with the STLs, are given in Table 5. The adjustment was applied as an additive constant to all temperatures in the record for a given instrument.

The processing steps described above resulted in time series of temperature at 17 depths between the surface and 310 m depth (Table 6).

The temperatures are plotted as overlapped time series in Figure 13a-i. The surface data are shown as a solid line, the 10 m data as a dashed line, etc., with successive depths alternating as solid and dashed. These data were averaged over

source	depth	8-hr mean	adjustment
VAWR	0	8.1205	+0.0099
USC MVMS	10	8.1091	+0.0213
Lamont MVMS	30	8.1791	-0.0487
USC MVMS	50	8.0964	+0.0340
Lamont MVMS	70	8.0568	+0.0736
Lamont MVMS	90	8.1409	-0.0105
Brancker STL	294	8.0198	+0.1106

Table 5: Temperature adjustments used to bring the seven instruments with un-reliable calibrations into agreement with the STLs between 80 m and 246 m. Mean temperatures over the first eight hours of 30 April were used in the comparisons.

2 hr prior to plotting. Note the occurrence of small, but persistent temperature inversions between the surface and 10 m depth (e.g. 5-7 May, 28-31 May). These are presumably not real, but rather a result of imperfect correction of the VAWR SST record. Inversions at other depths can occasionally be seen, which may be the result of the crude nature of the temperature adjustments described above.

The temperature data are shown vs. depth and time as contour plots in Figure 14a-i. The data were averaged over 18 hr prior to contouring.

3.4 Upper-Ocean Currents

A complete record of currents was obtained from the RDI ADCP. Currents in earth coordinates (i.e. rotated from a coordinate system relative to the instrument into a geographical coordinate system using the measured pitch, roll and heading) were averaged to create time series in 16 m depth cells between 86 m and 310 m (Table 6). The ADCP recorded one profile (an average of 60 transmissions) every

depth	temperature	currents
0	VAWR 706	-
10	USC MVMS	USC MVMS
30	Lamont MVMS	Lamont MVMS
50	USC MVMS	USC MVMS
70	Lamont MVMS	Lamont MVMS
80	Brancker STL	-
90	-	ADCP (86 m)
102	Brancker STL	ADCP
118	Brancker STL	ADCP
134	-	ADCP
150	Brancker STL	ADCP
166	Brancker STL	ADCP
182	Brancker STL	ADCP
198	Brancker STL	ADCP
214	Brancker STL	ADCP
230	Brancker STL	ADCP
246	Brancker STL	ADCP
262	-	ADCP
278	-	ADCP
294	Brancker STL	ADCP
310	Brancker STL	ADCP

Table 6: The sensors used to provide temperature and current data at a given depth are shown. If no sensor is shown then no data were available at that depth (except for the 90 m temperature which was available, but not used due to an unresolved timing problem).

15 minutes. The earth-coordinate current profiles were computed on a ping-by-ping basis by the ADCP, so no further processing was necessary. Although the ADCP passed all pre and post deployment diagnostic tests, no laboratory calibration of the ADCP currents was possible. Instead, the ADCP currents at 86 m were compared statistically to the MVMS currents at 50 and 70 m. The comparison showed rms differences in speed of 2-3 cm/s. and in direction of about 7°. Since these differences were near the expected instrumental error level and comparable to differences between the 50 m and 70 m MVMS records, it was concluded that the ADCP was performing properly. Coherence between the ADCP and MVMSs was significant out to a frequency of about 0.3 cph where the ADCP spectra reached a noise floor.

Currents were also obtained from the USC and Lamont MVMSs at 10, 30, 50, and 70 m (Table 6). As with the temperature data, the 1 min USC samples and 4 min Lamont samples were averaged to 15 min to be compatible with our nominal sampling interval. The current records from the two USC instruments and the 70 m Lamont instrument were complete, and no further processing was done. The Lamont record from 30 m stopped on 9 July due to a broken rotor. The missing data were filled using linear interpolation between the 10 m and 50 m USC MVMSs. The Lamont MVMS at 90 m recorded good data only for the first three days of the deployment due to a compass problem, and was eliminated from any further processing. Instead, the ADCP currents from the 86 m depth bin were used.

Figures 15a-i and 16a-i show the east and north velocity components from 11 depths as overplotted lines. Time series from the MVMSs at 10, 30, 50, and 70 m are shown along with ADCP data from bins at 86, 102, 118, 150, 182, 214, and 246 m. Data were smoothed over 8 hr prior to plotting. In order to distinguish data from different depths, a variety of line types is used. The 10 m data is plotted as a solid line and data from 30, 50, and 70 m use progressively longer dashes. At 102 m and below all lines are solid. The currents below 100 m have little variation

with depth and form a "clump" of solid lines. When there is substantial shear in the upper 100 m the solid 10 m line and the dashed lines at 30, 50 and 70 m separate from the clump of solid lines from 102 m and below.

Figure 17a-i shows currents at selected depths between 10 m and 250 m as vector stick plots. The nine panels, from top to bottom, show data from 10, 30, 50, 70, 86, 118, 150, 198, and 246 meters. A stick pointing upwards represents a current towards the north. These data were averaged over 8 hr prior to plotting.

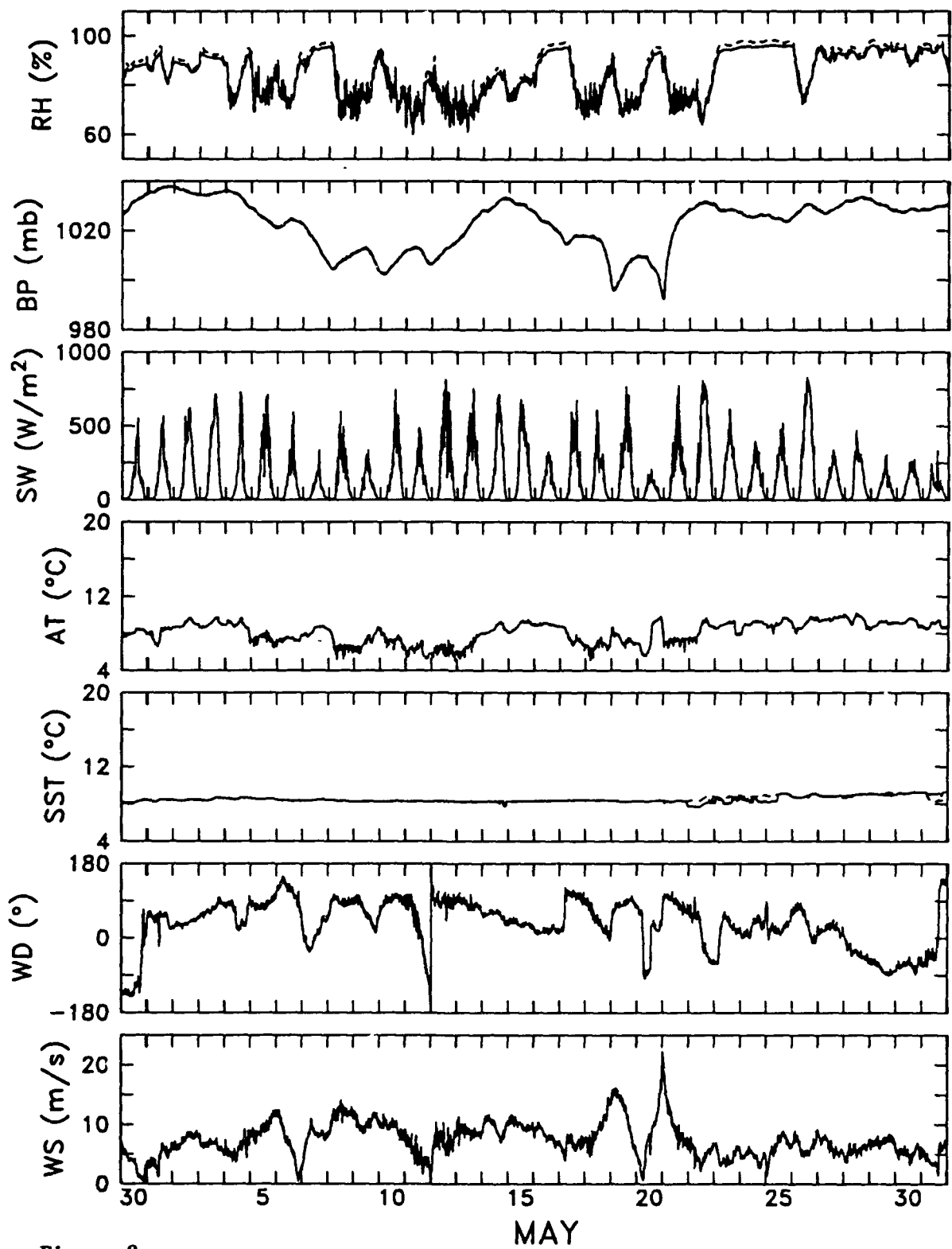


Figure 8a
Meteorological variables from the two VAWRs.

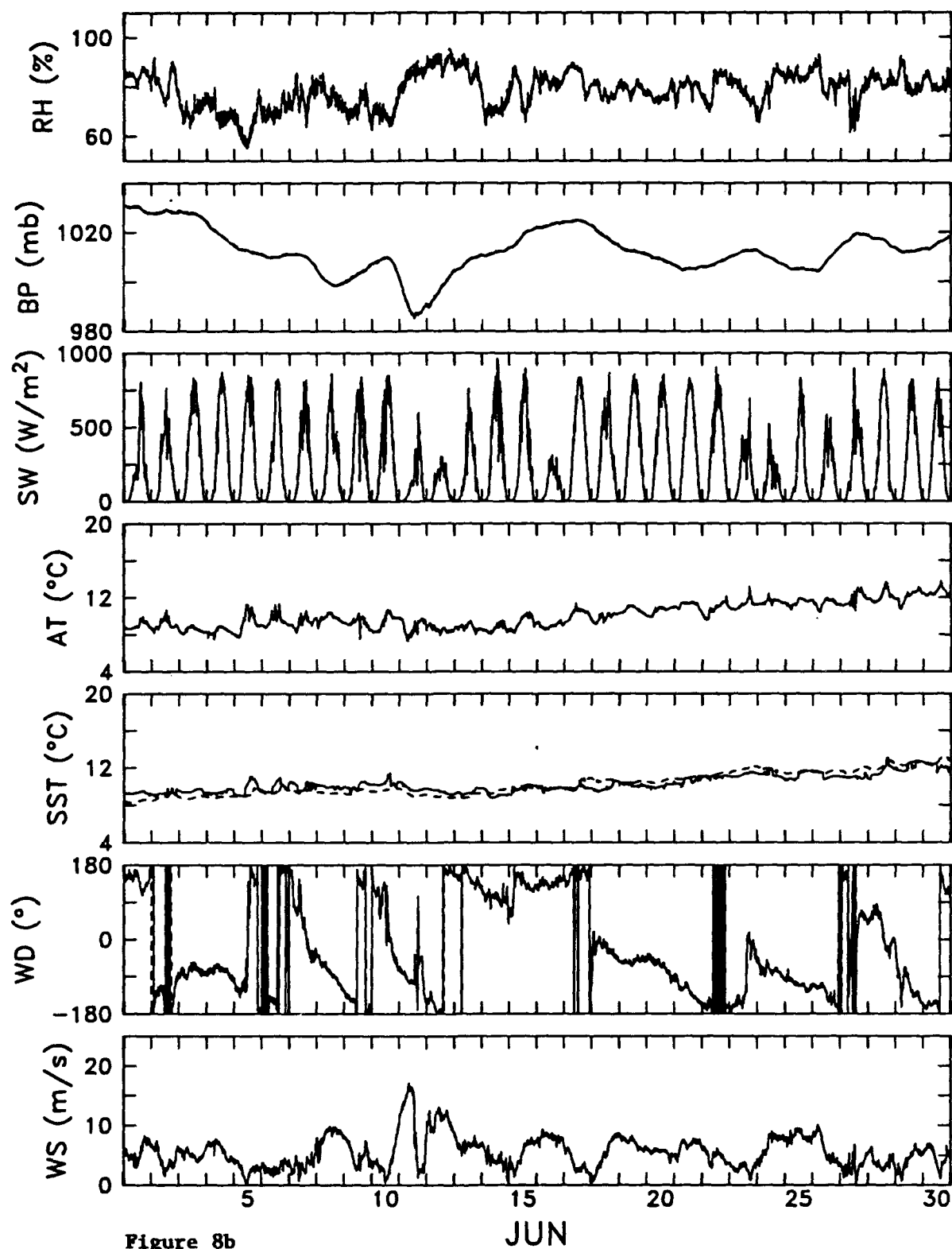


Figure 8b
Meteorological variables from the two VAWRs.

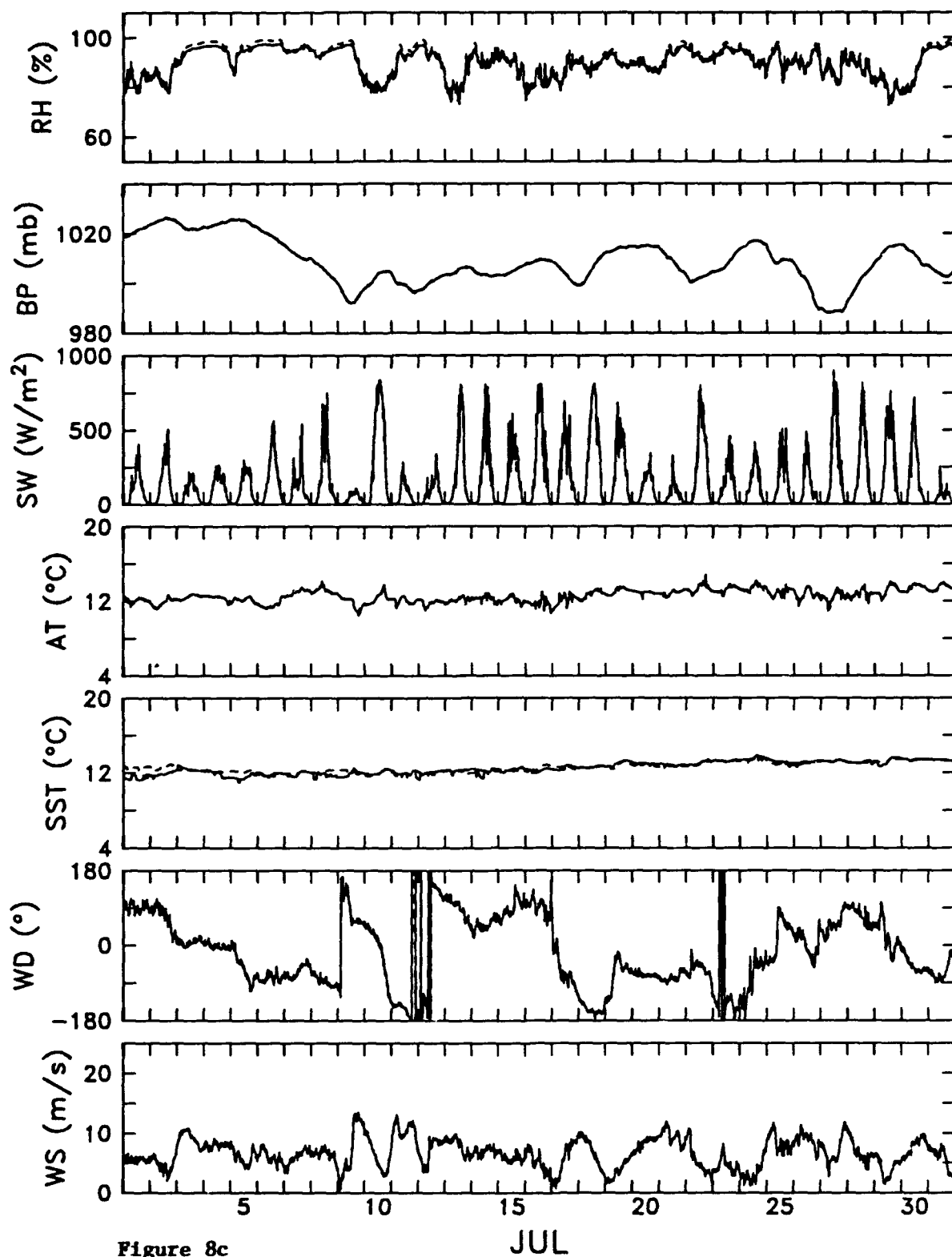


Figure 8c
Meteorological variables from the two VAWRs.

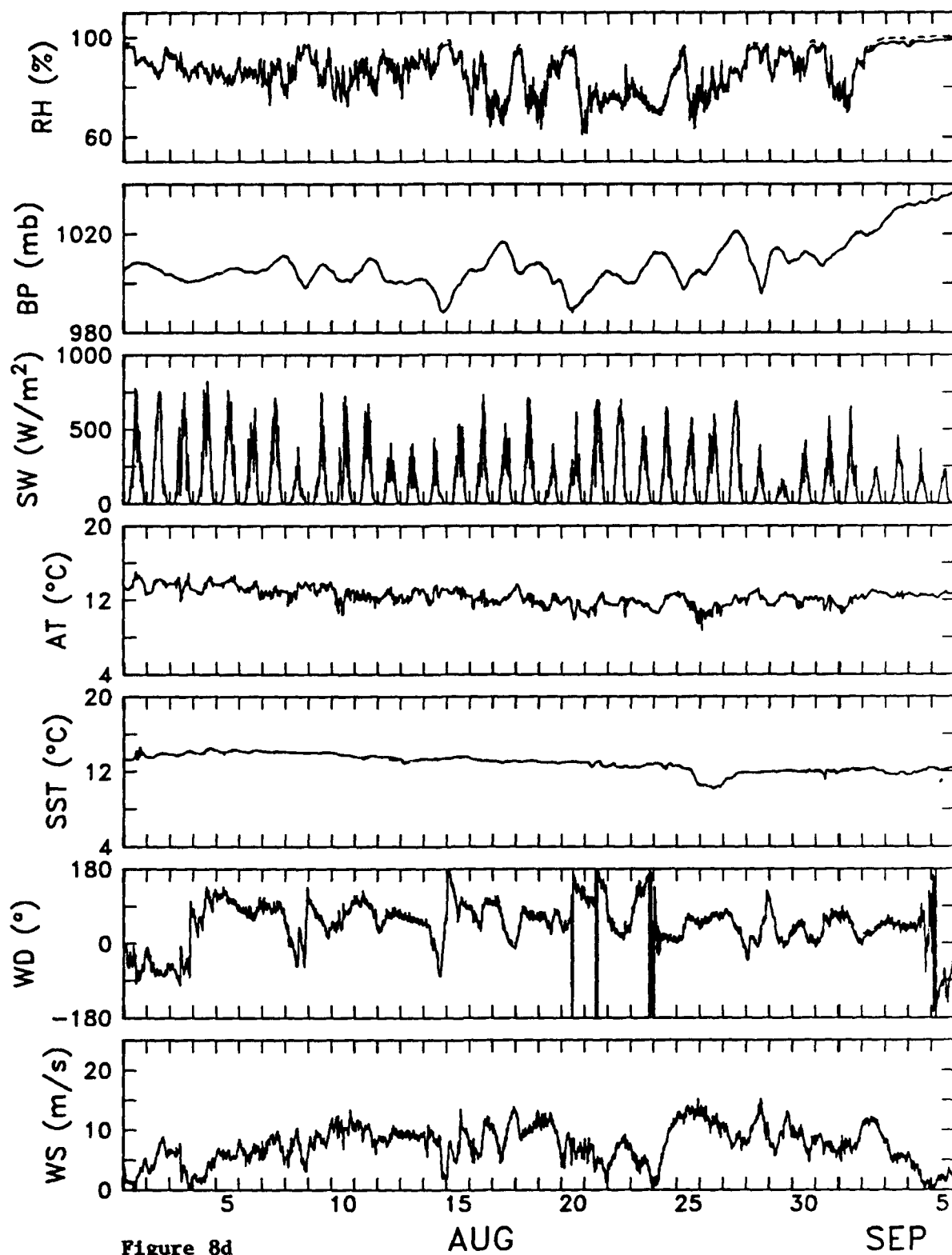


Figure 8d
Meteorological variables from the two VAWRs.

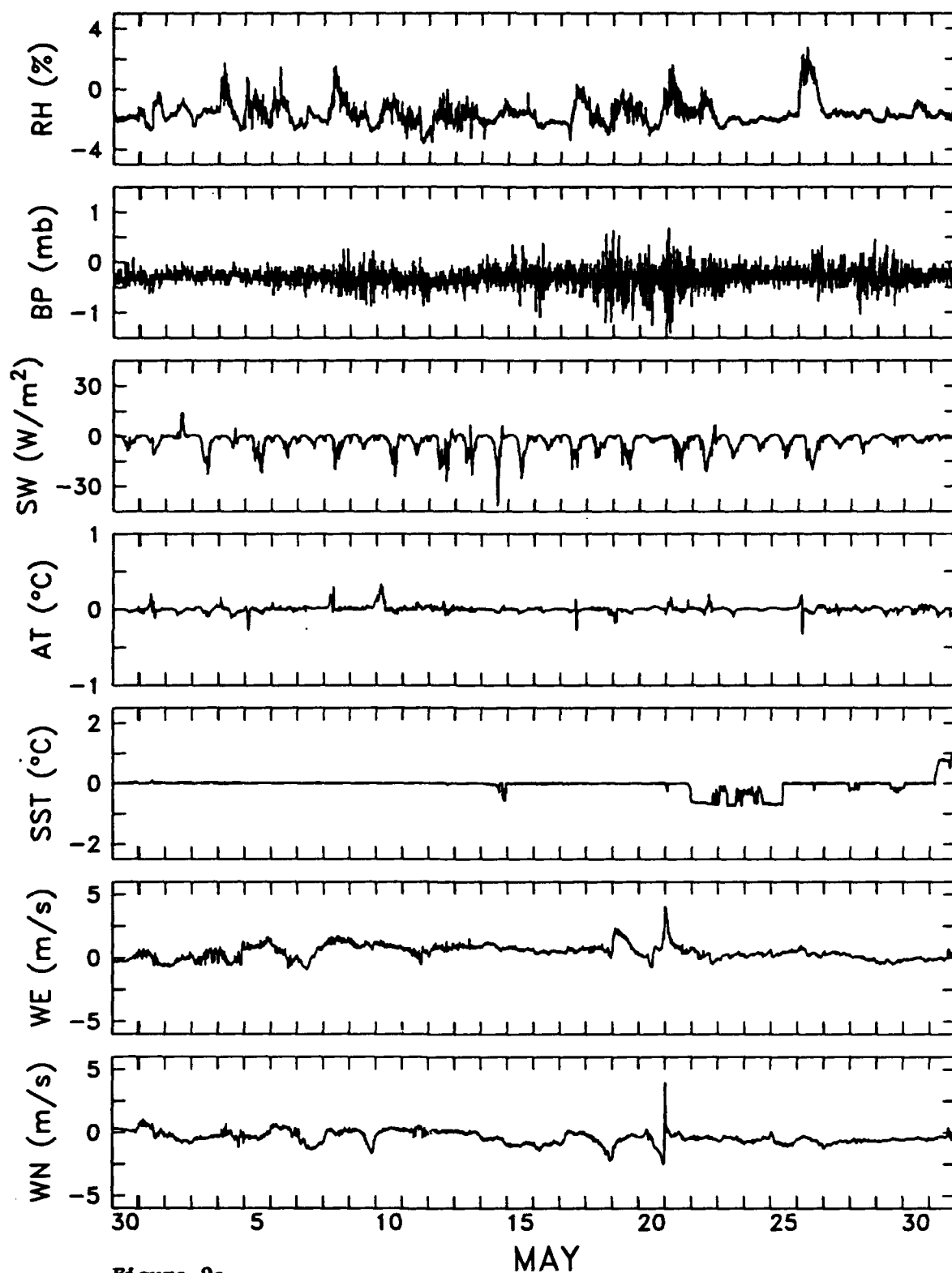


Figure 9a
Differences between meteorological variables.

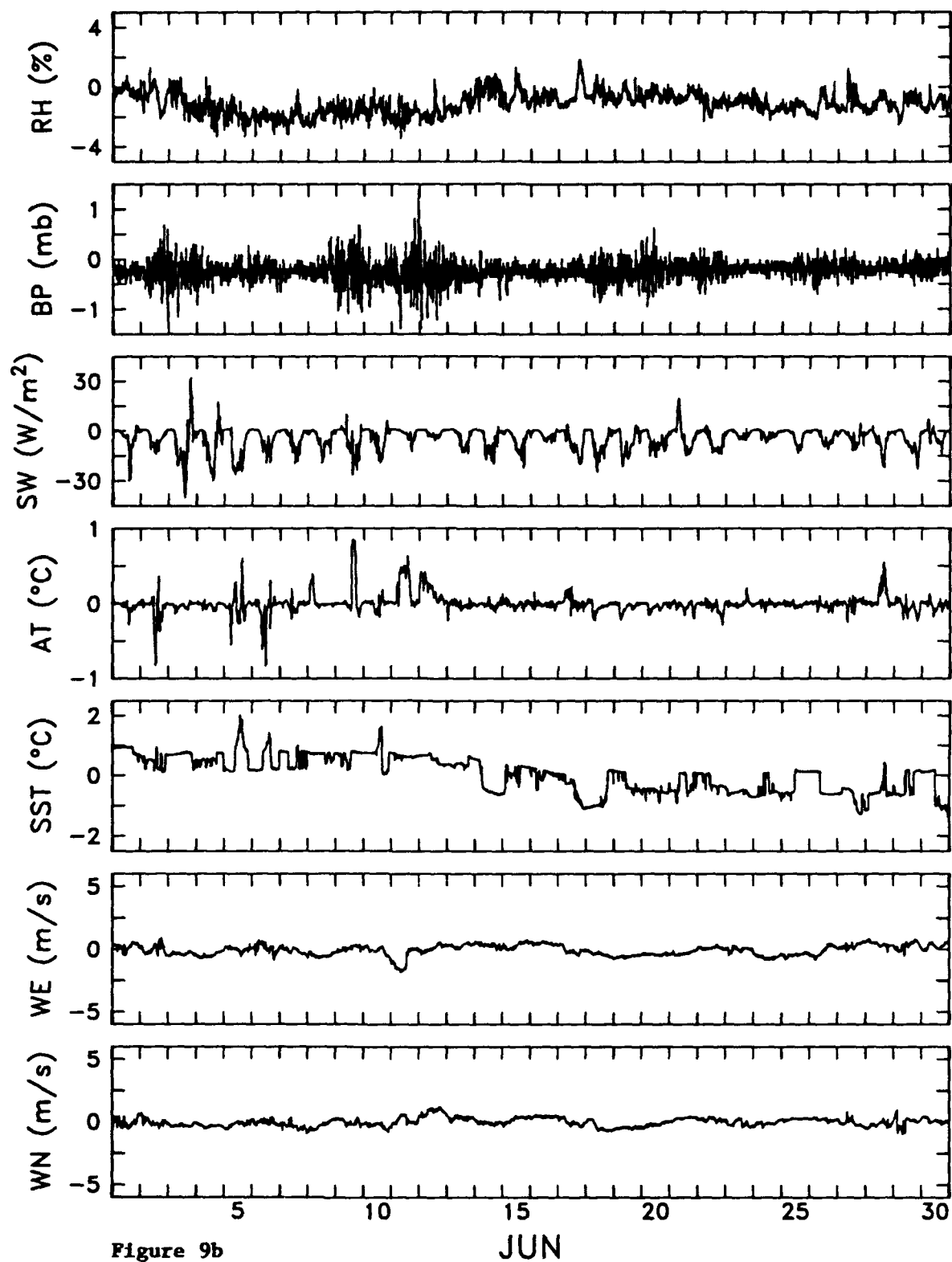


Figure 9b
Differences between meteorological variables.

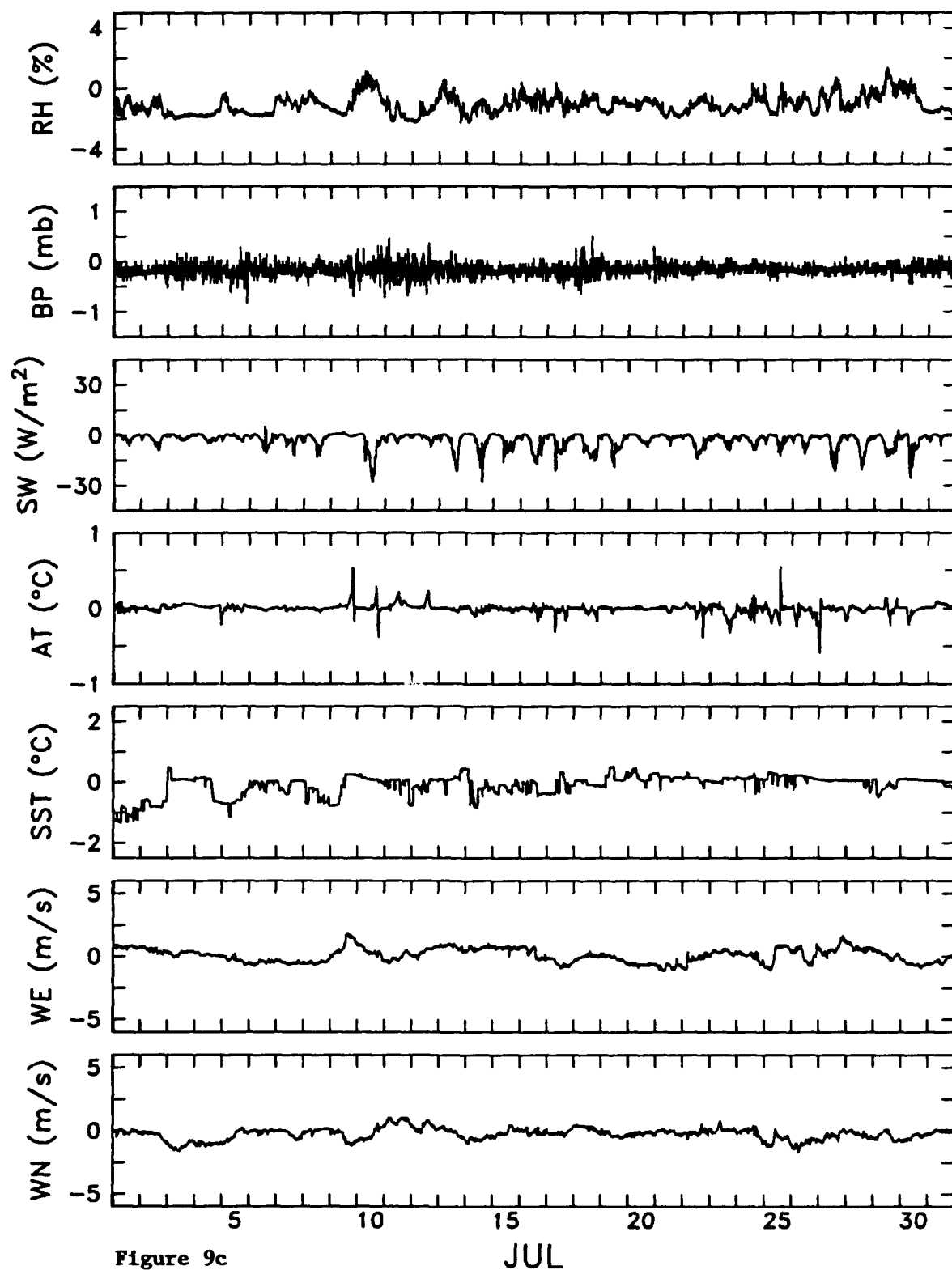


Figure 9c
Differences between meteorological variables.

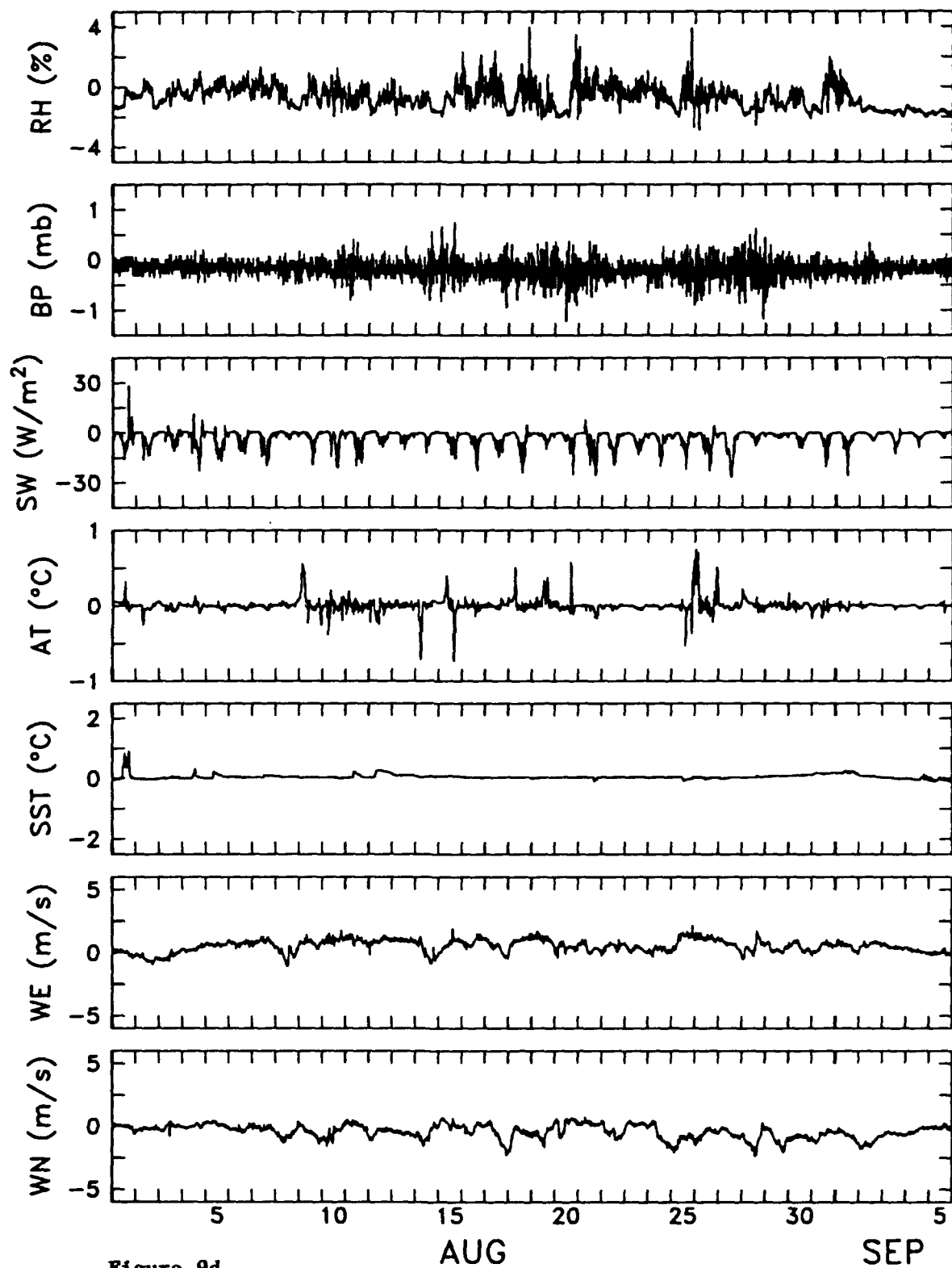


Figure 9d
Differences between meteorological variables.

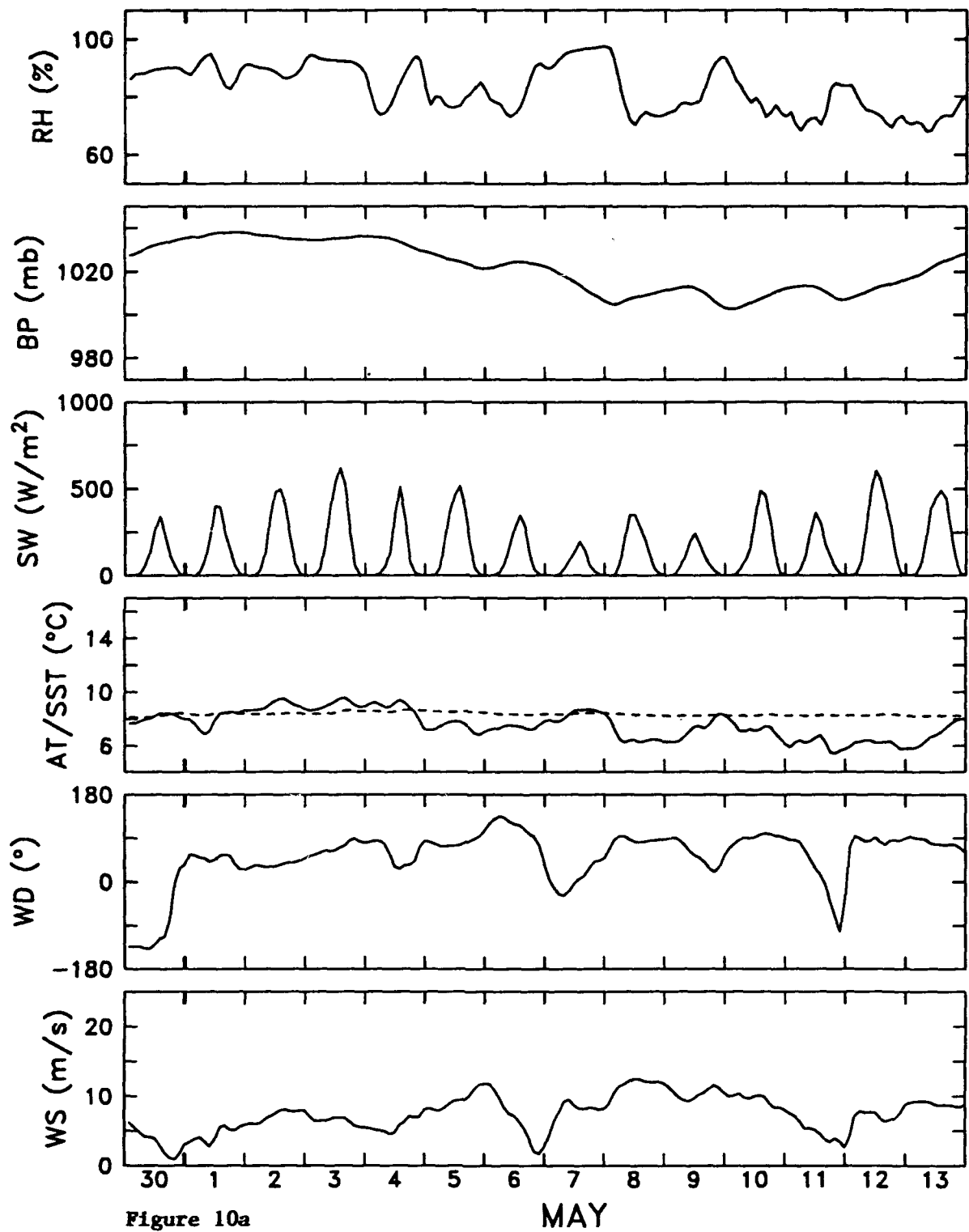


Figure 10a
Best available meteorological variables.

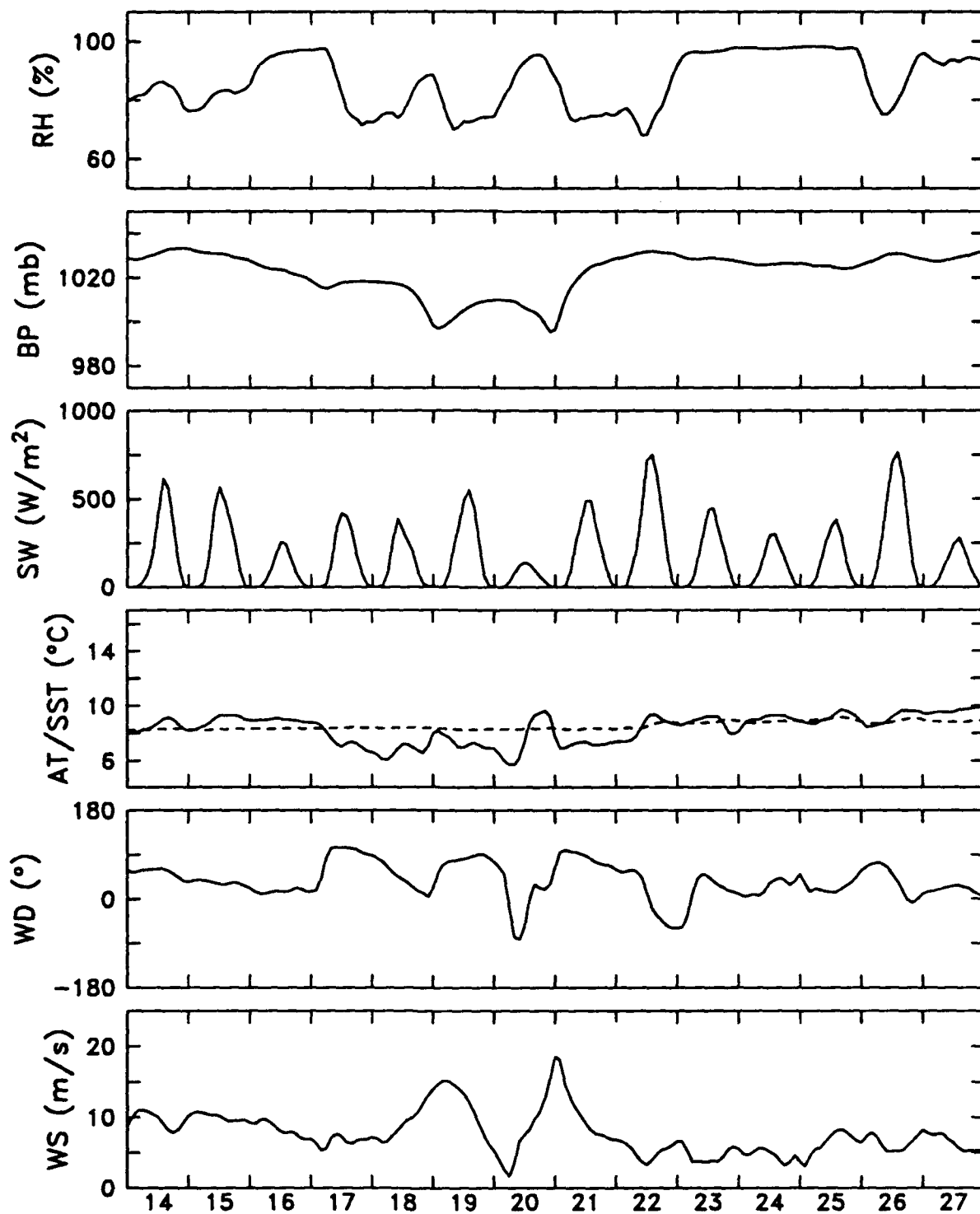


Figure 10b
MAY
 Best available meteorological variables.

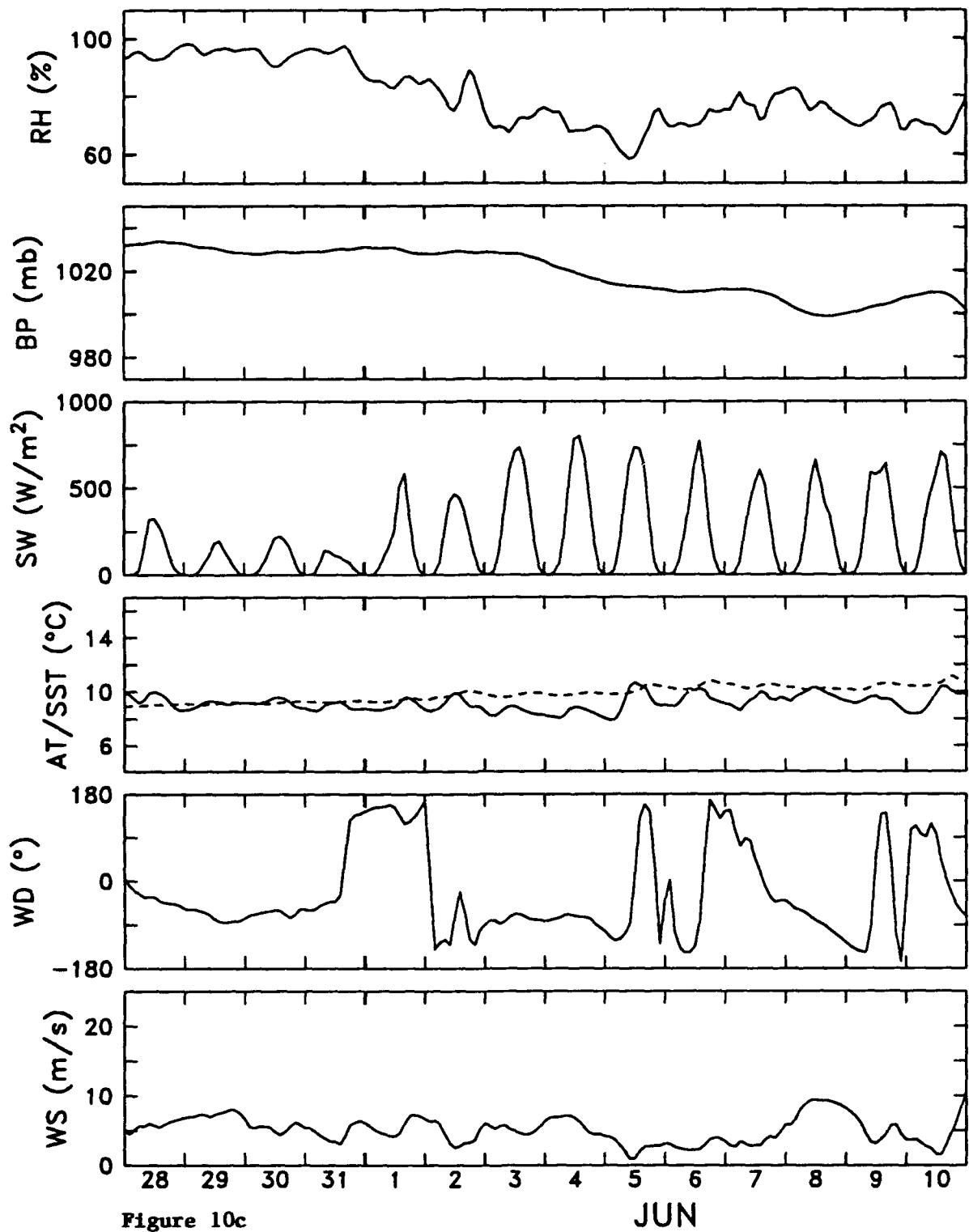


Figure 10c
Best available meteorological variables.

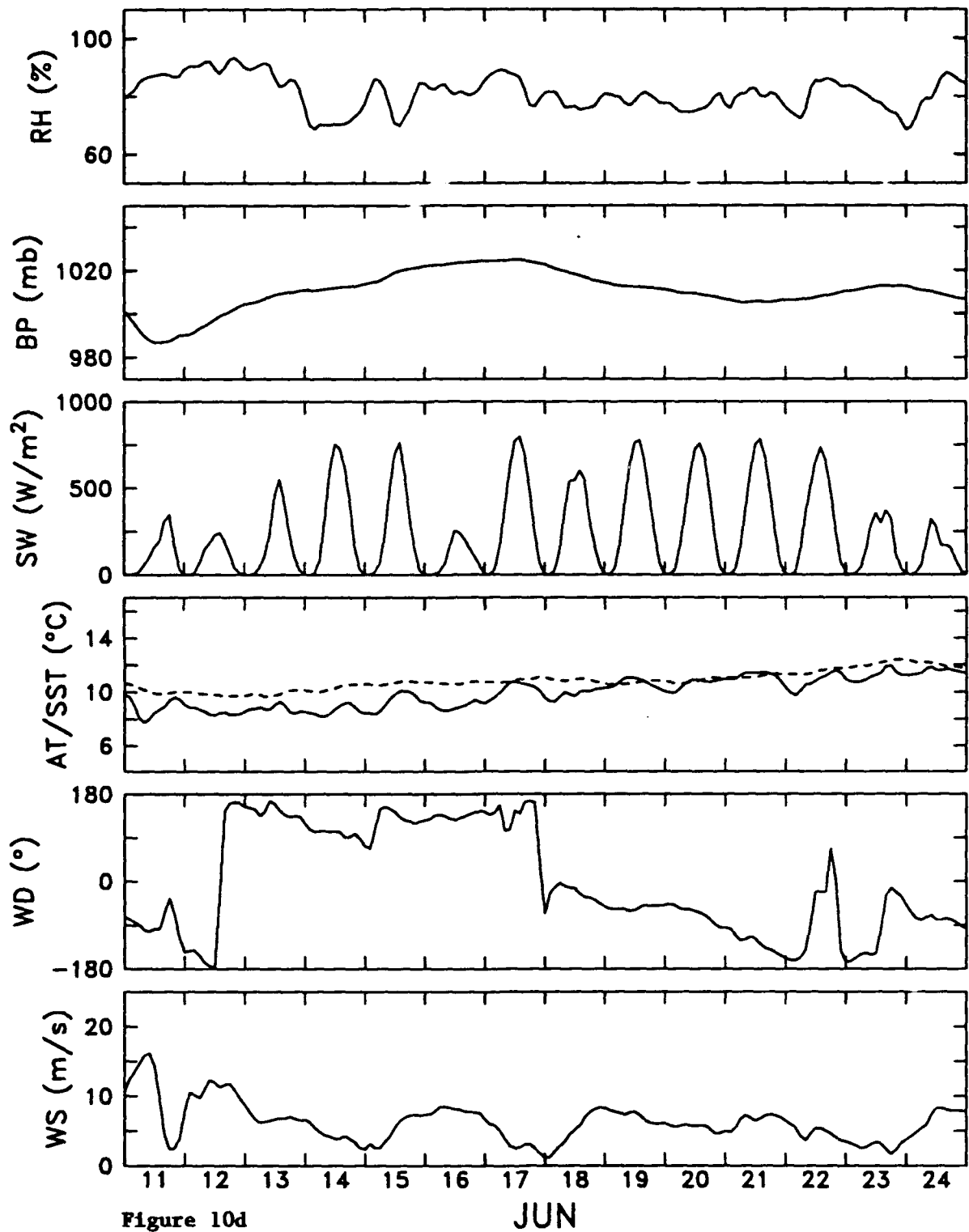


Figure 10d
Best available meteorological variables.

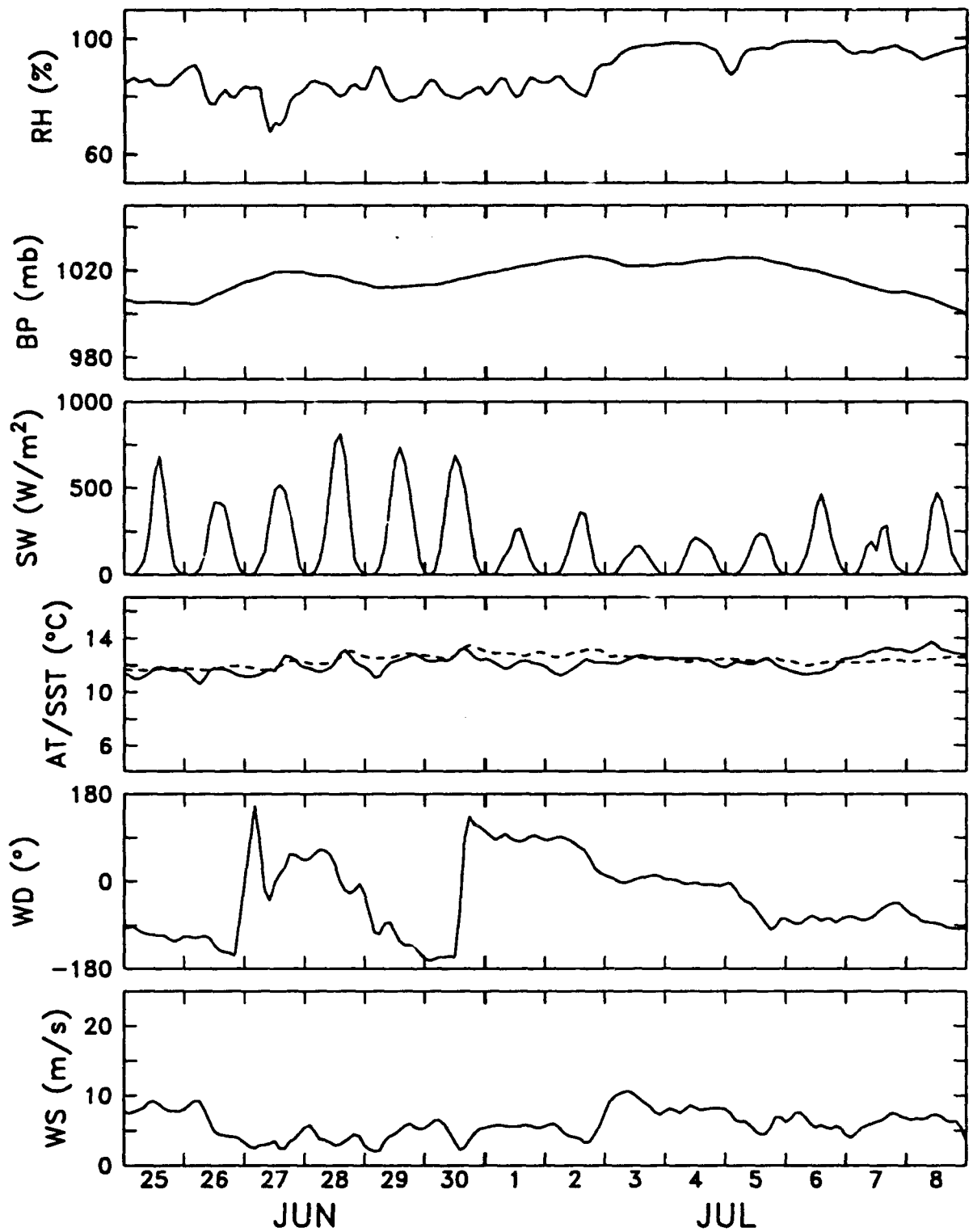


Figure 10e
Best available meteorological variables.

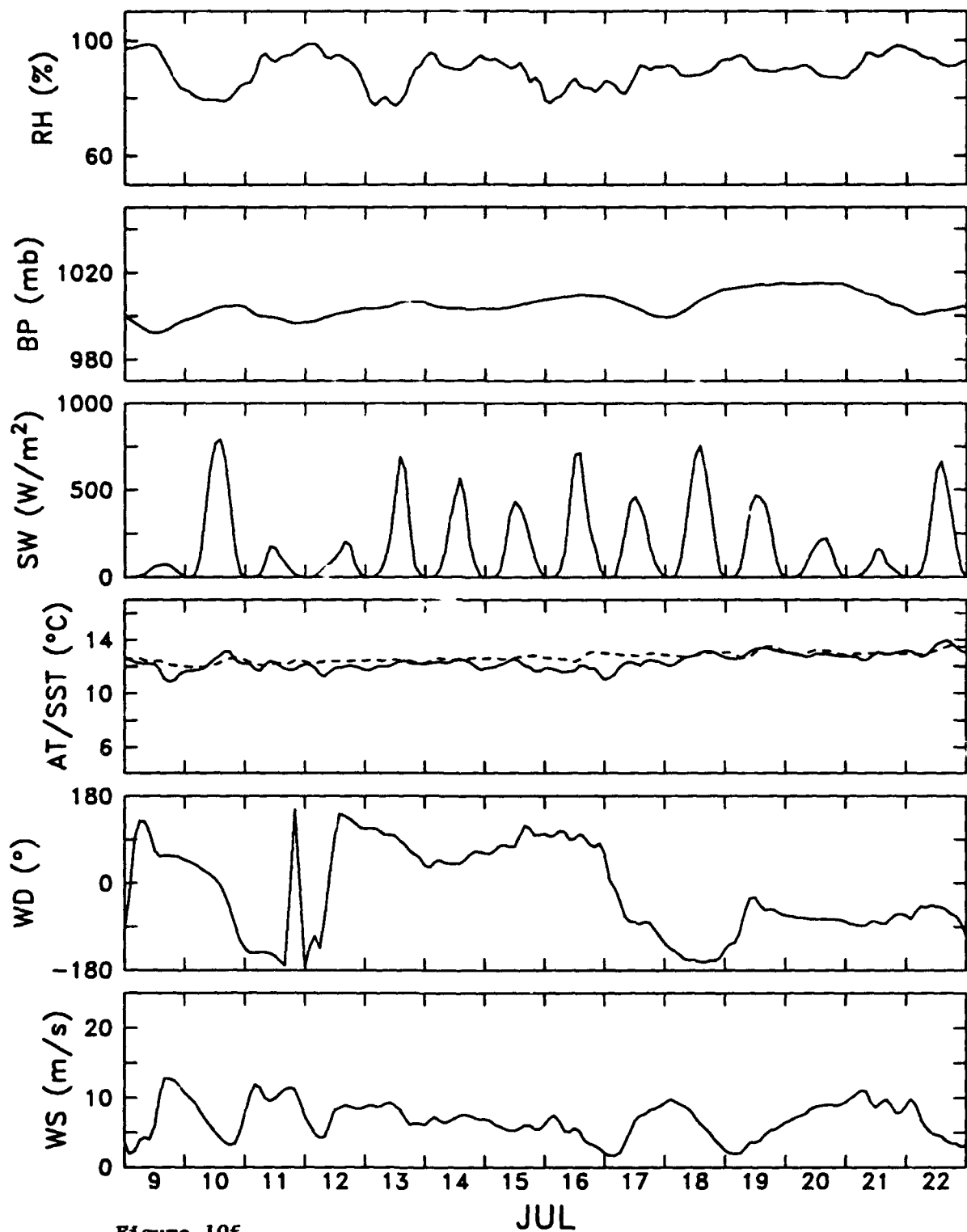


Figure 10f
Best available meteorological variables.

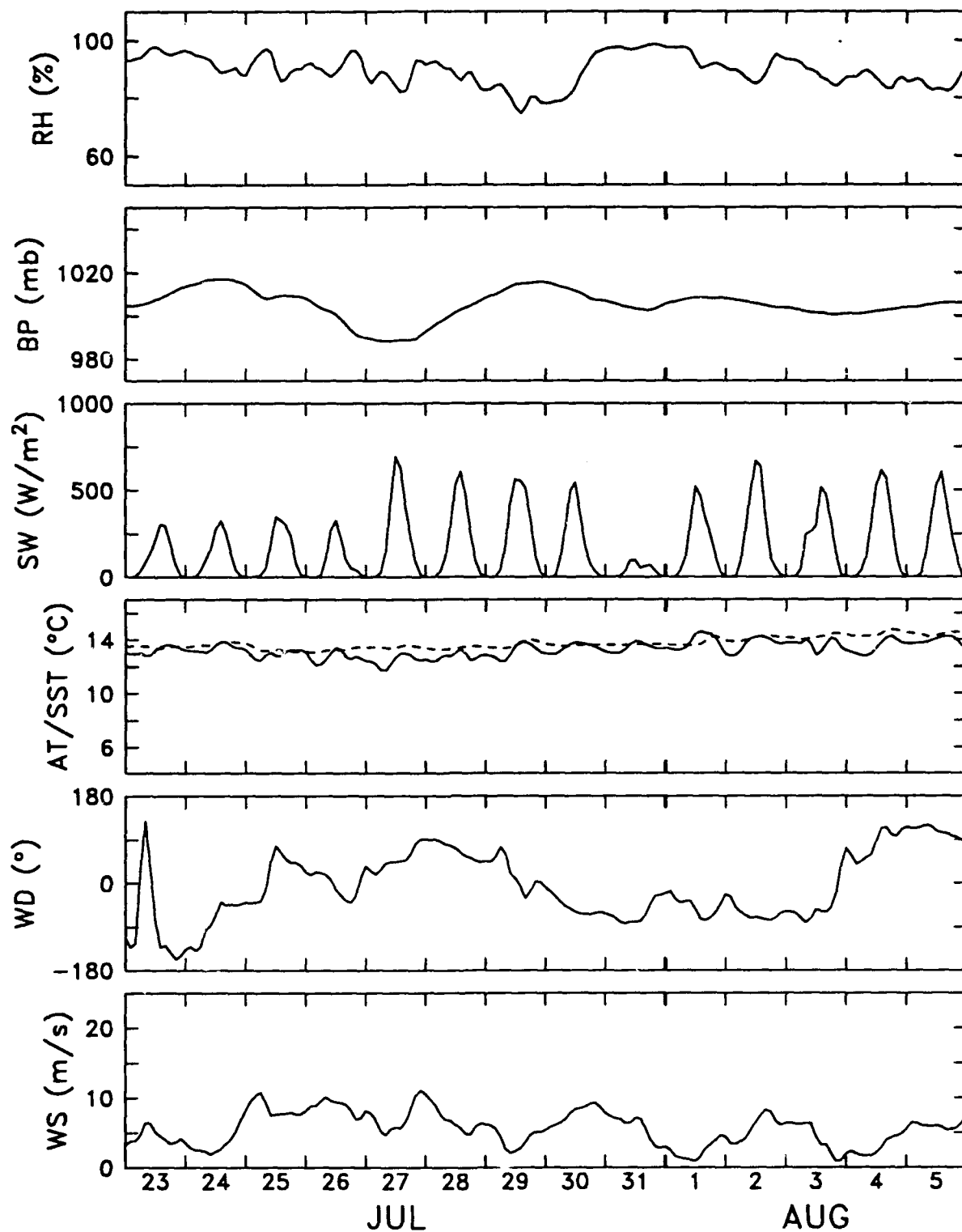


Figure 10g
Best available meteorological variables.

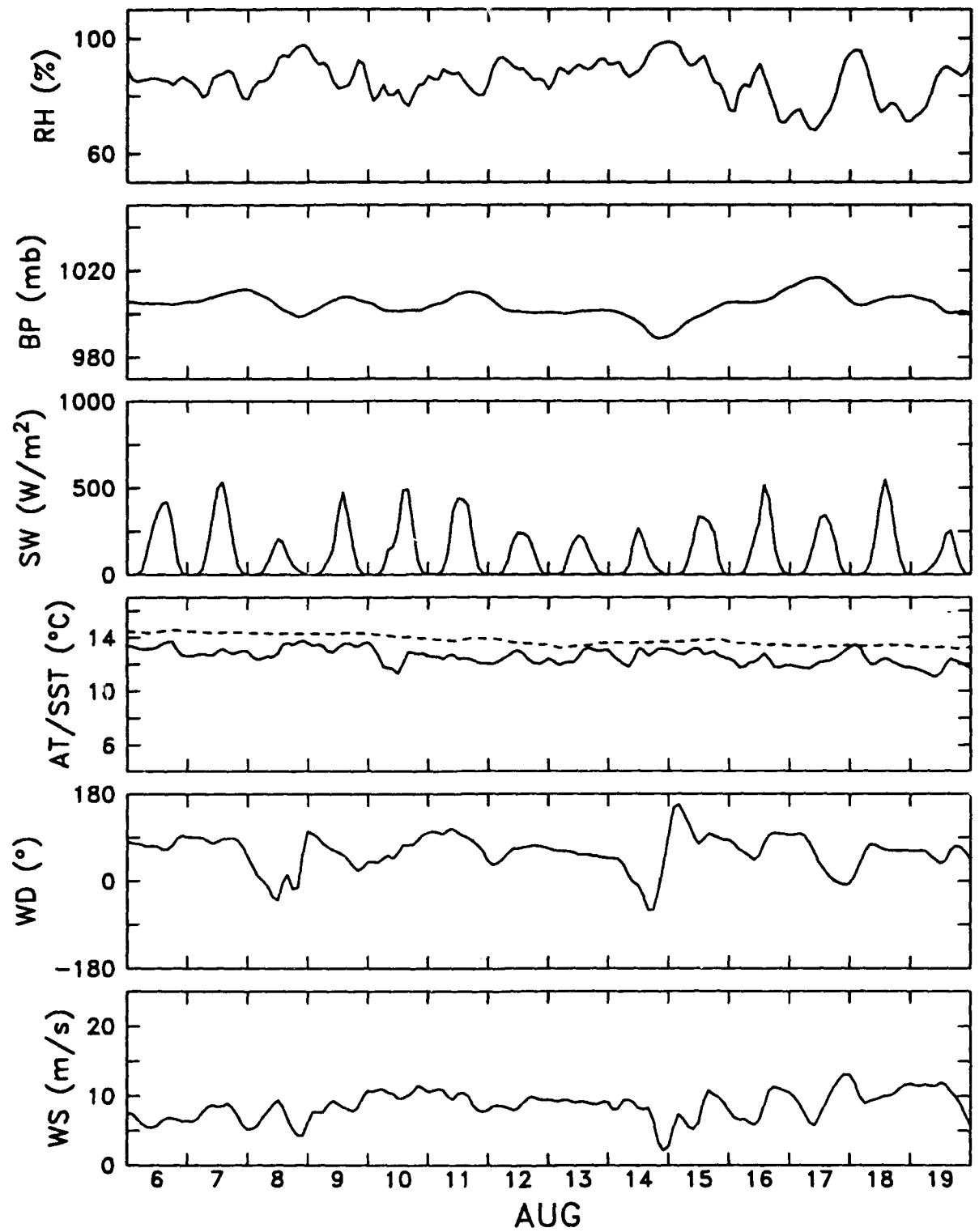


Figure 10h
Best available meteorological variables.

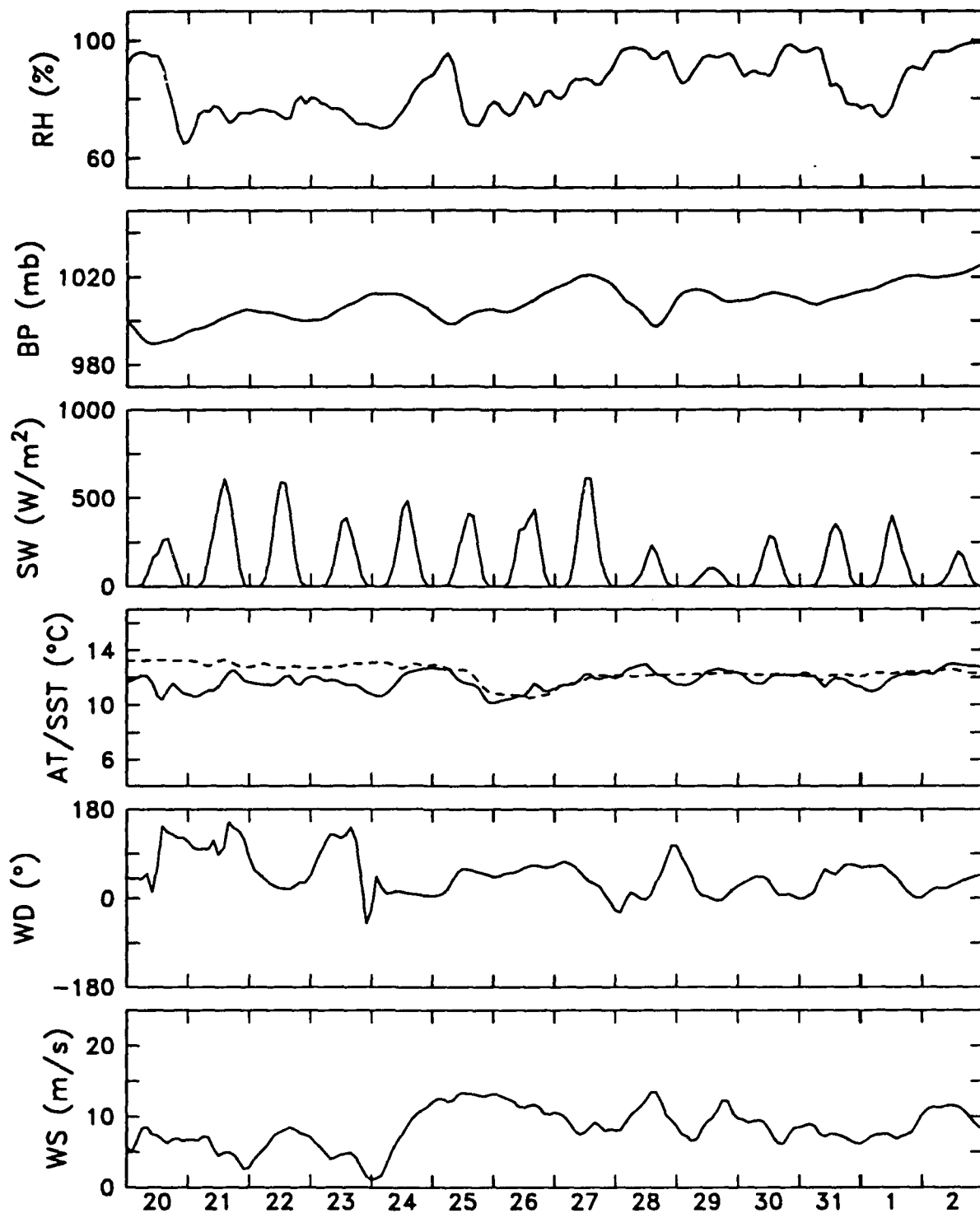


Figure 10i
AUG
Best available meteorological variables.

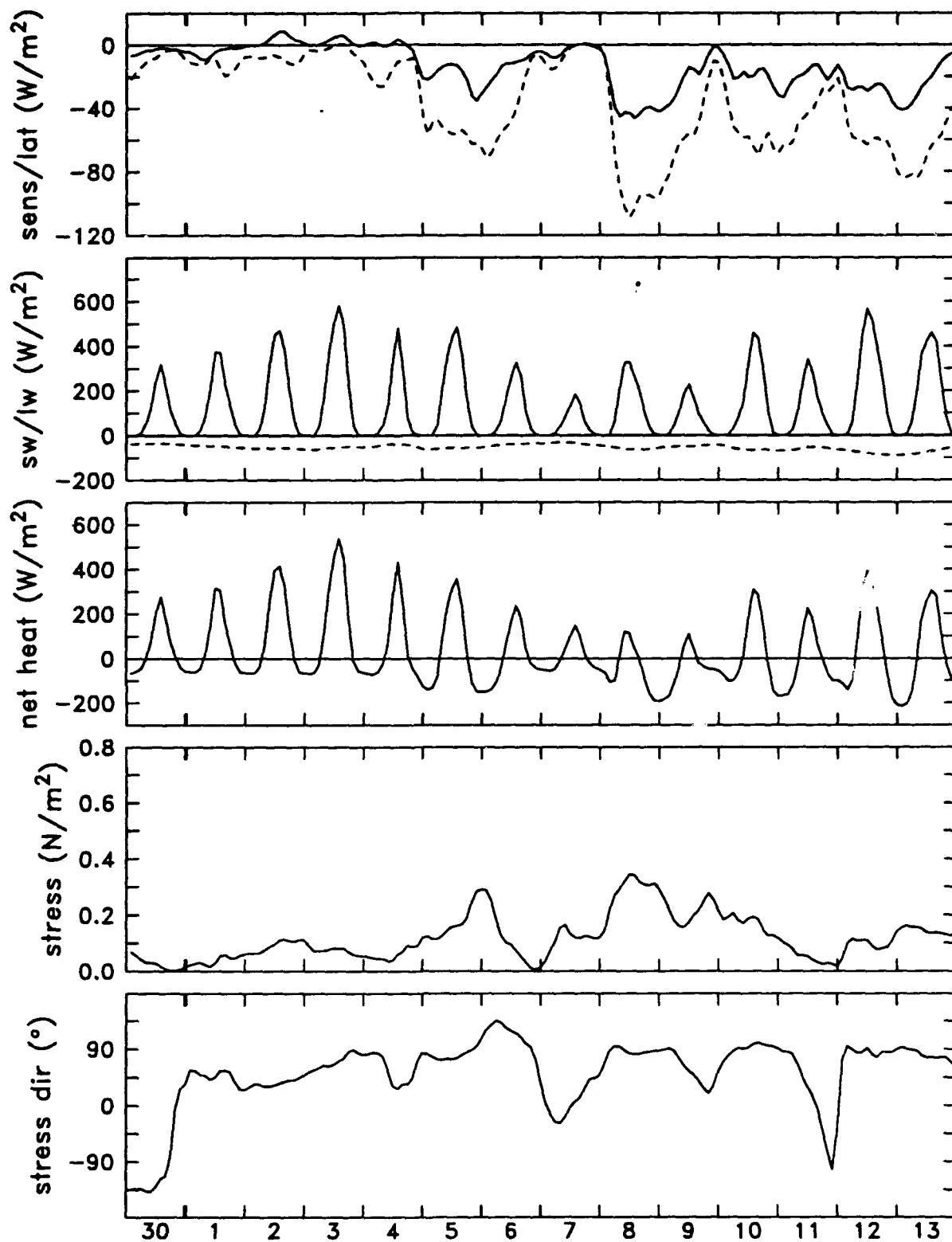


Figure 11a
Air-sea fluxes from bulk formulae.

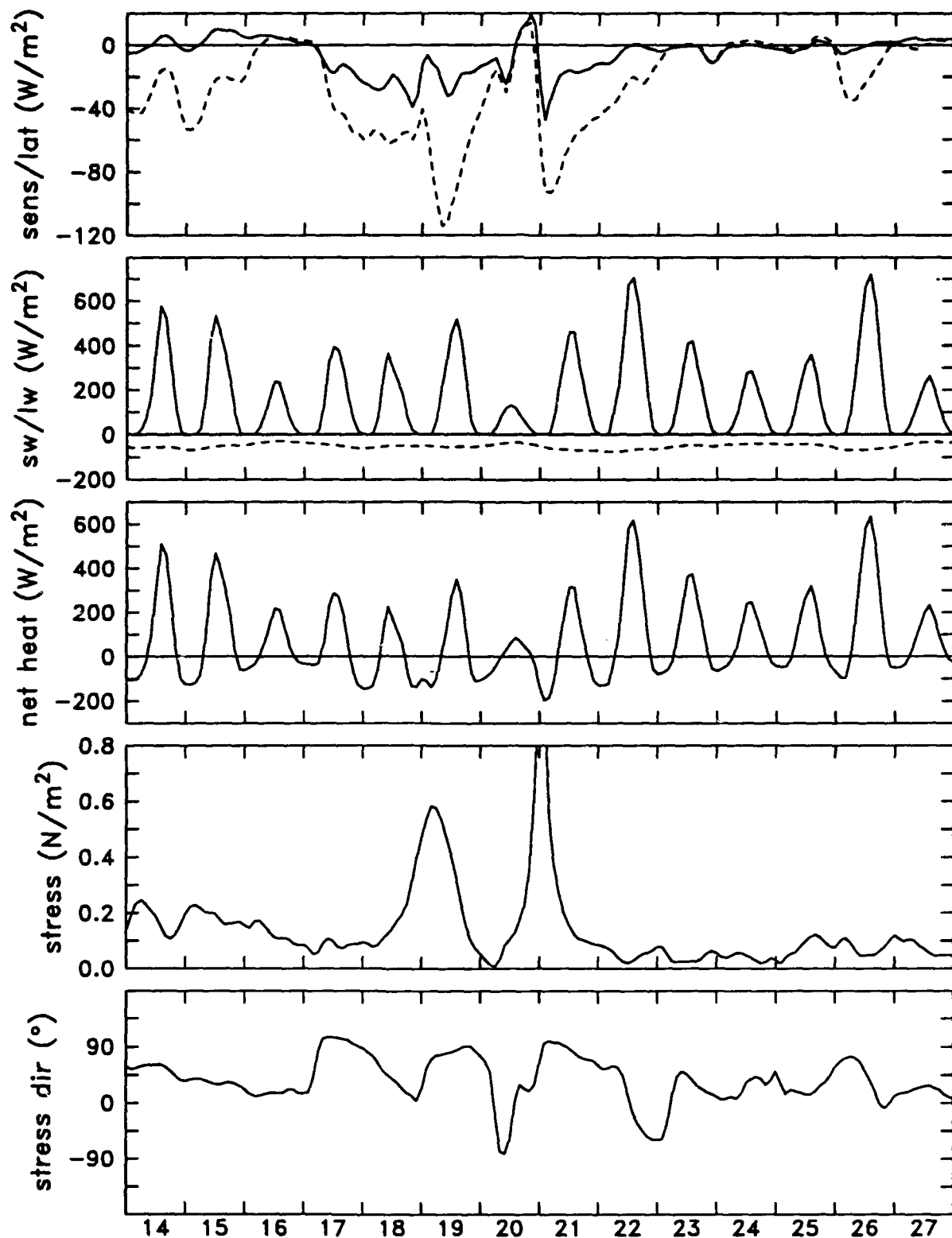


Figure 11b
Air-sea fluxes from bulk formulae.

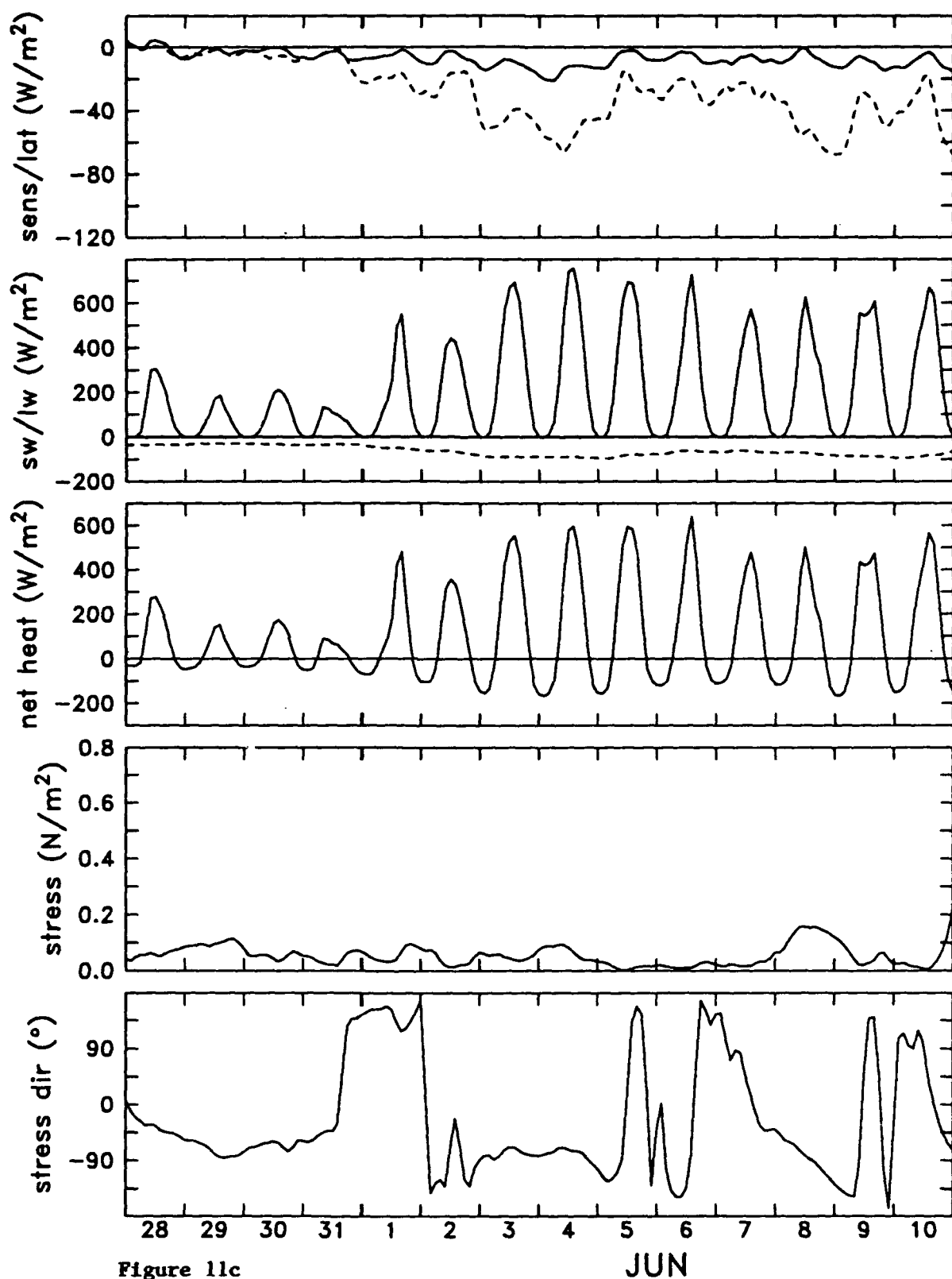


Figure 11c
Air-sea fluxes from bulk formulae.

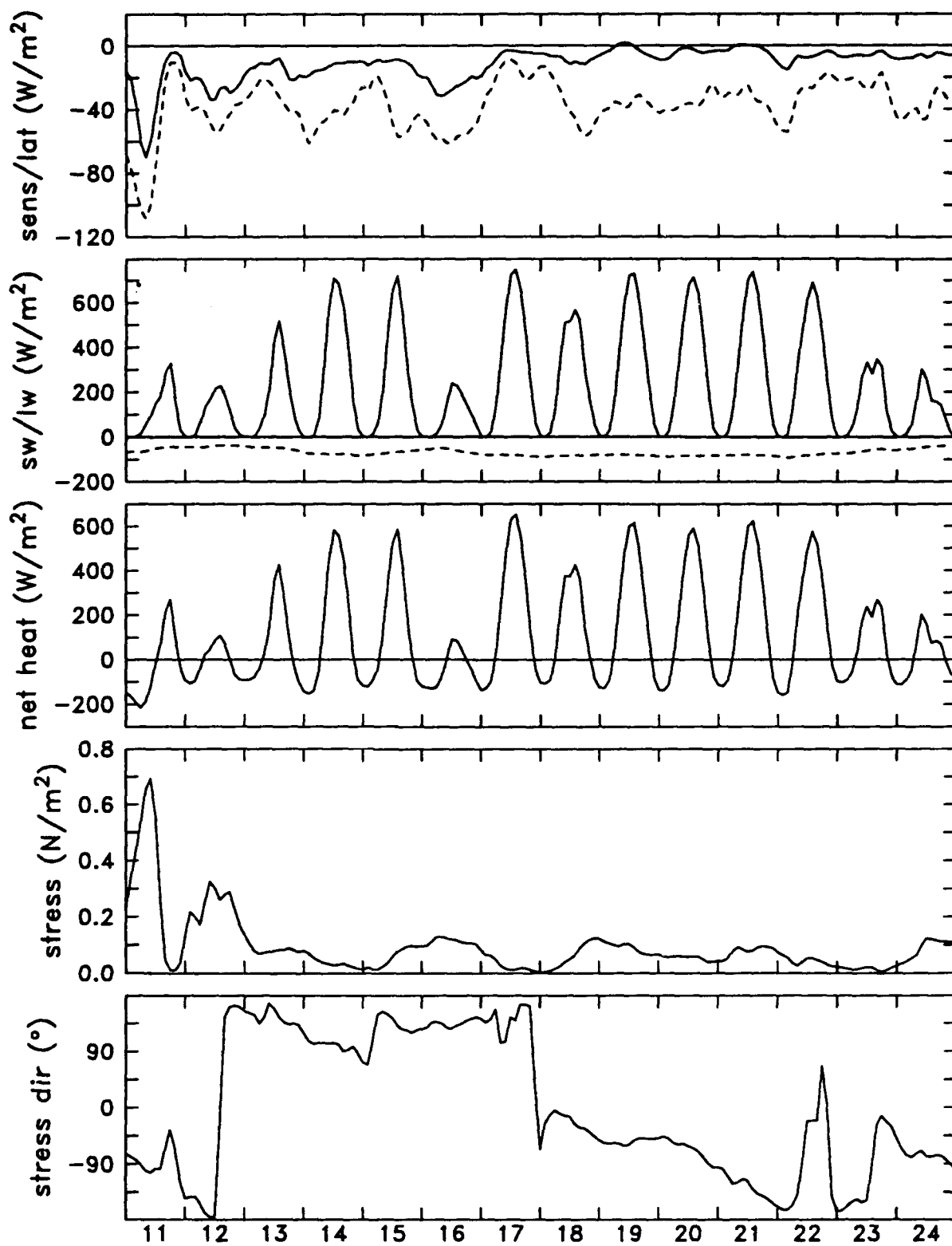


Figure 11d
Air-sea fluxes from bulk formulae.

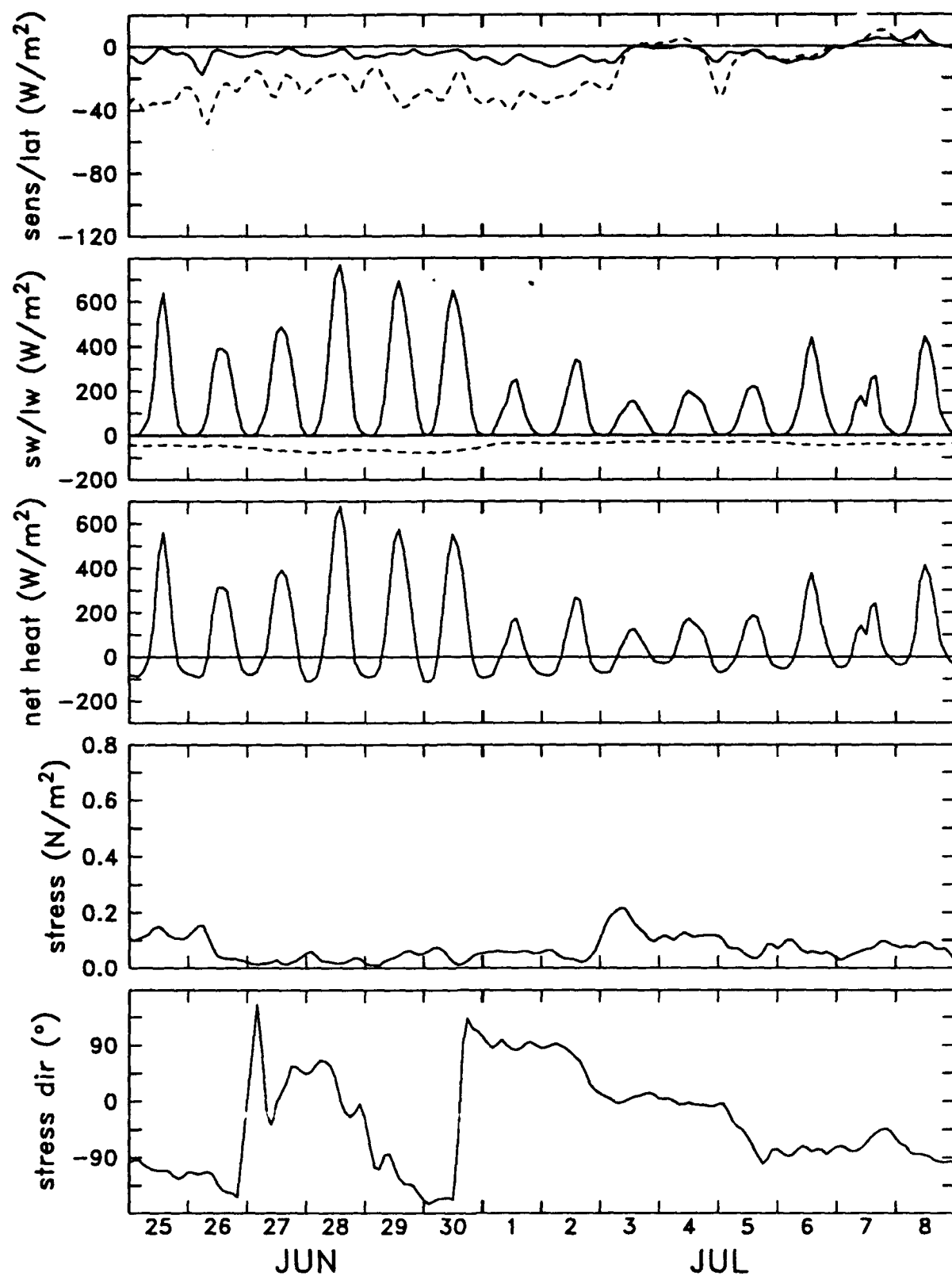


Figure 11e
Air-sea fluxes from bulk formulae.

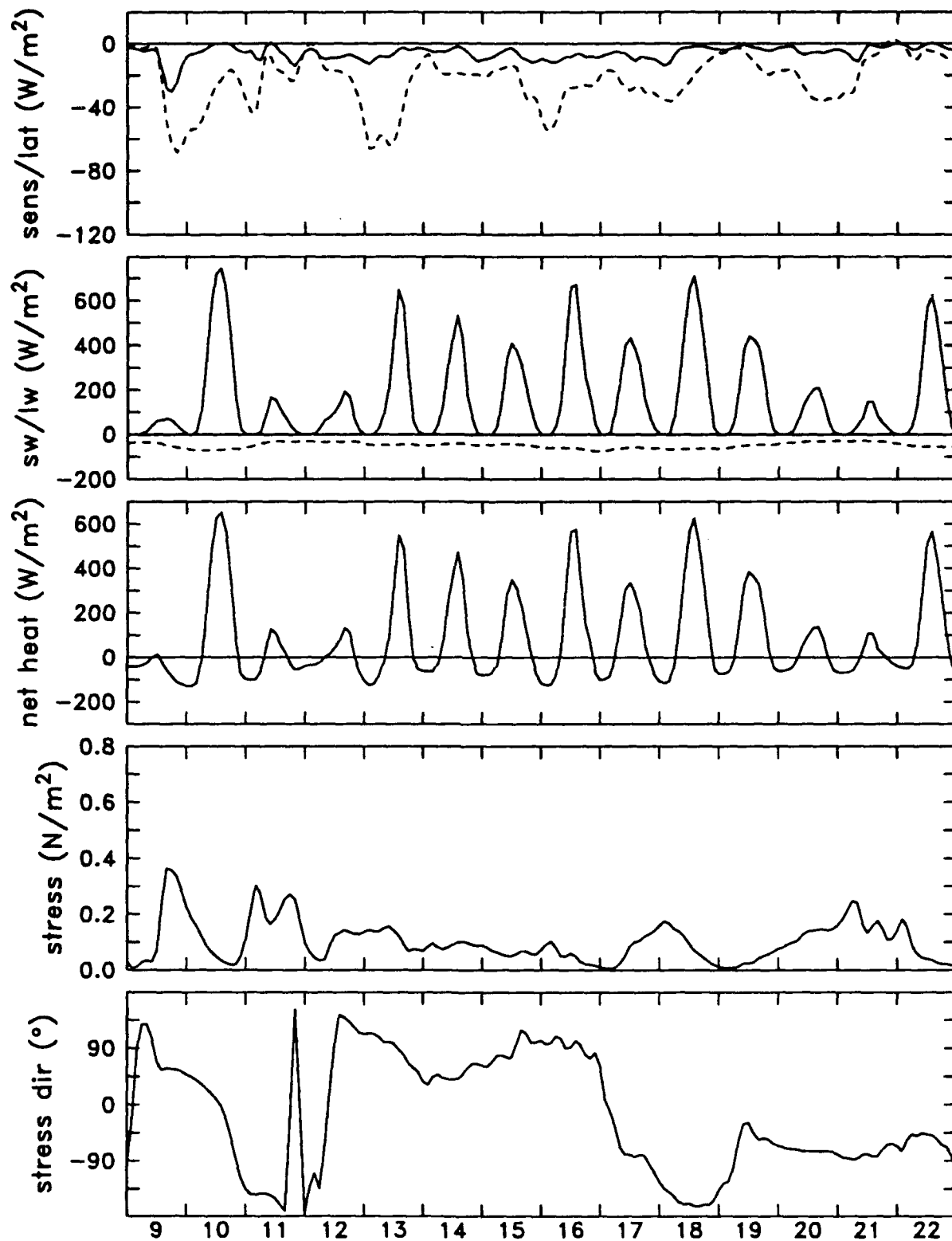


Figure 11f JUL
Air-sea fluxes from bulk formulae.

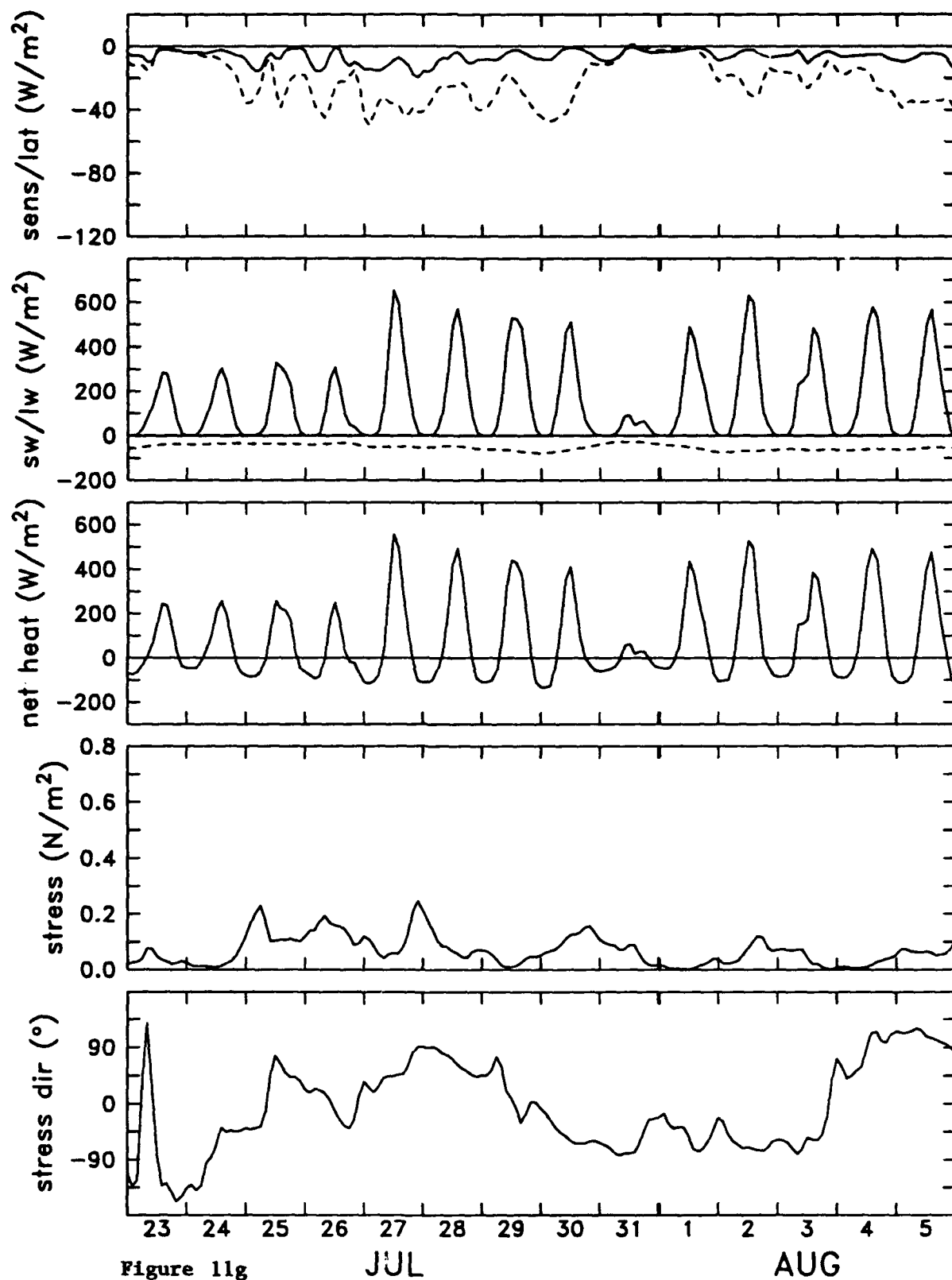


Figure 11g
Air-sea fluxes from bulk formulae.

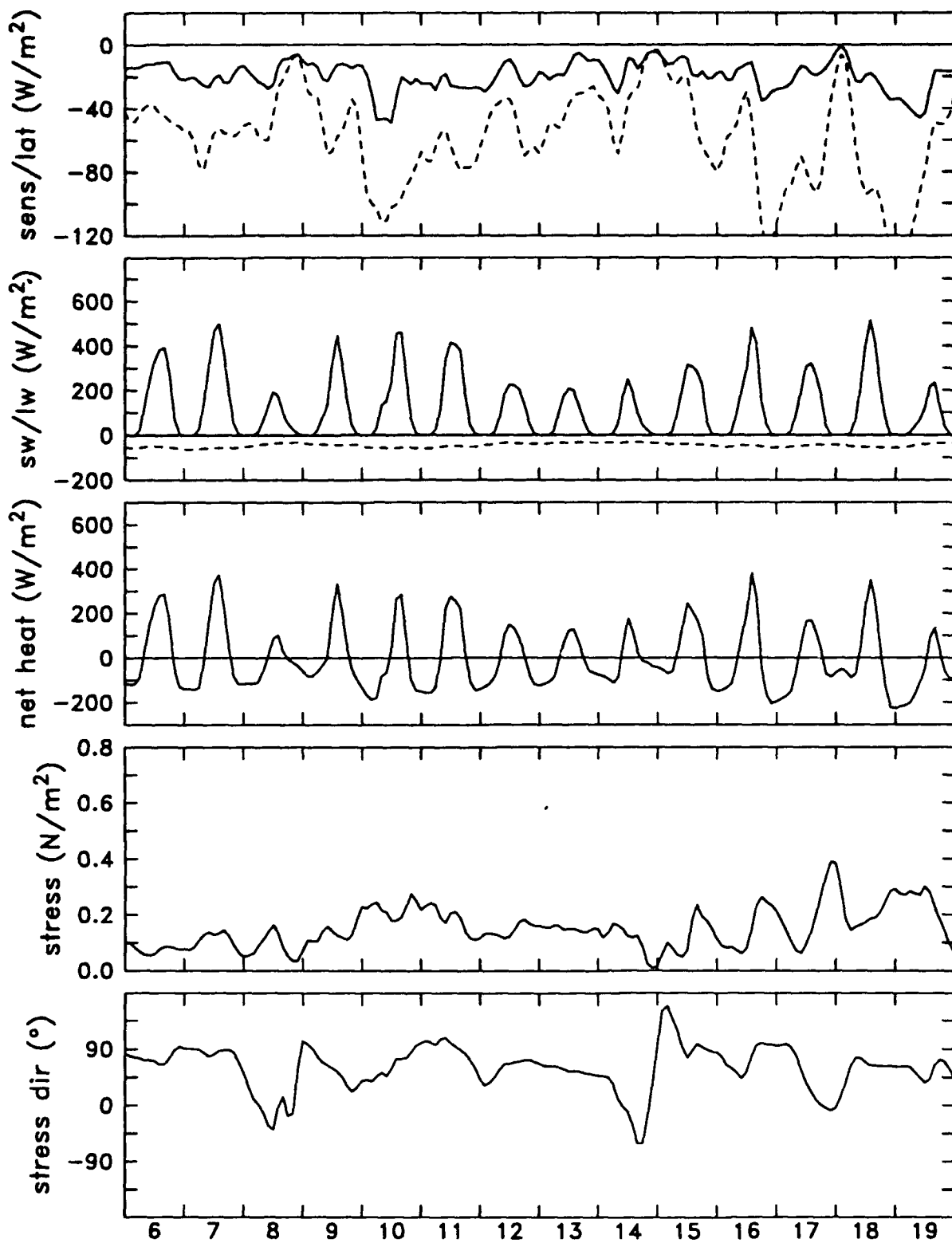


Figure 11h
AUG
Air-sea fluxes from bulk formulae.

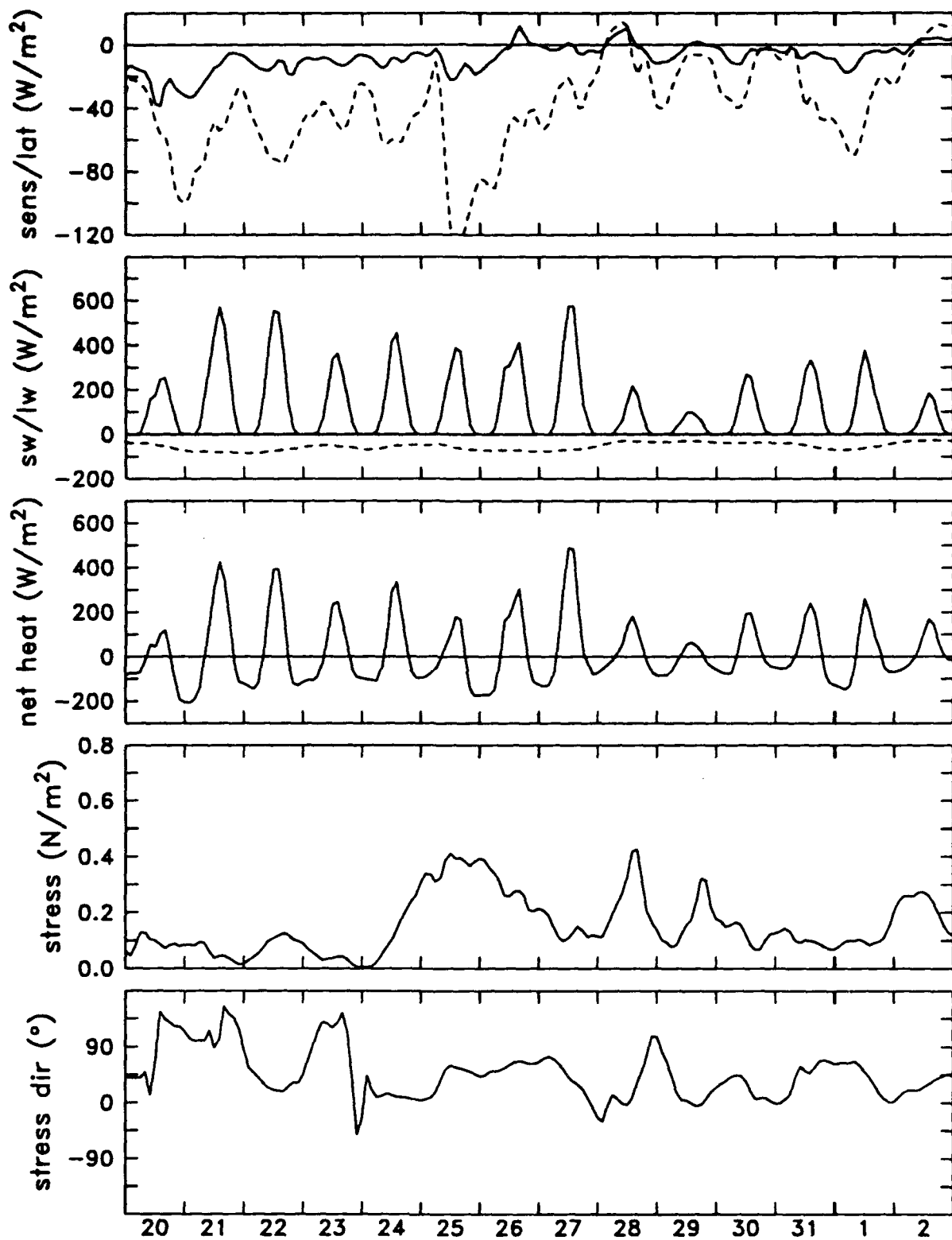


Figure 111

AUG

Air-sea fluxes from bulk formulae.

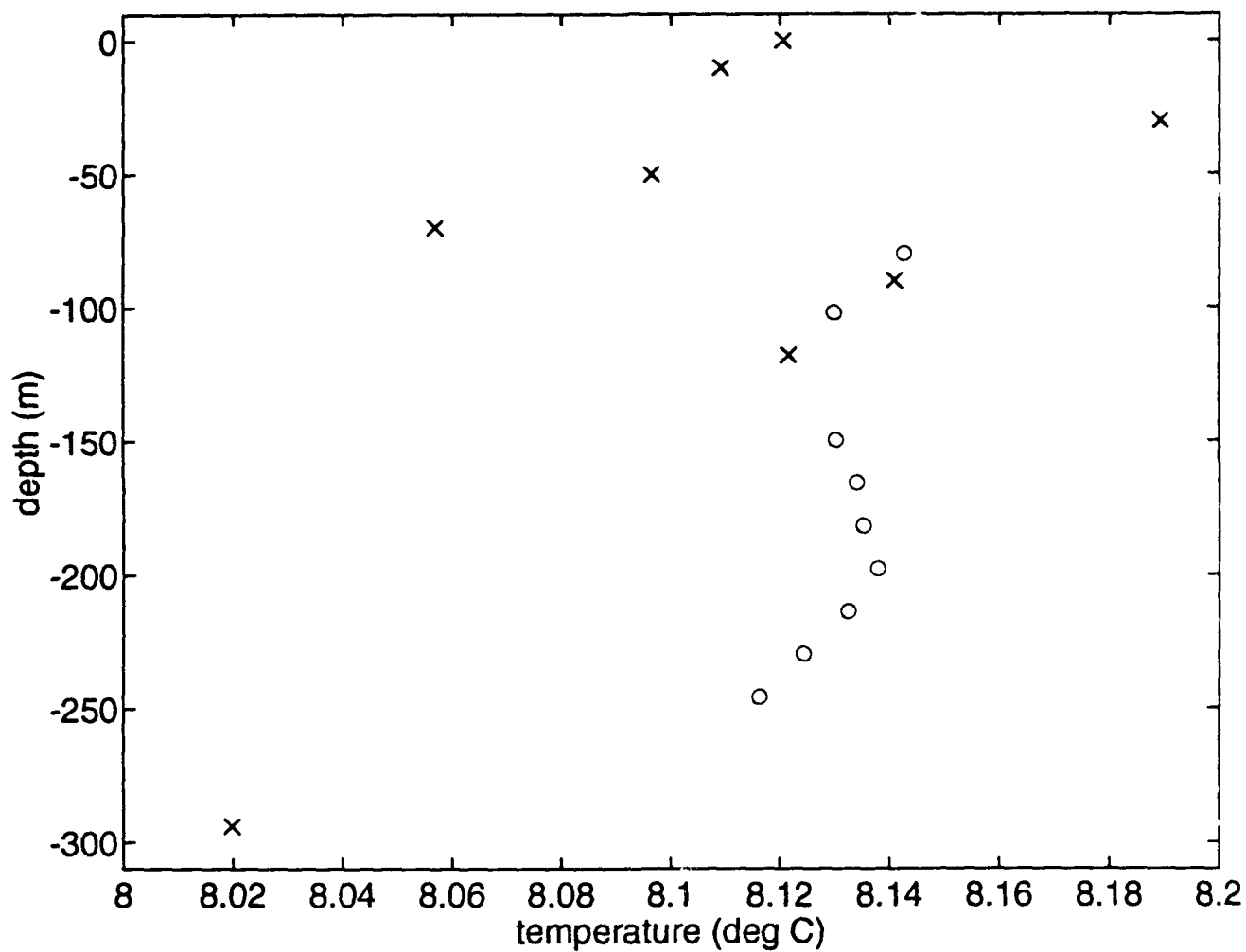


Figure 12
Eight-hour mean temperatures versus depth.

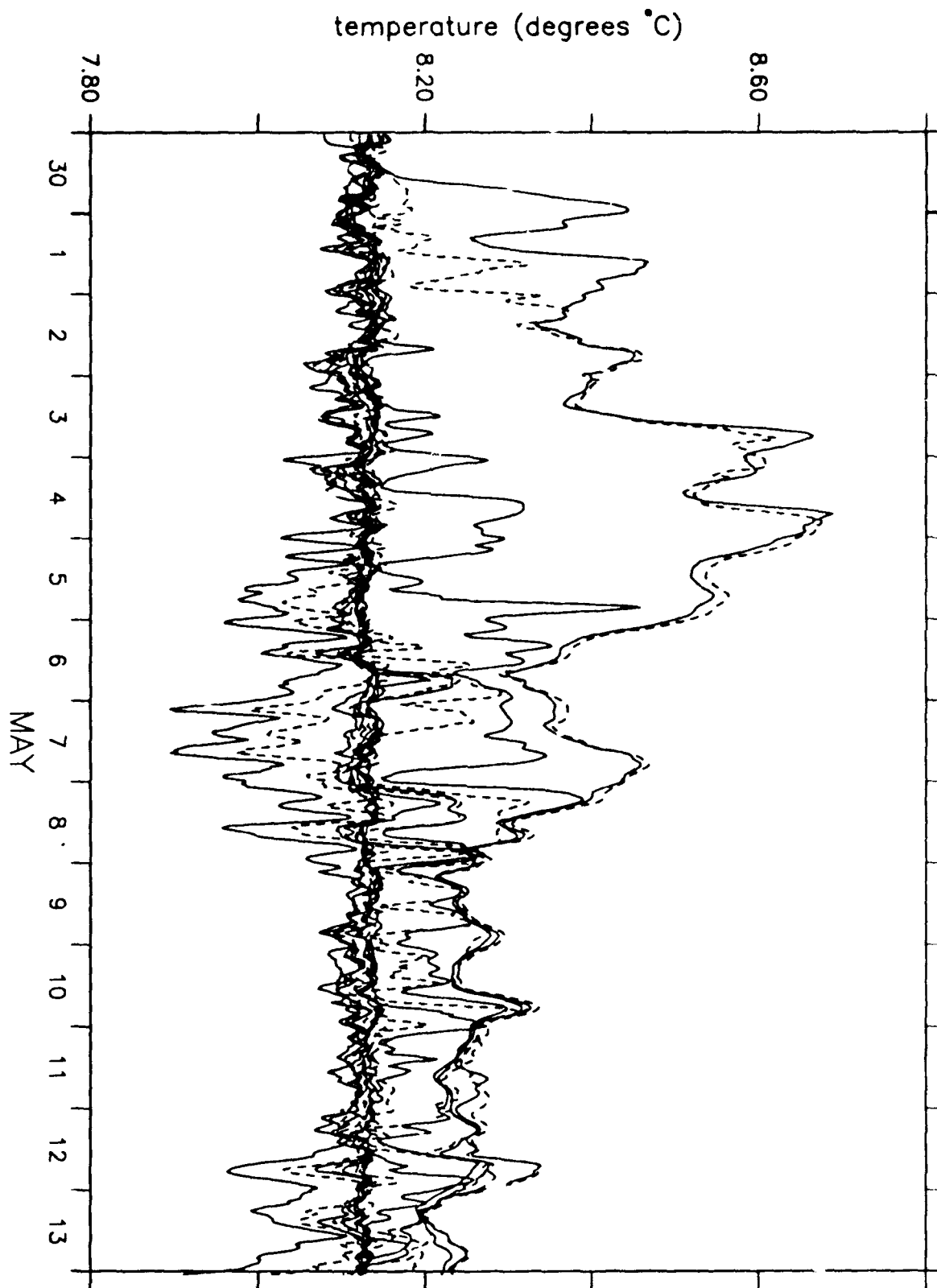


Figure 13a
Sub-surface temperature time series.

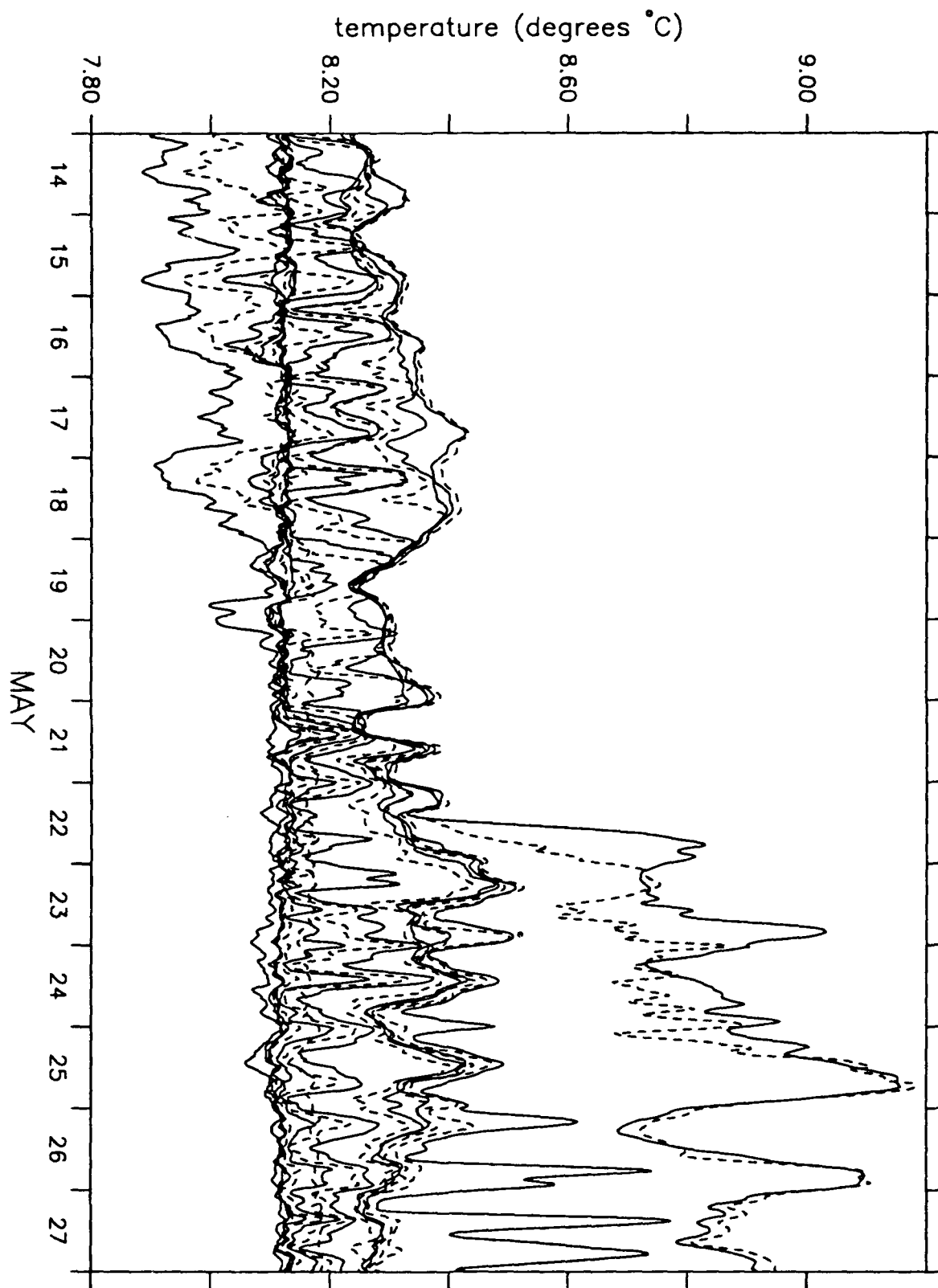


Figure 13b
Sub-surface temperature time series.

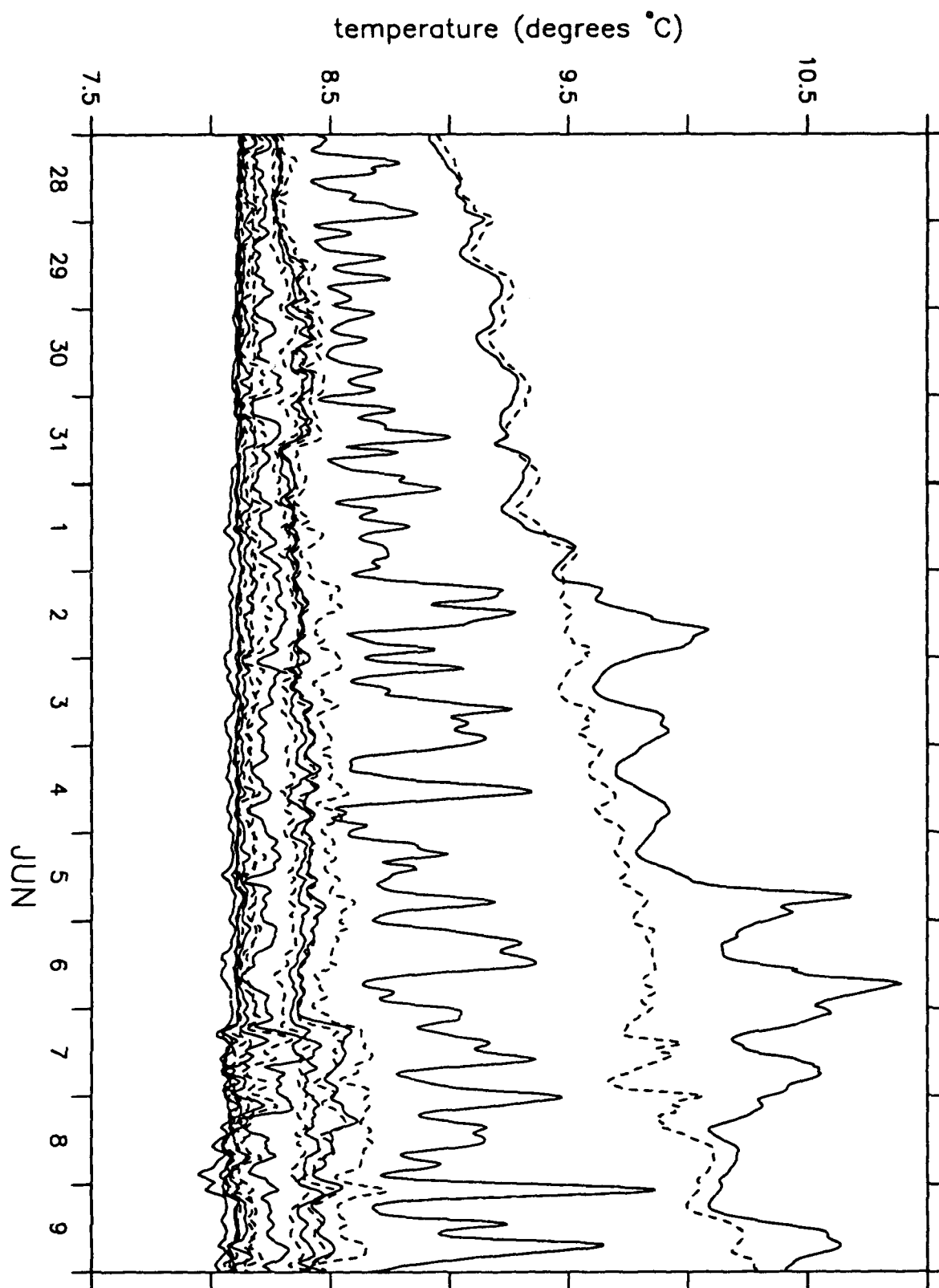


Figure 13c
Sub-surface temperature time series.

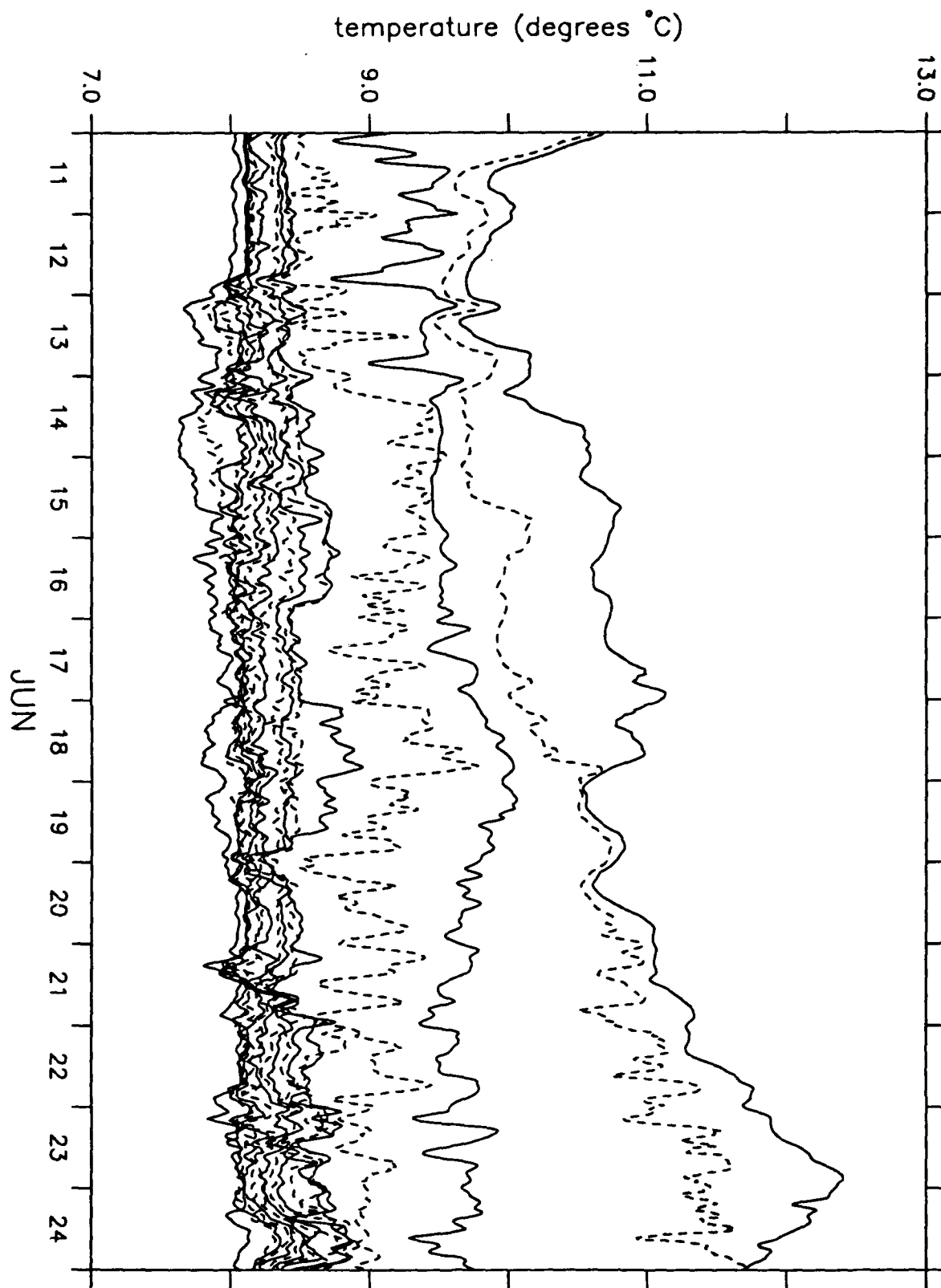


Figure 13d
Sub-surface temperature time series.

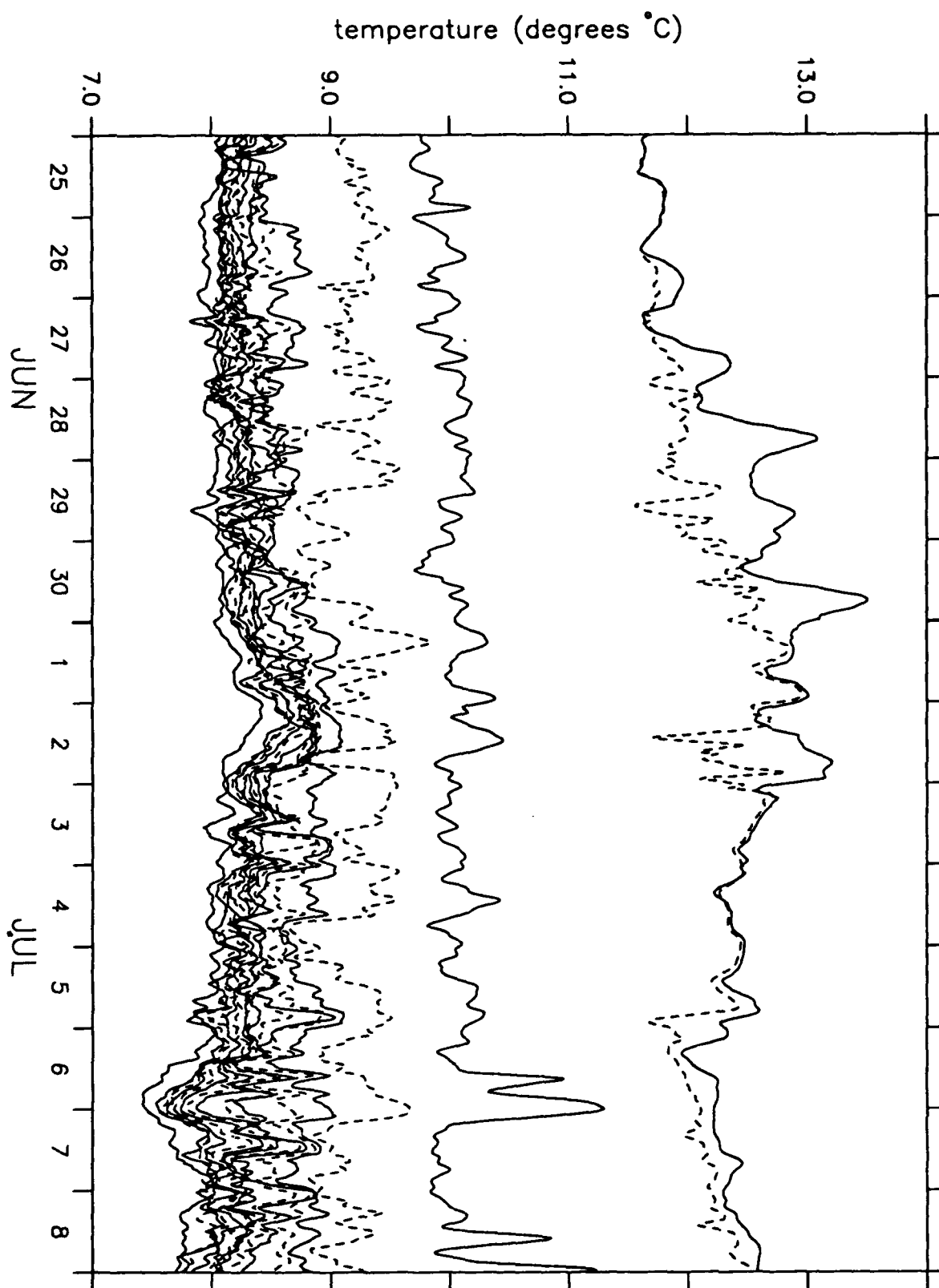


Figure 13e
Sub-surface temperature time series.

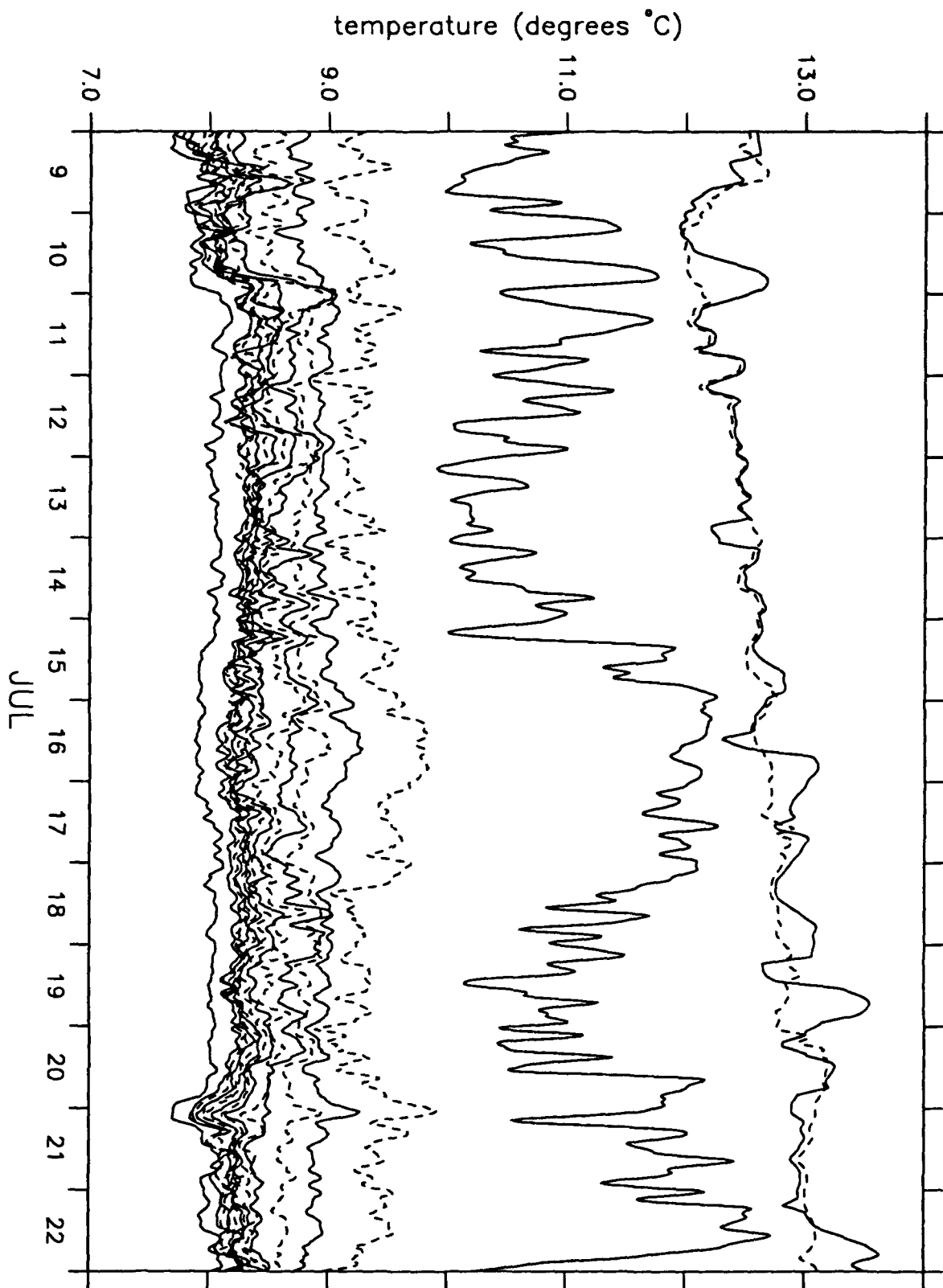


Figure 13f
Sub-surface temperature time series.

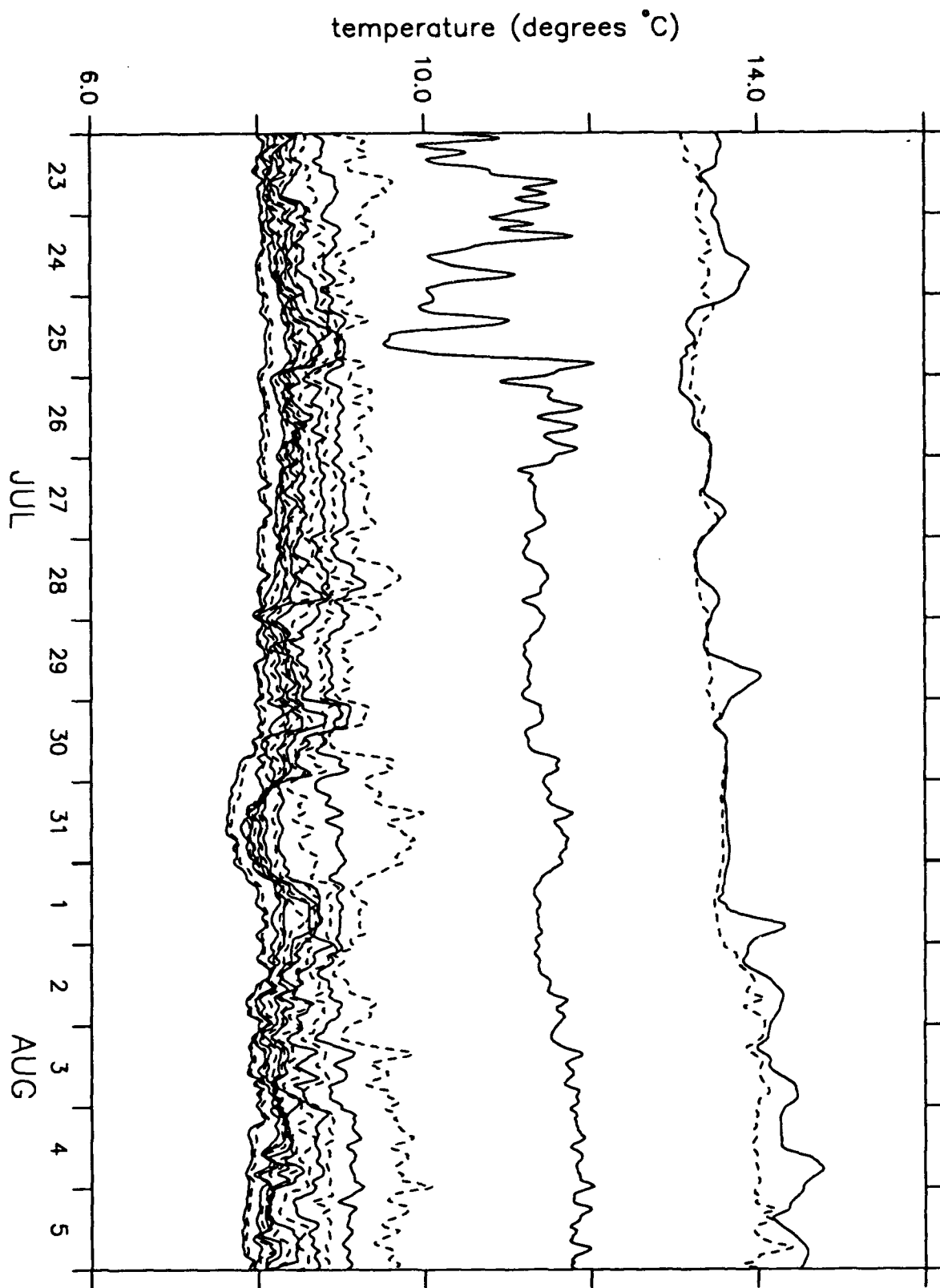


Figure 13g
Sub-surface temperature time series.

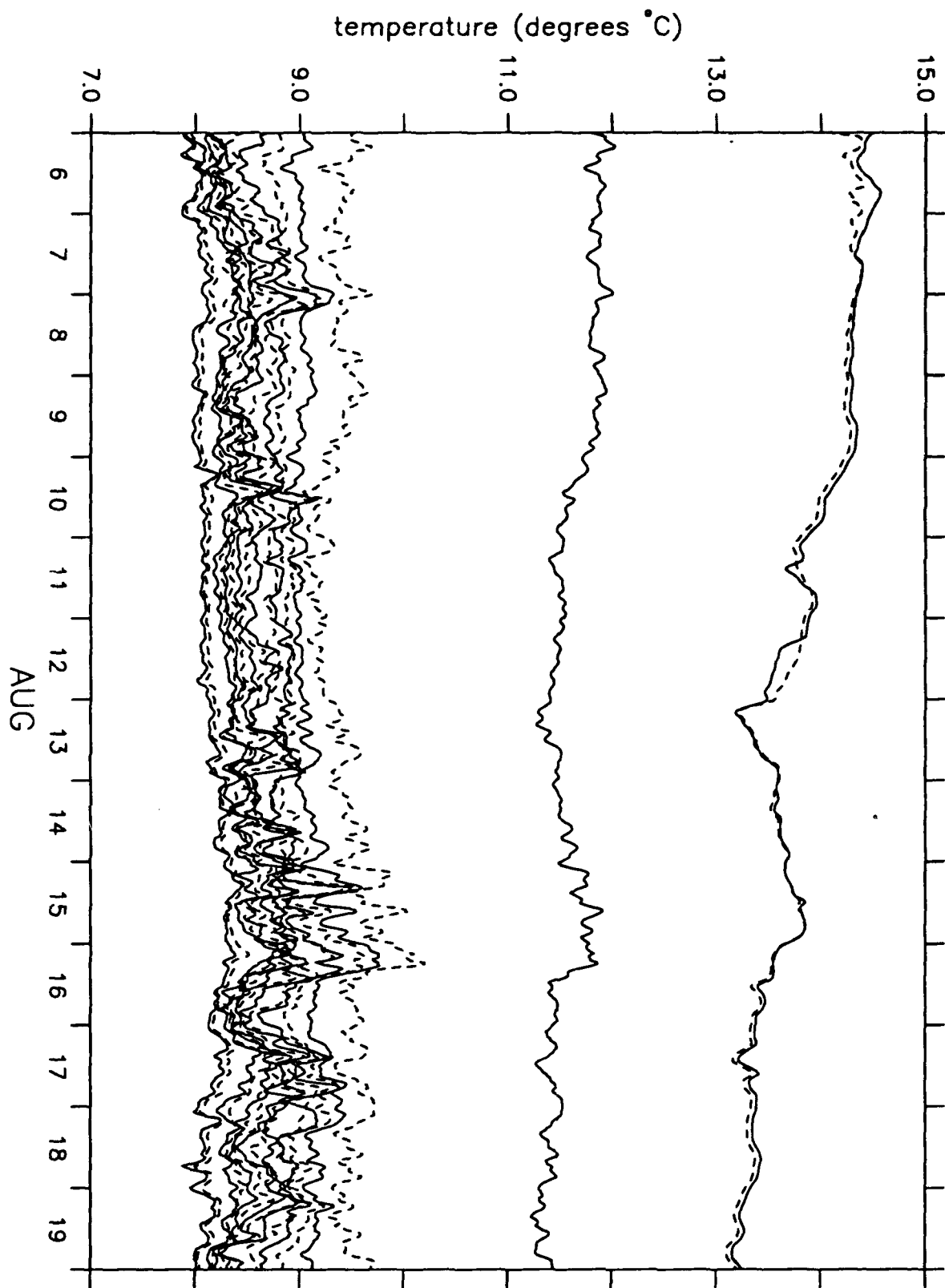


Figure 13h
Sub-surface temperature time series.

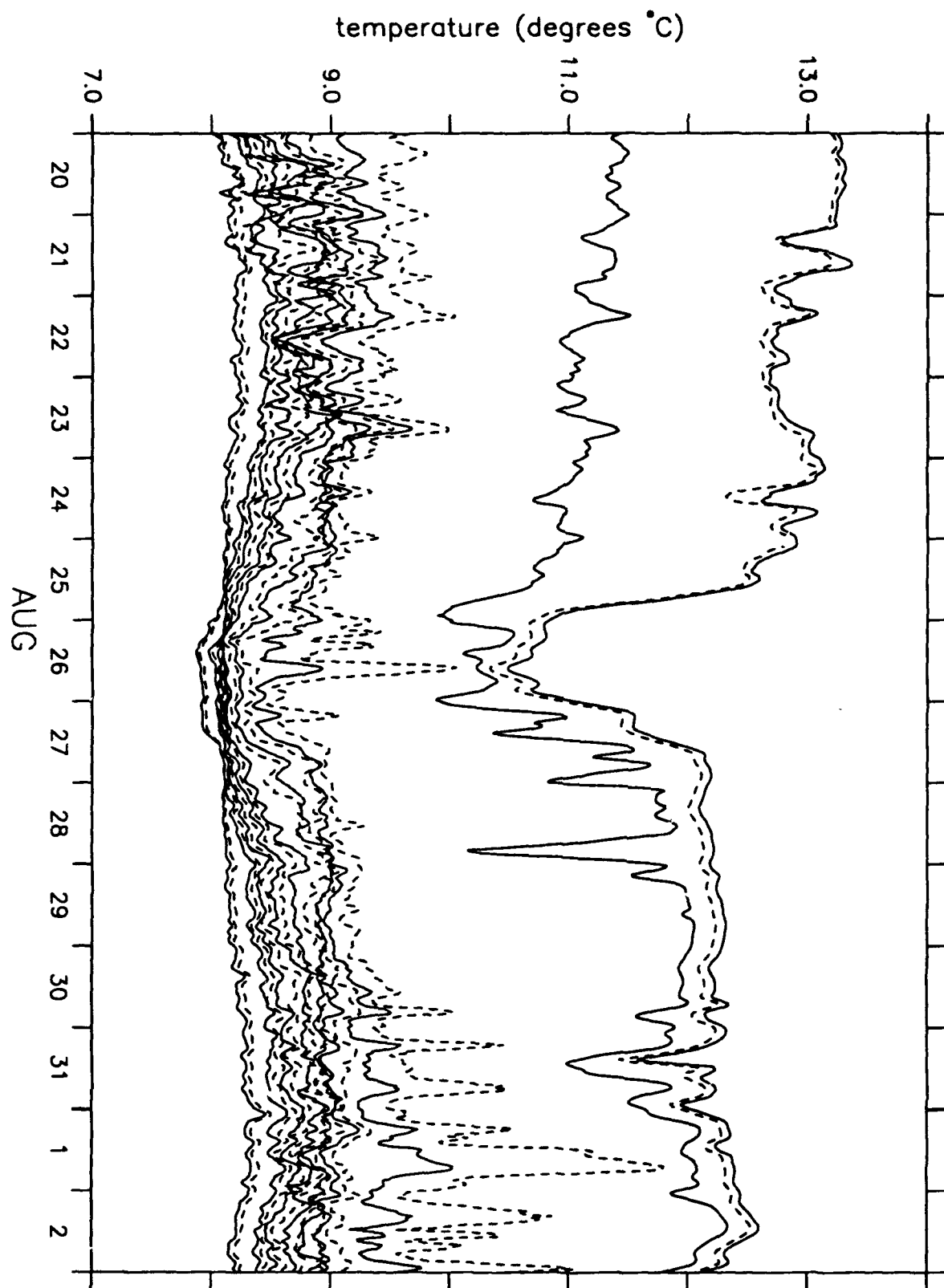


Figure 131
Sub-surface temperature time series.

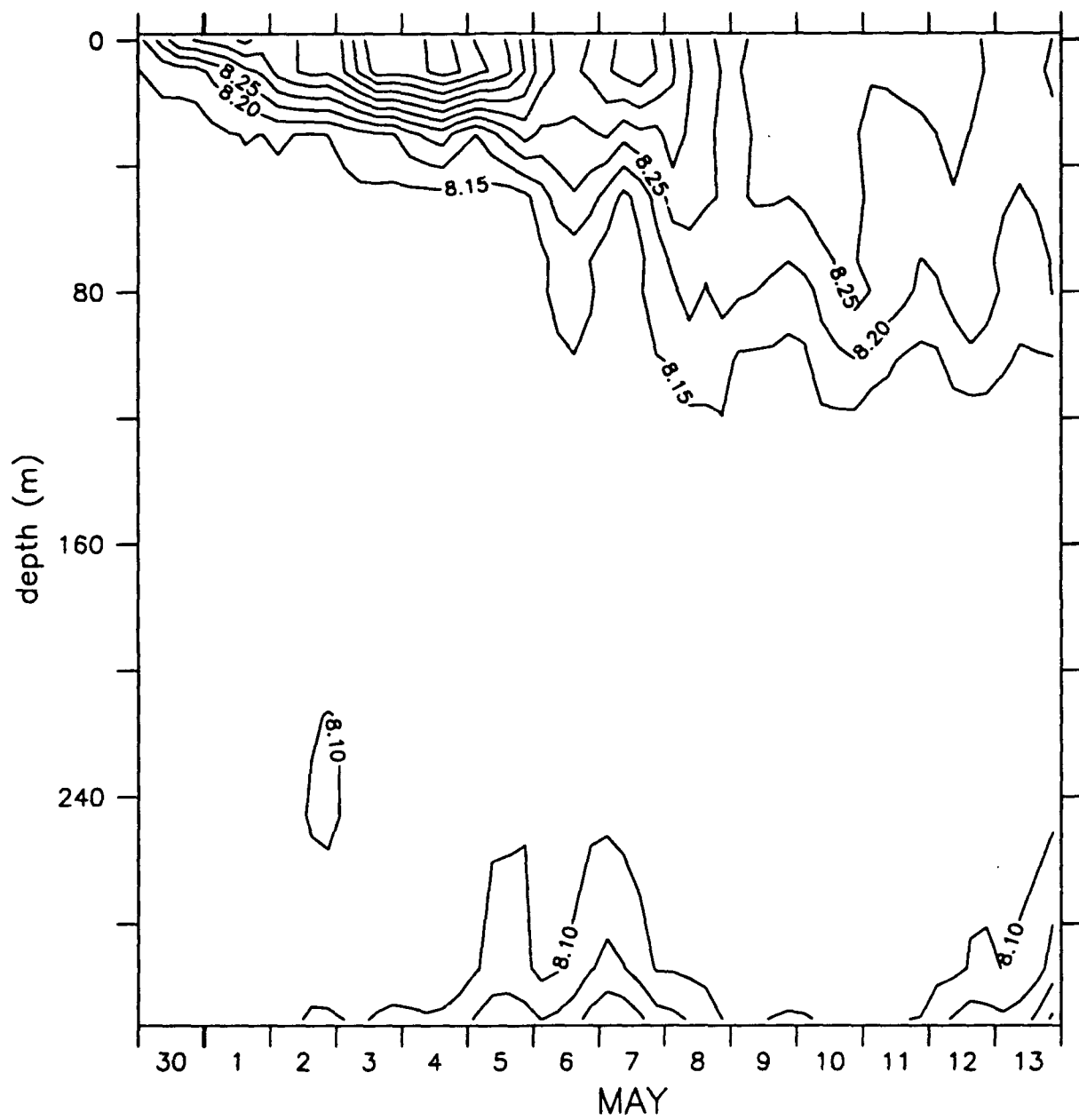


Figure 14a
Contours of sub-surface temperature.

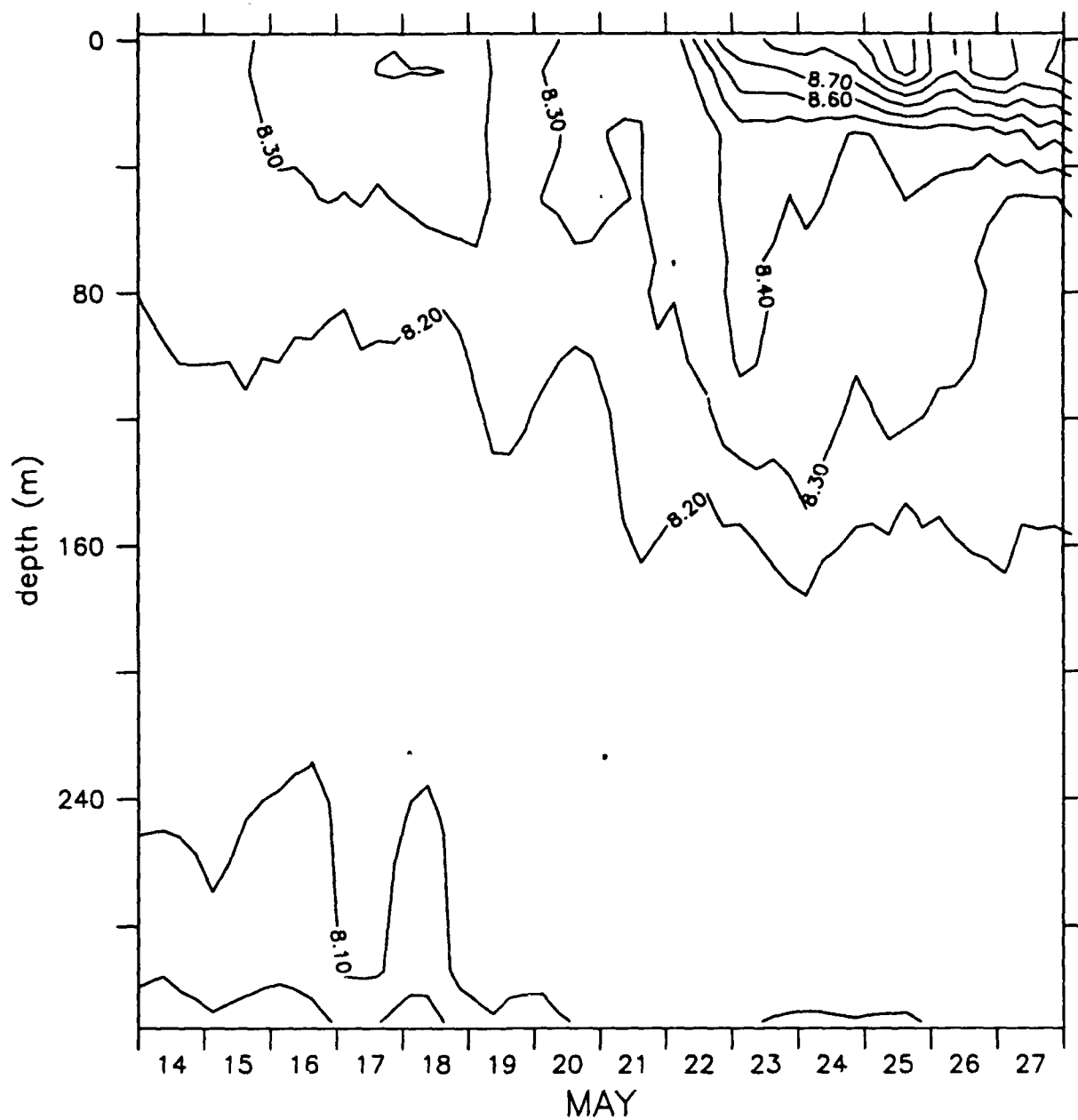


Figure 14b
Contours of sub-surface temperature.

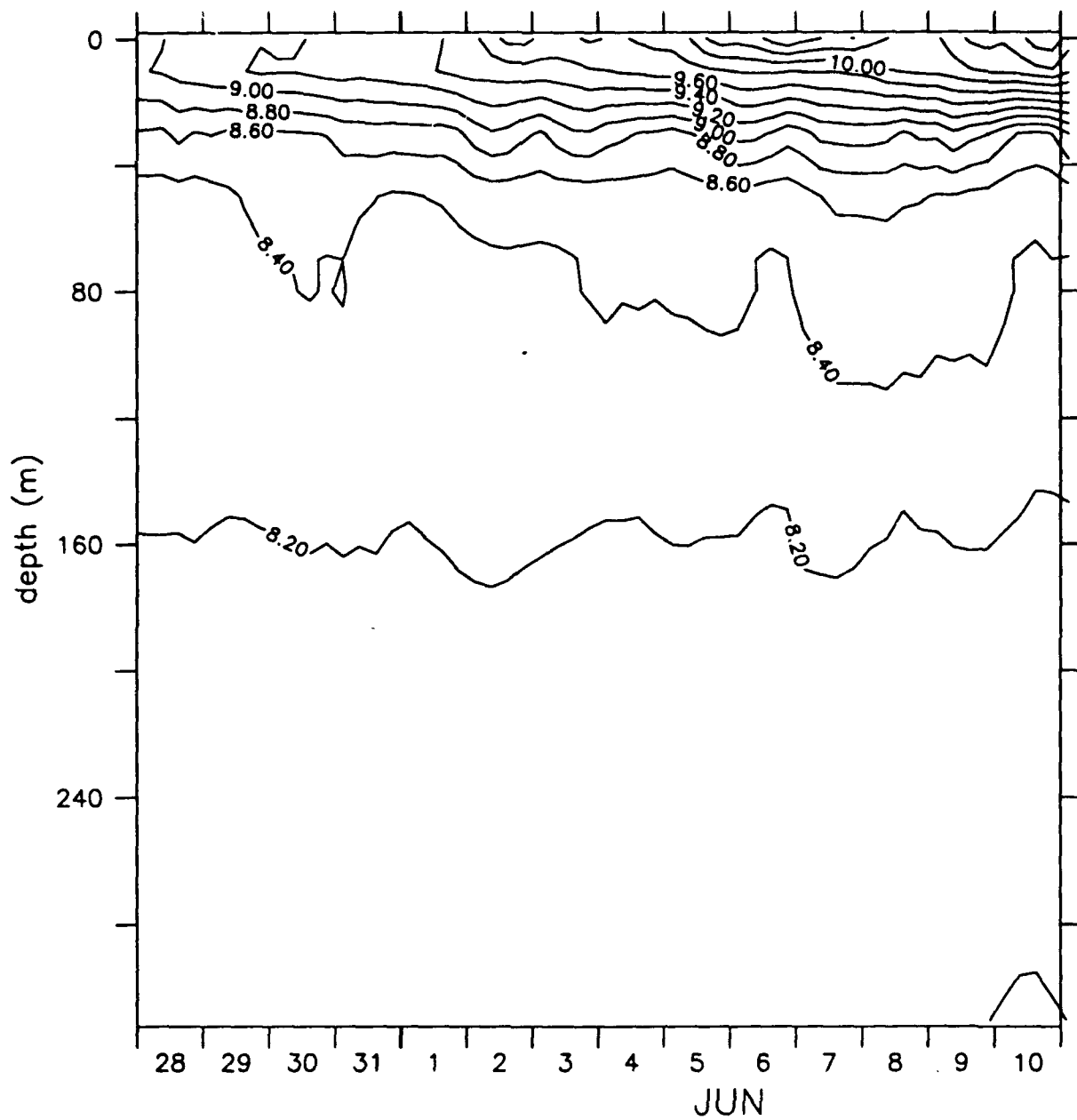


Figure 14c
Contours of sub-surface temperature.

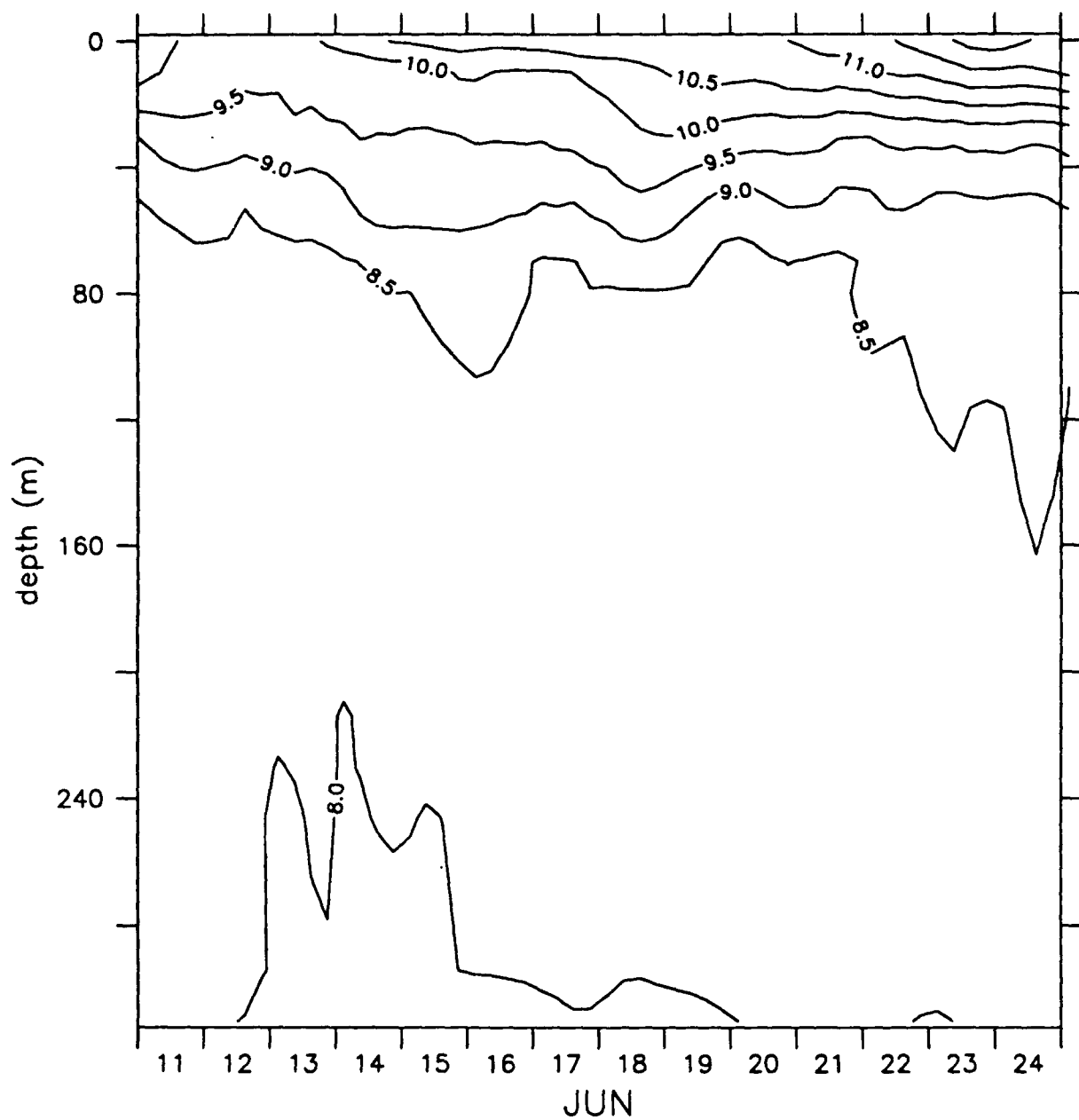


Figure 14d

Contours of sub-surface temperature.

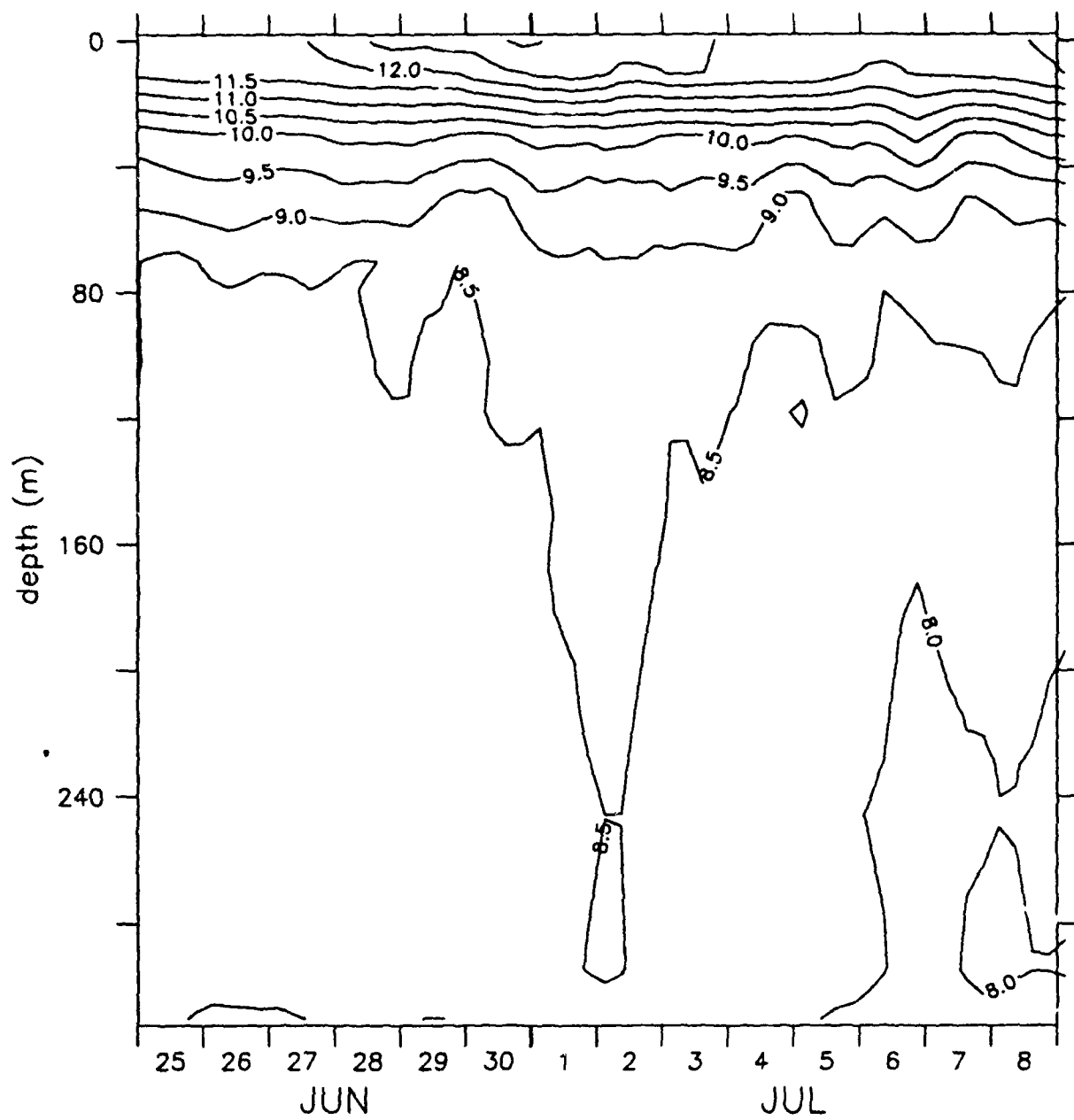


Figure 14e
Contours of sub-surface temperature.

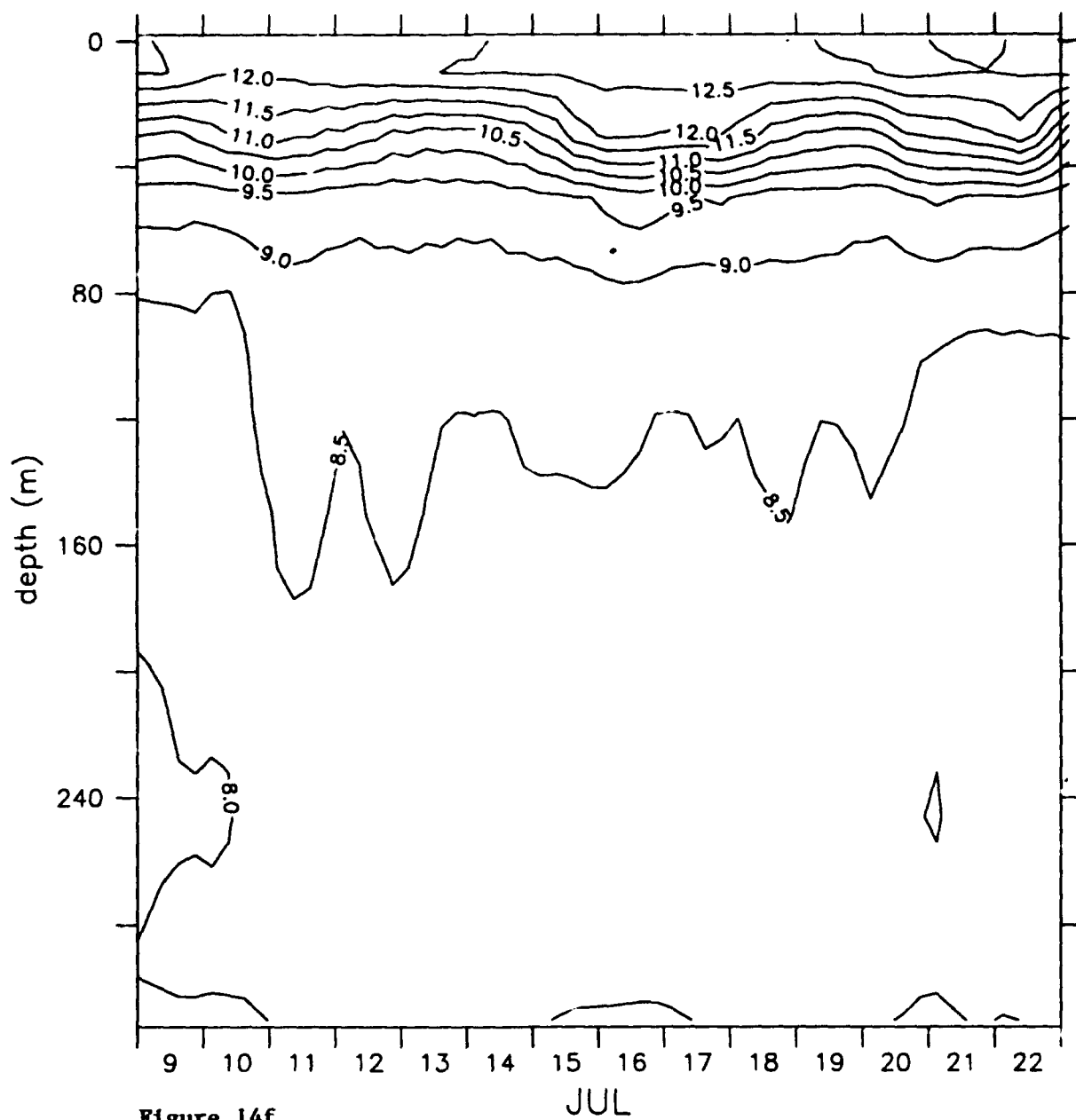


Figure 14f
Contours of sub-surface temperature.

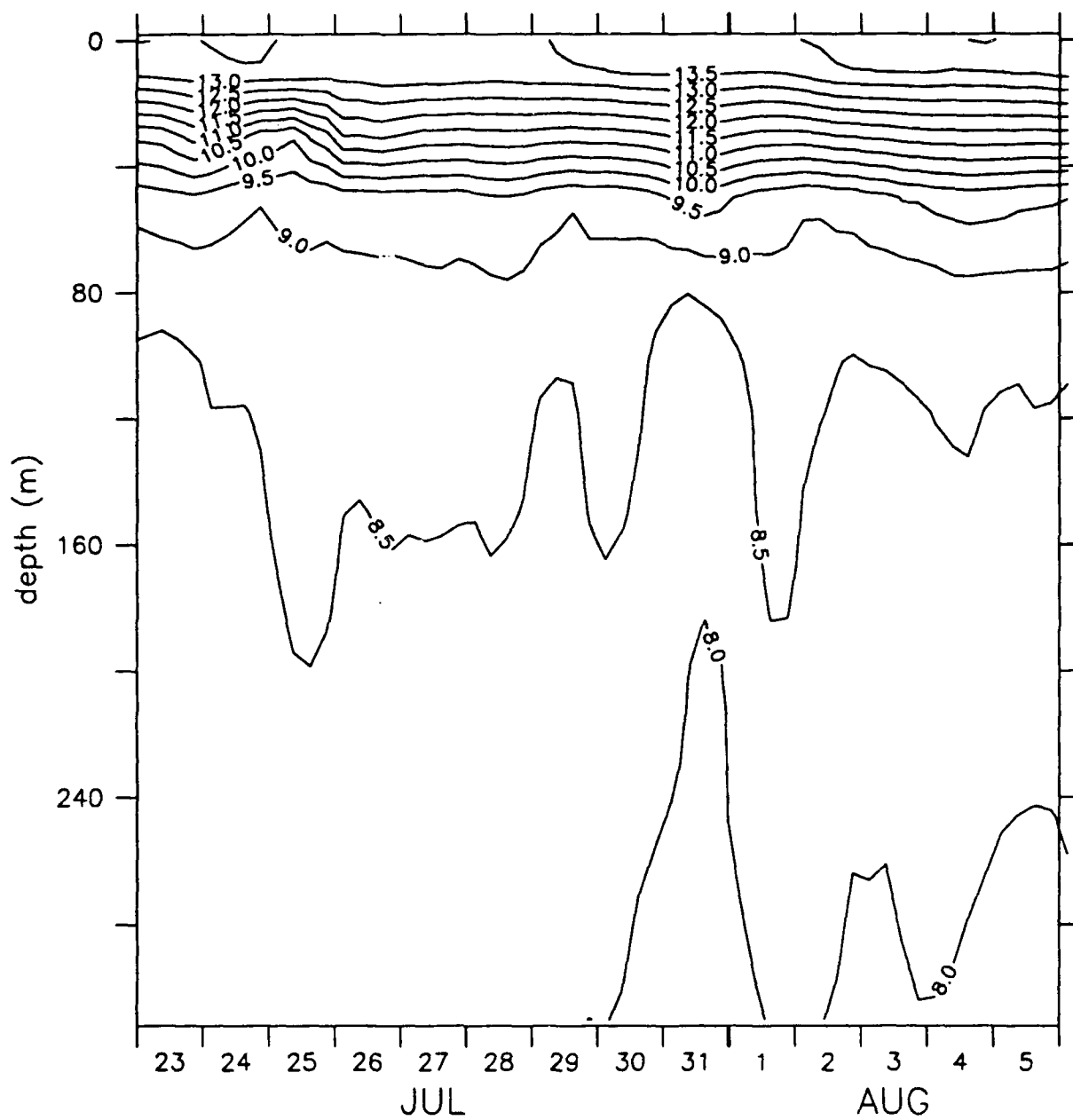


Figure 14g
Contours of sub-surface temperature.

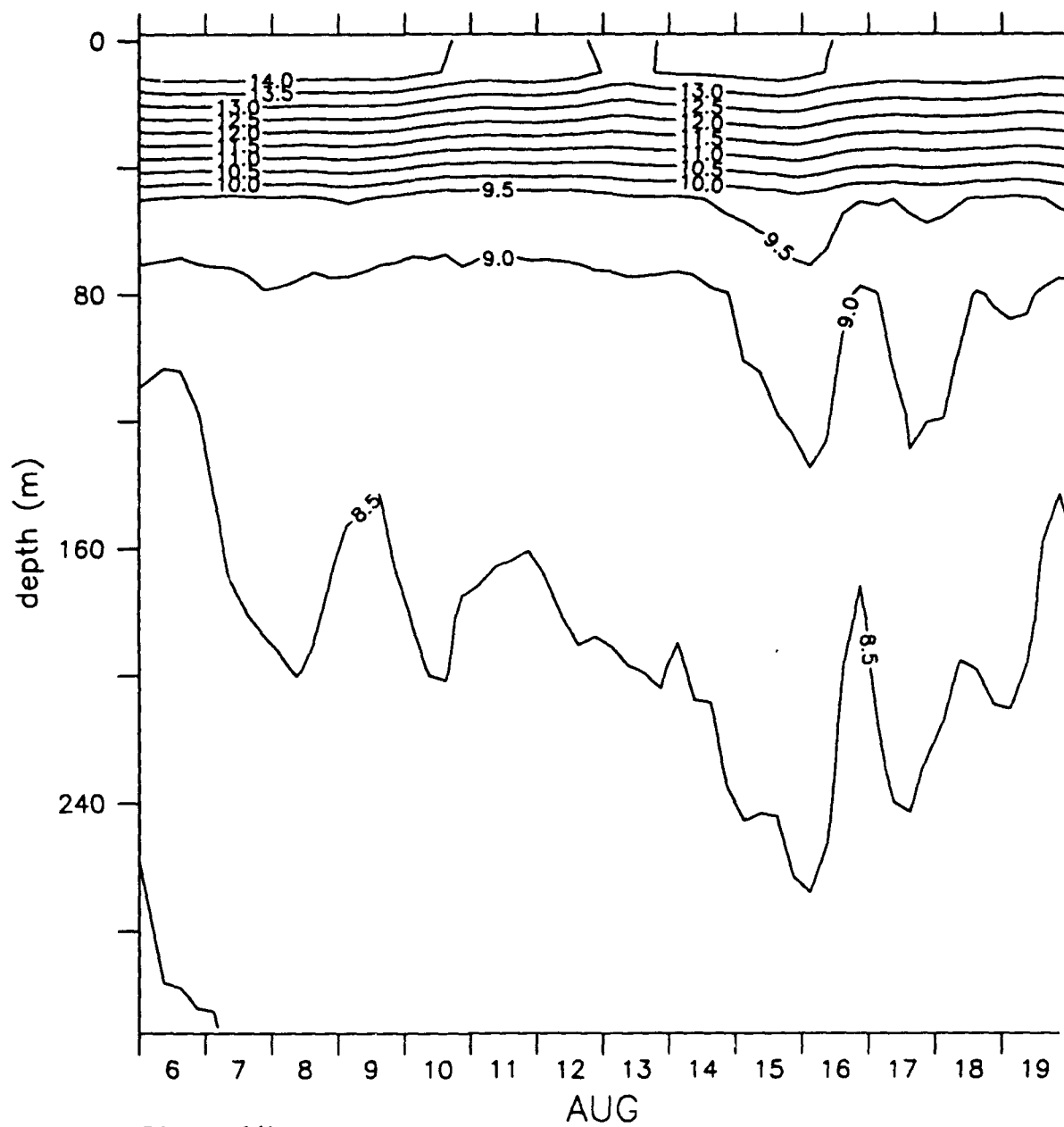


Figure 14h
Contours of sub-surface temperature.

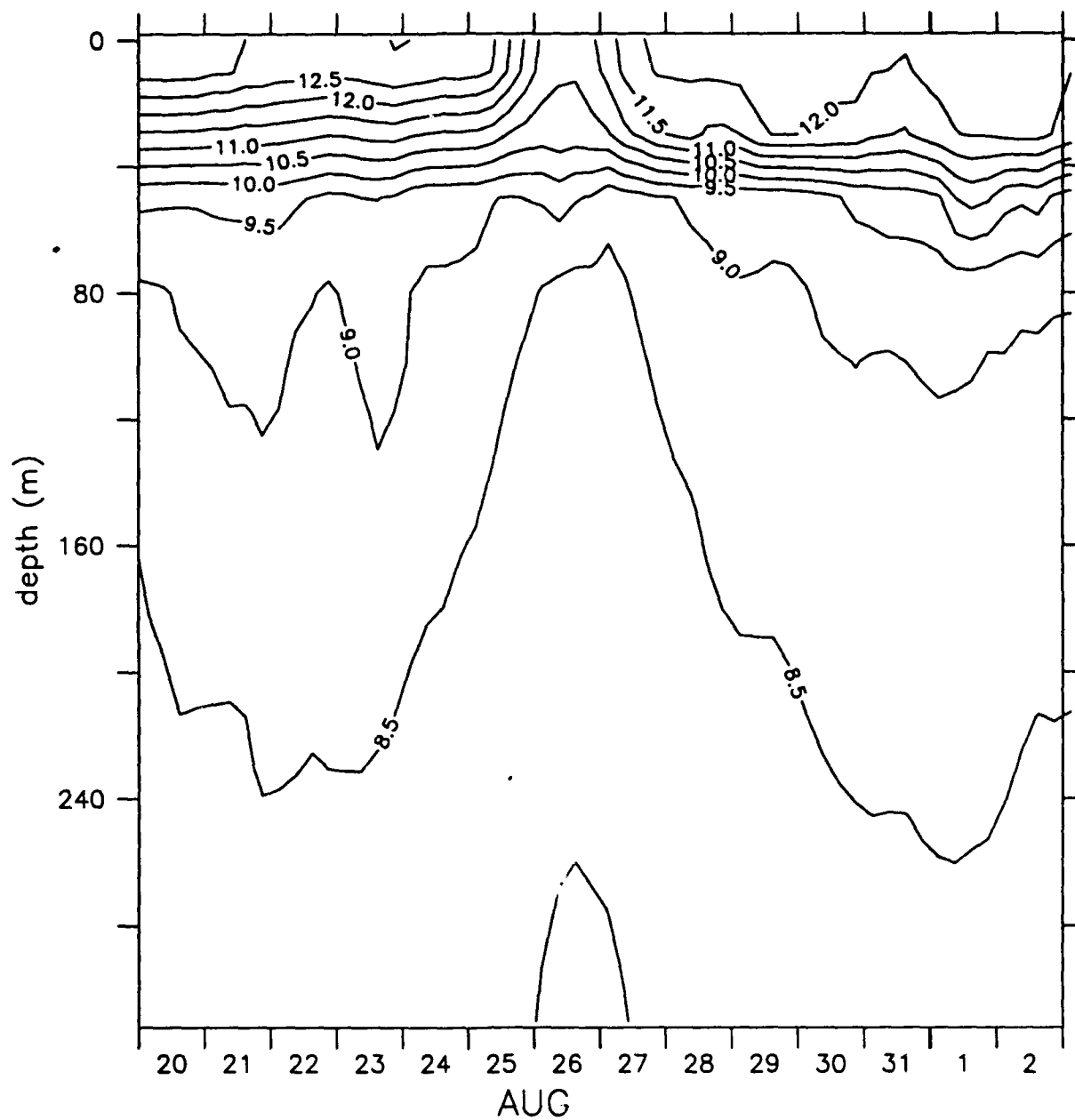


Figure 141
Contours of sub-surface temperature.

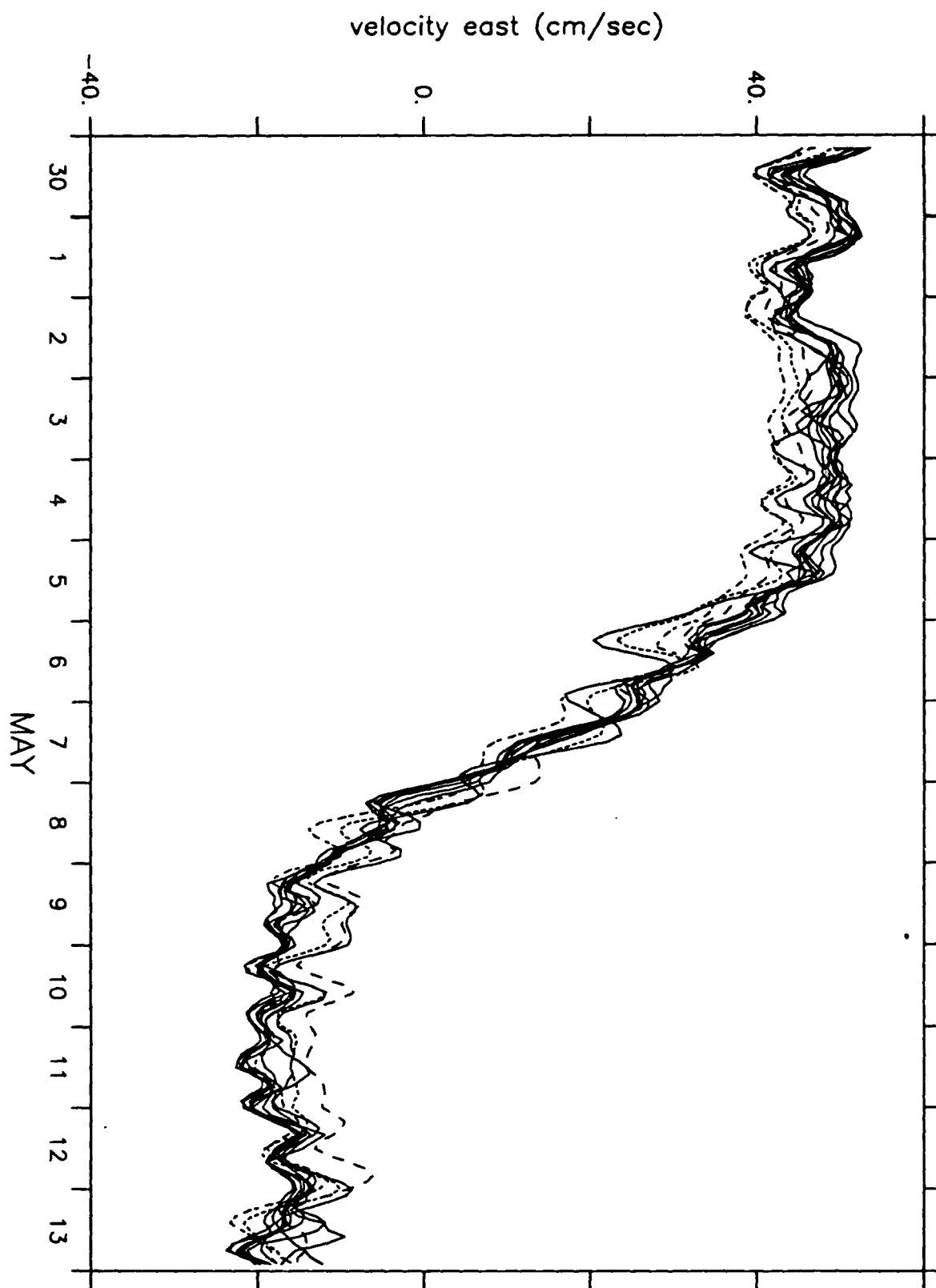


Figure 15a
Velocity time series, East component.

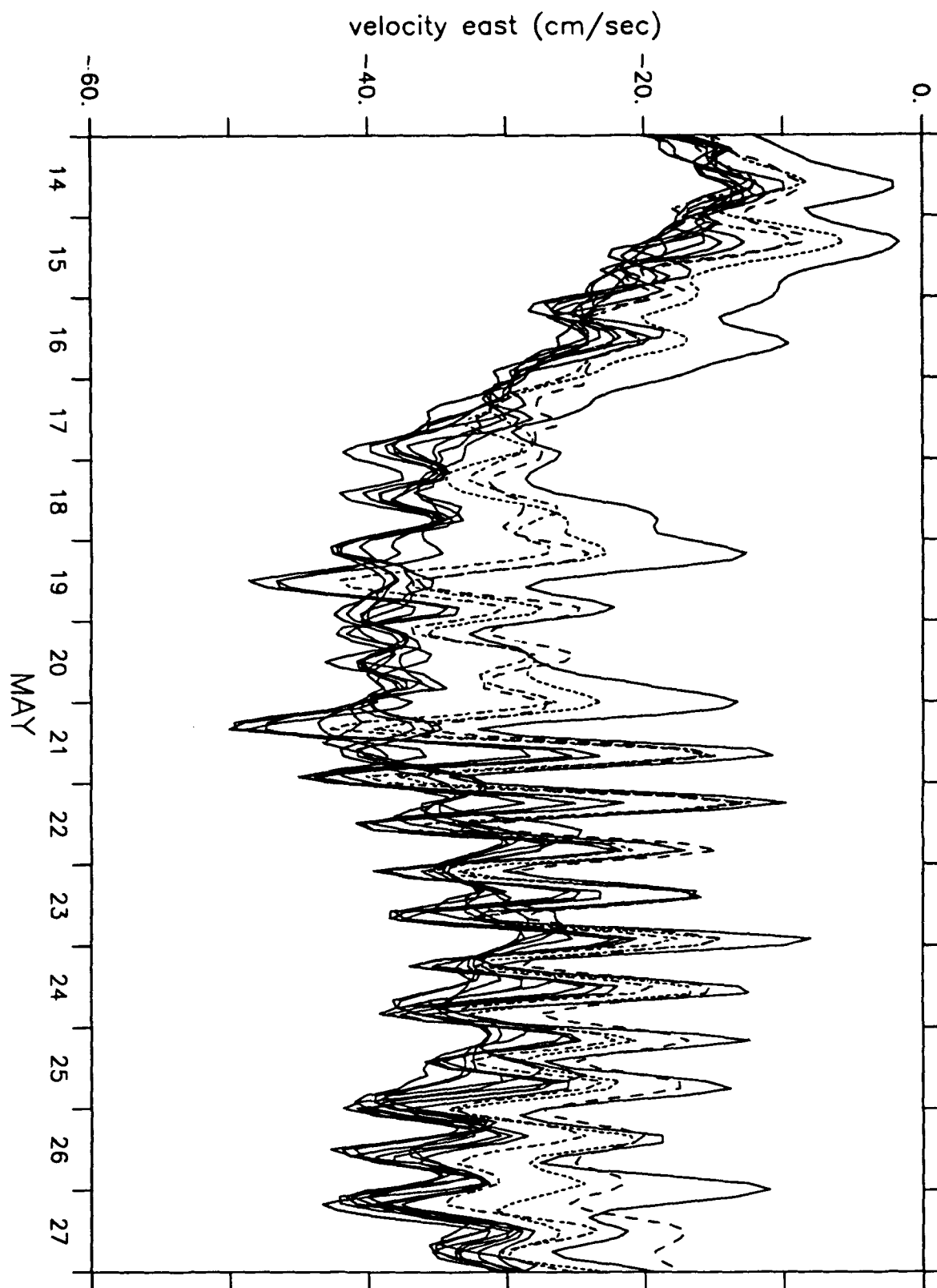


Figure 15b
Velocity time series, East component.

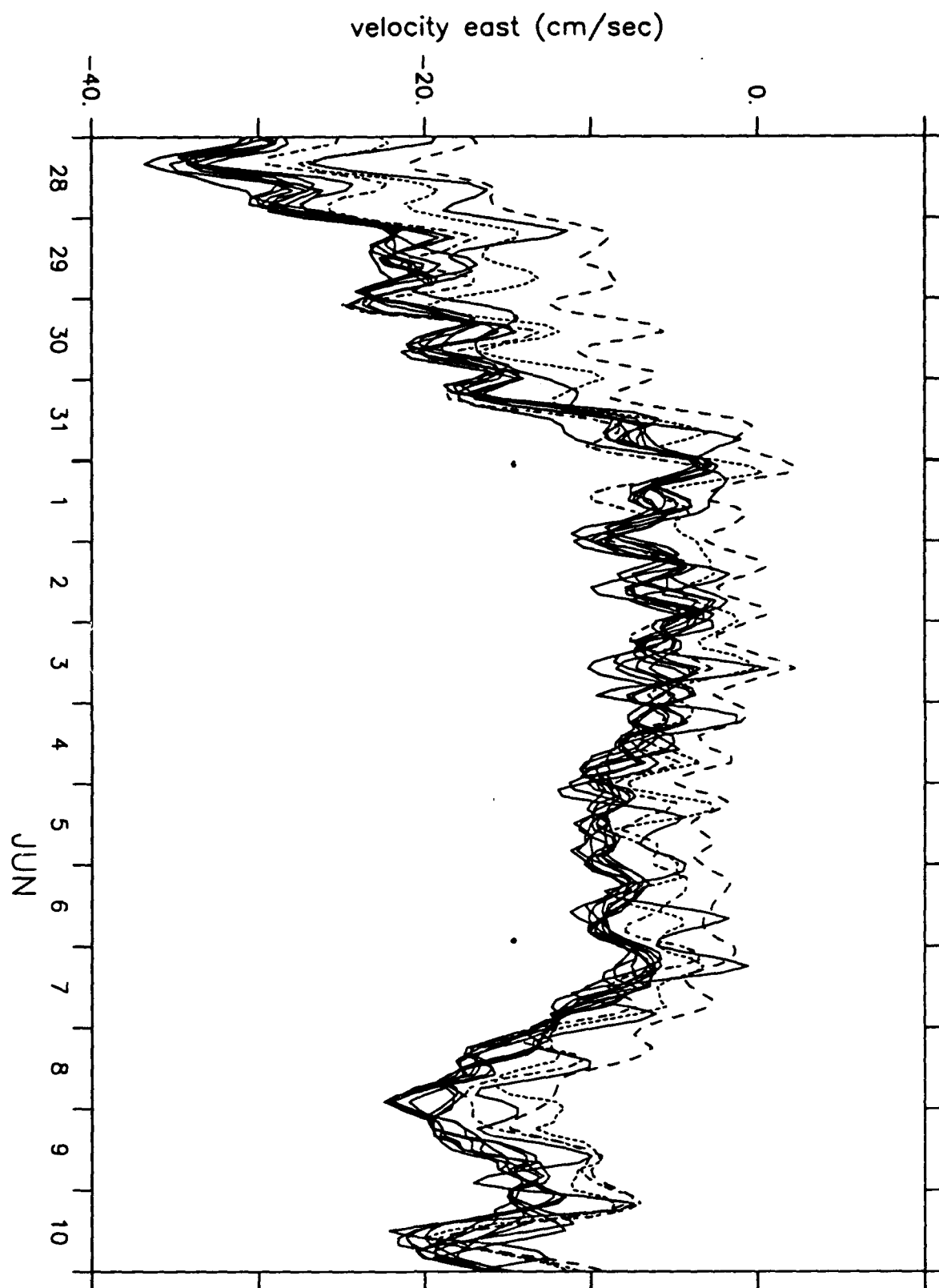


Figure 15c
Velocity time series, East component.

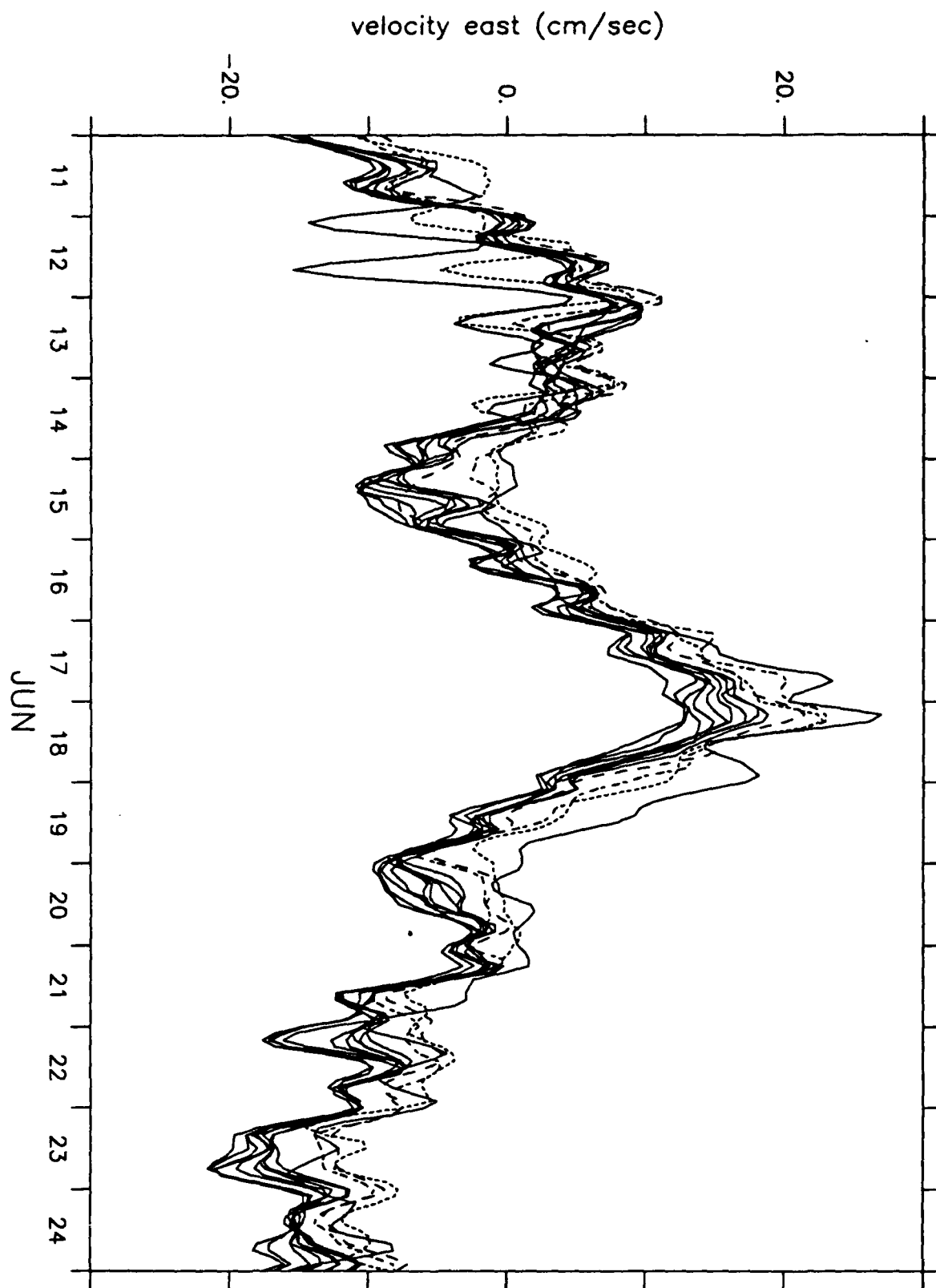


Figure 15d
Velocity time series, East component.

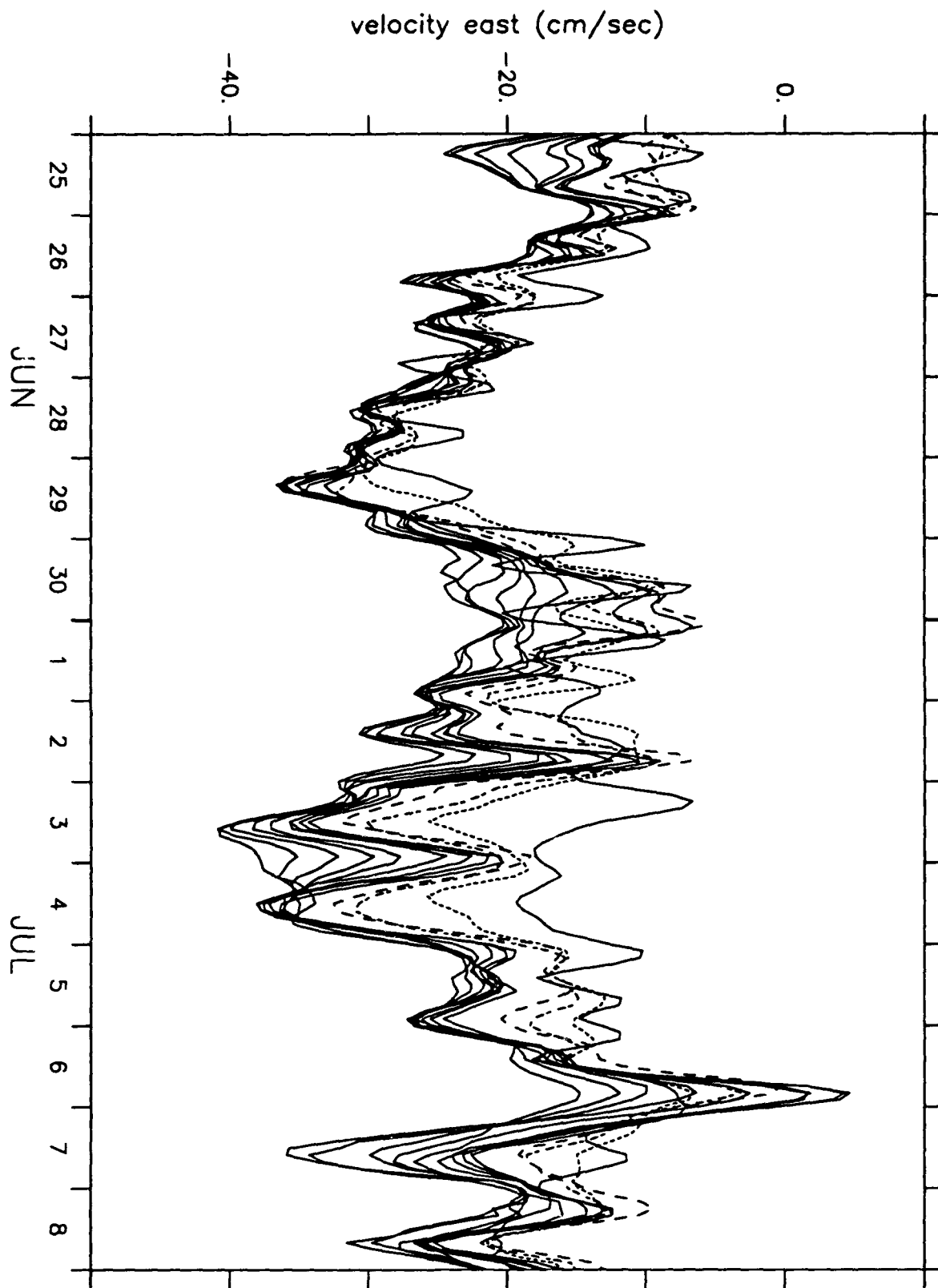


Figure 15e
Velocity time series, East component.

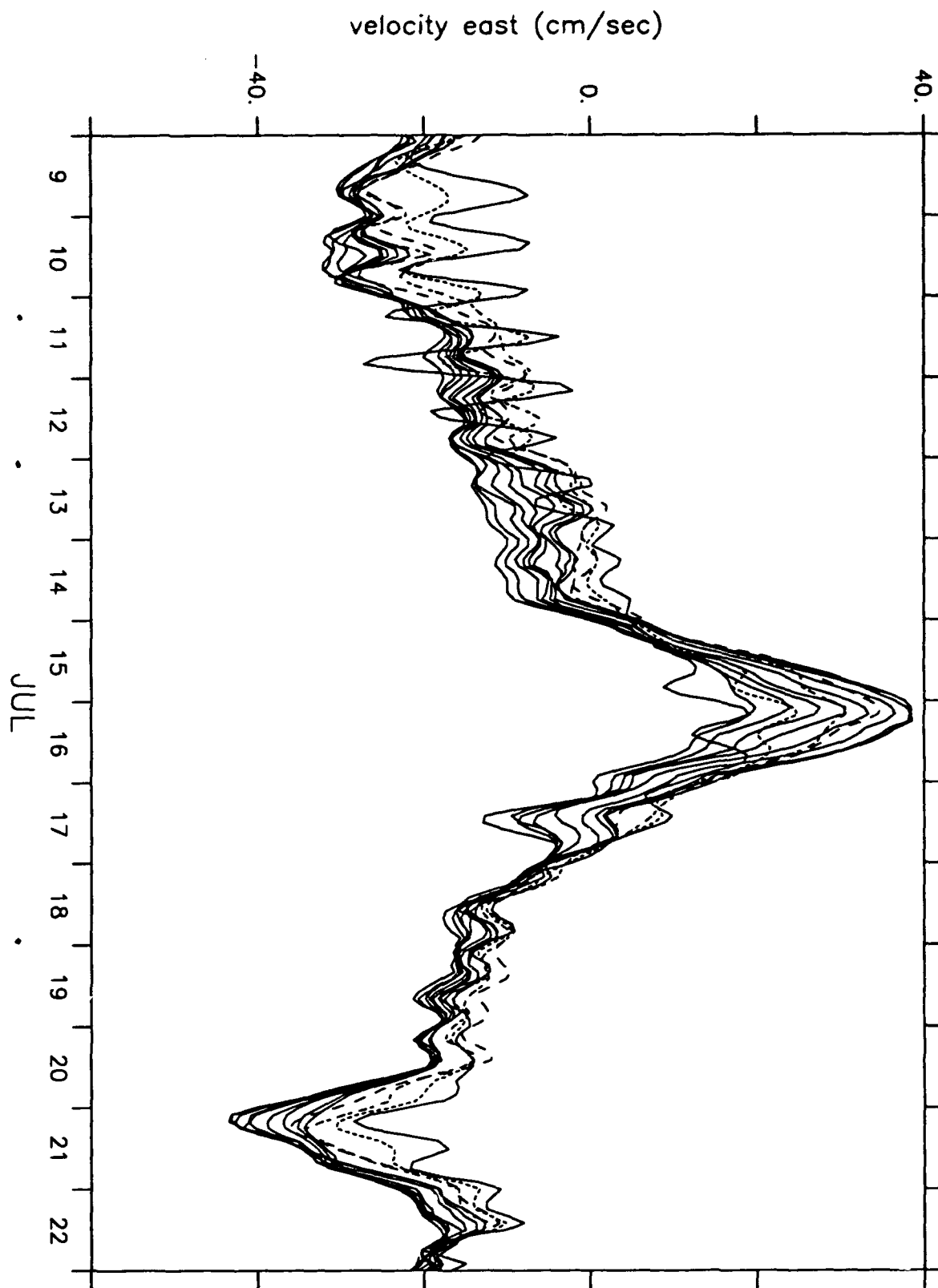


Figure 15f
Velocity time series, East component.

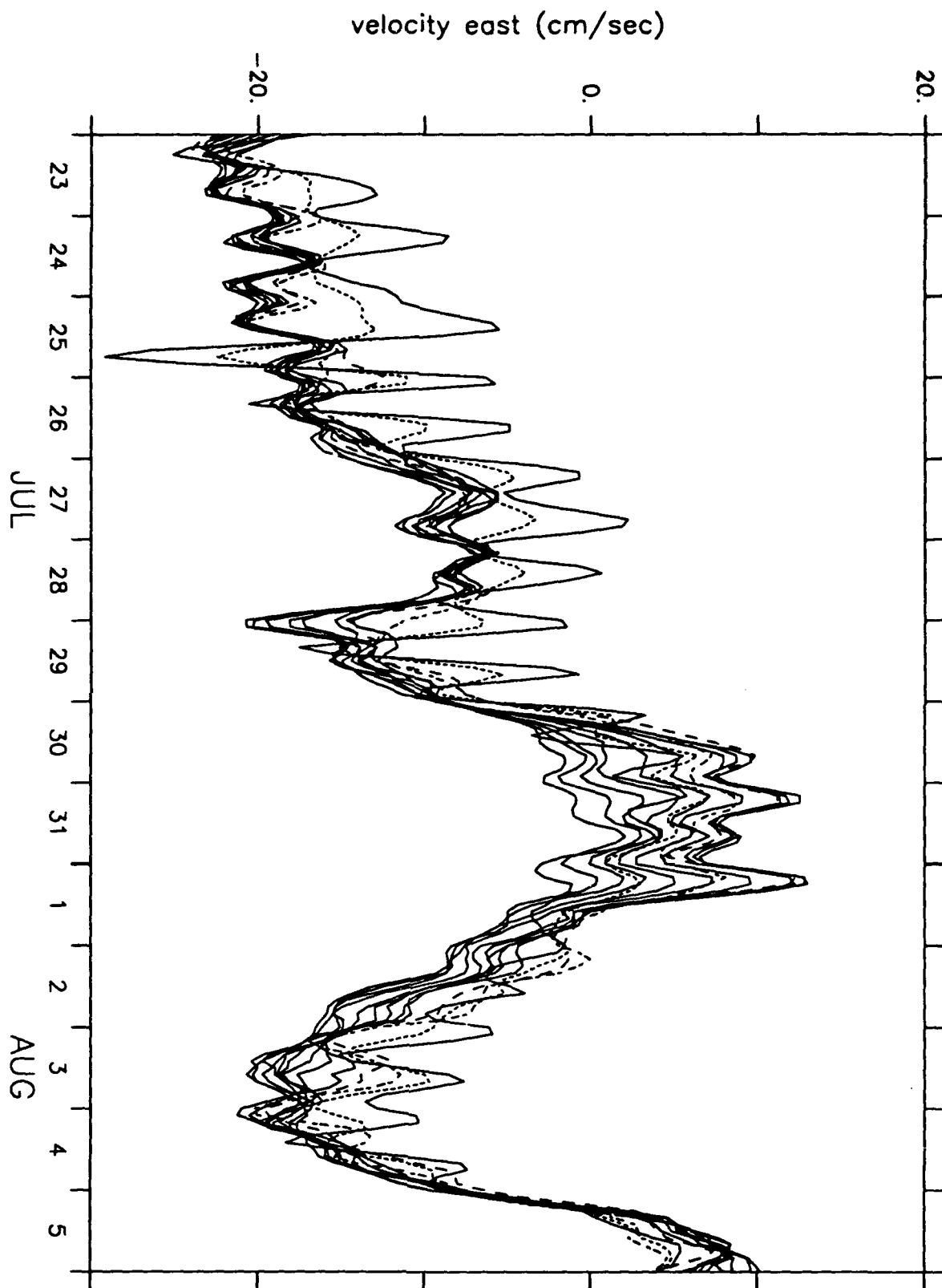


Figure 15g
Velocity time series, East component.

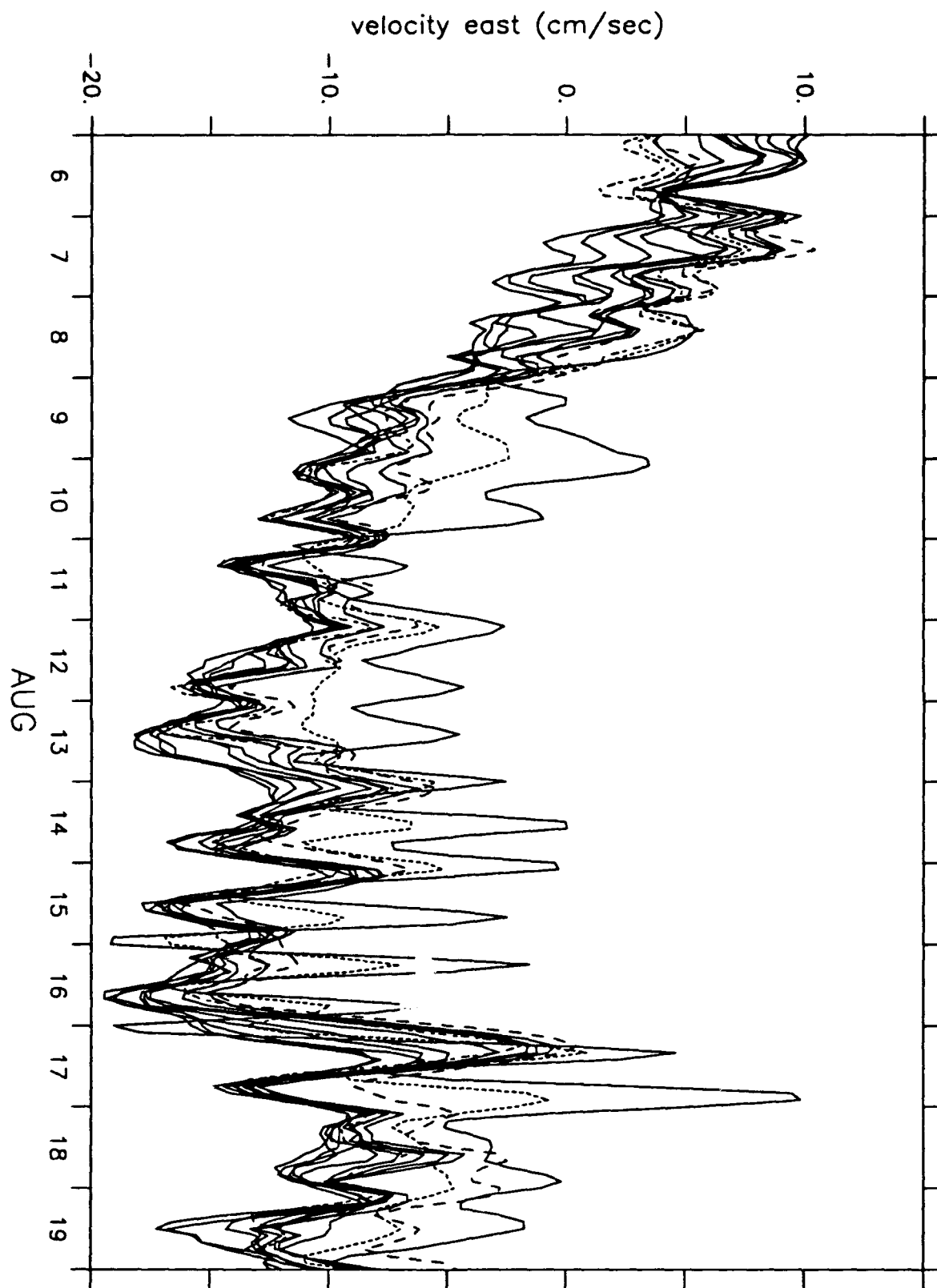


Figure 15h
Velocity time series, East component.

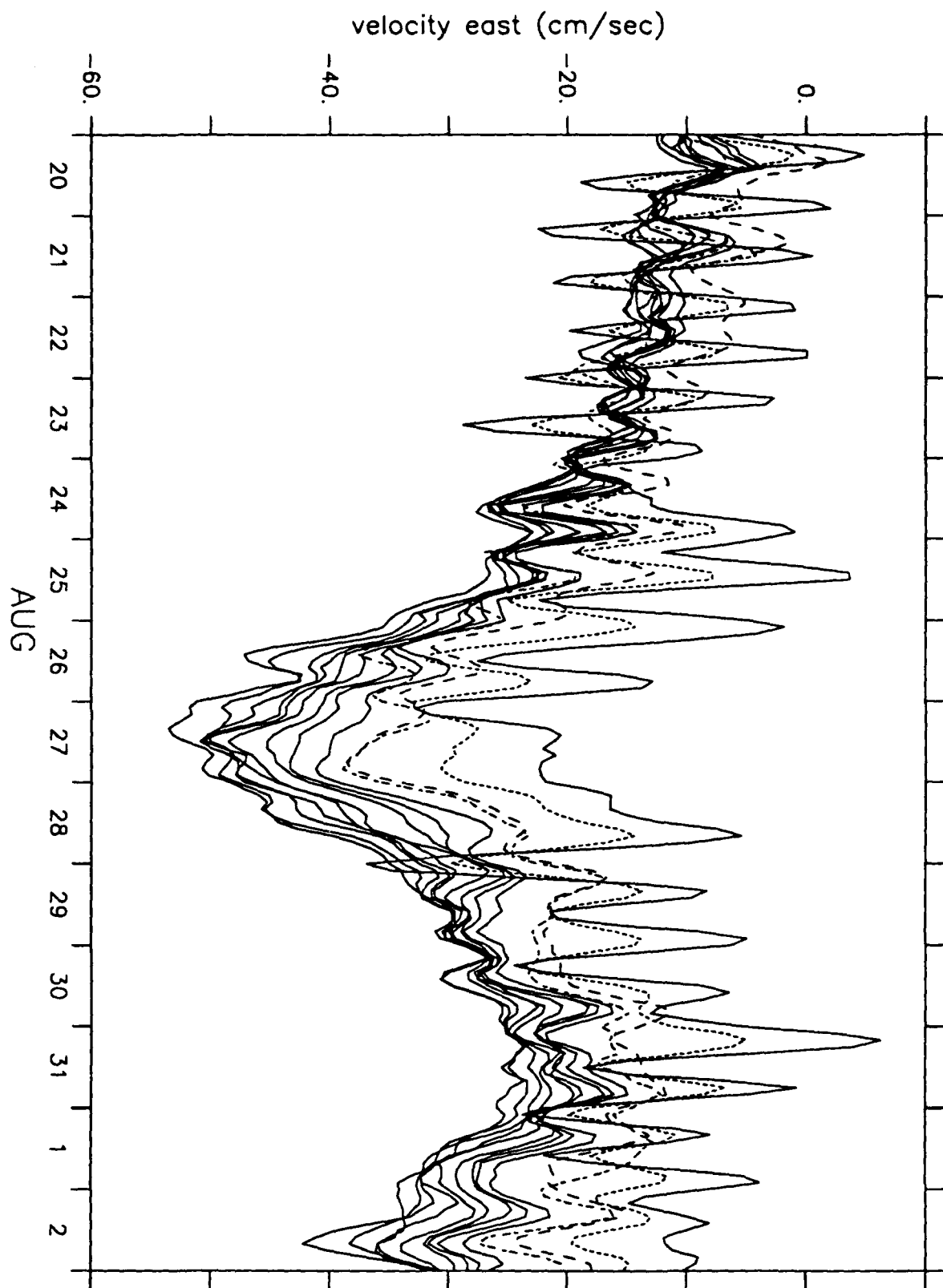


Figure 151
Velocity time series, East component.

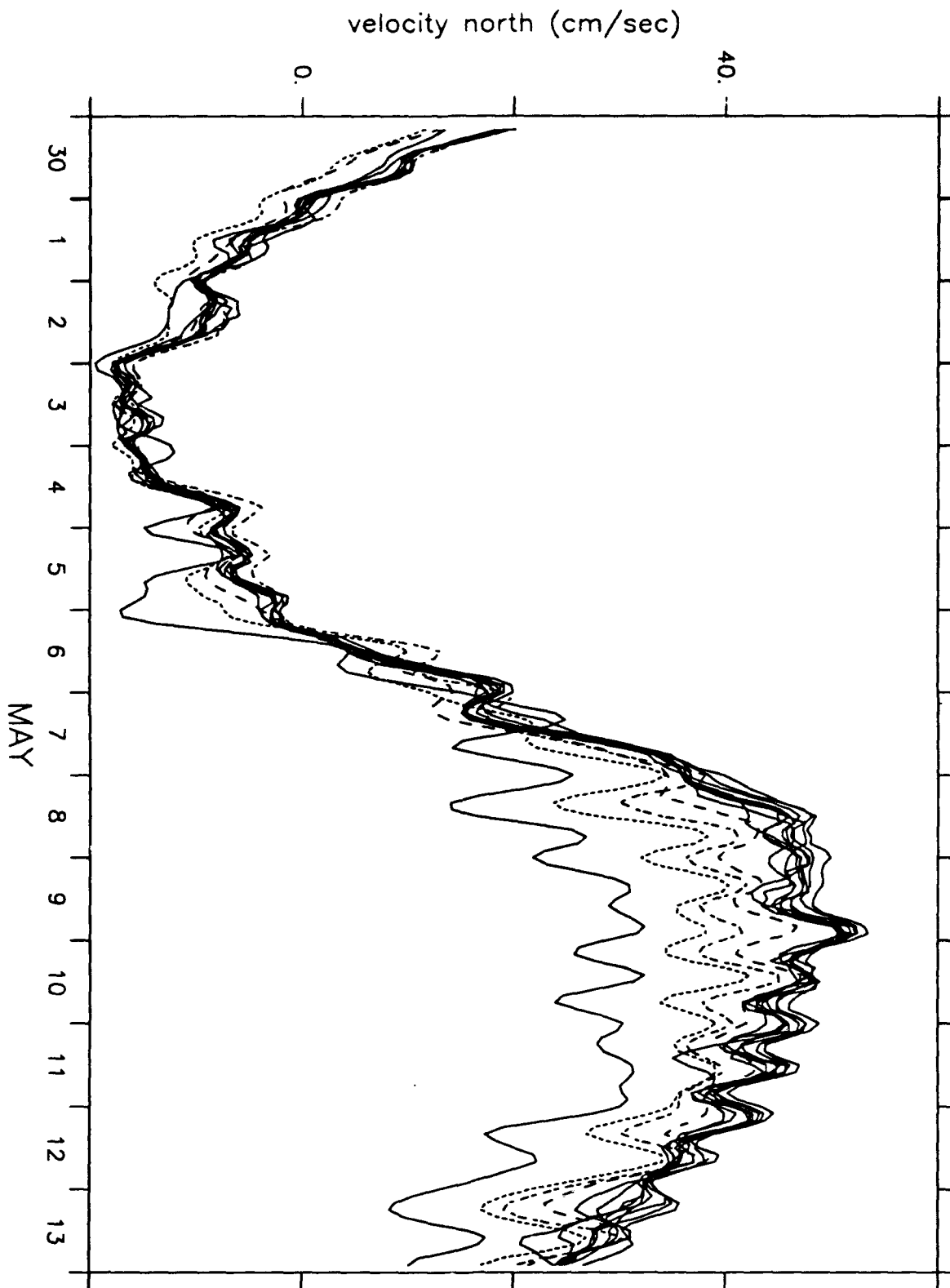


Figure 16a
Velocity time series, North component.

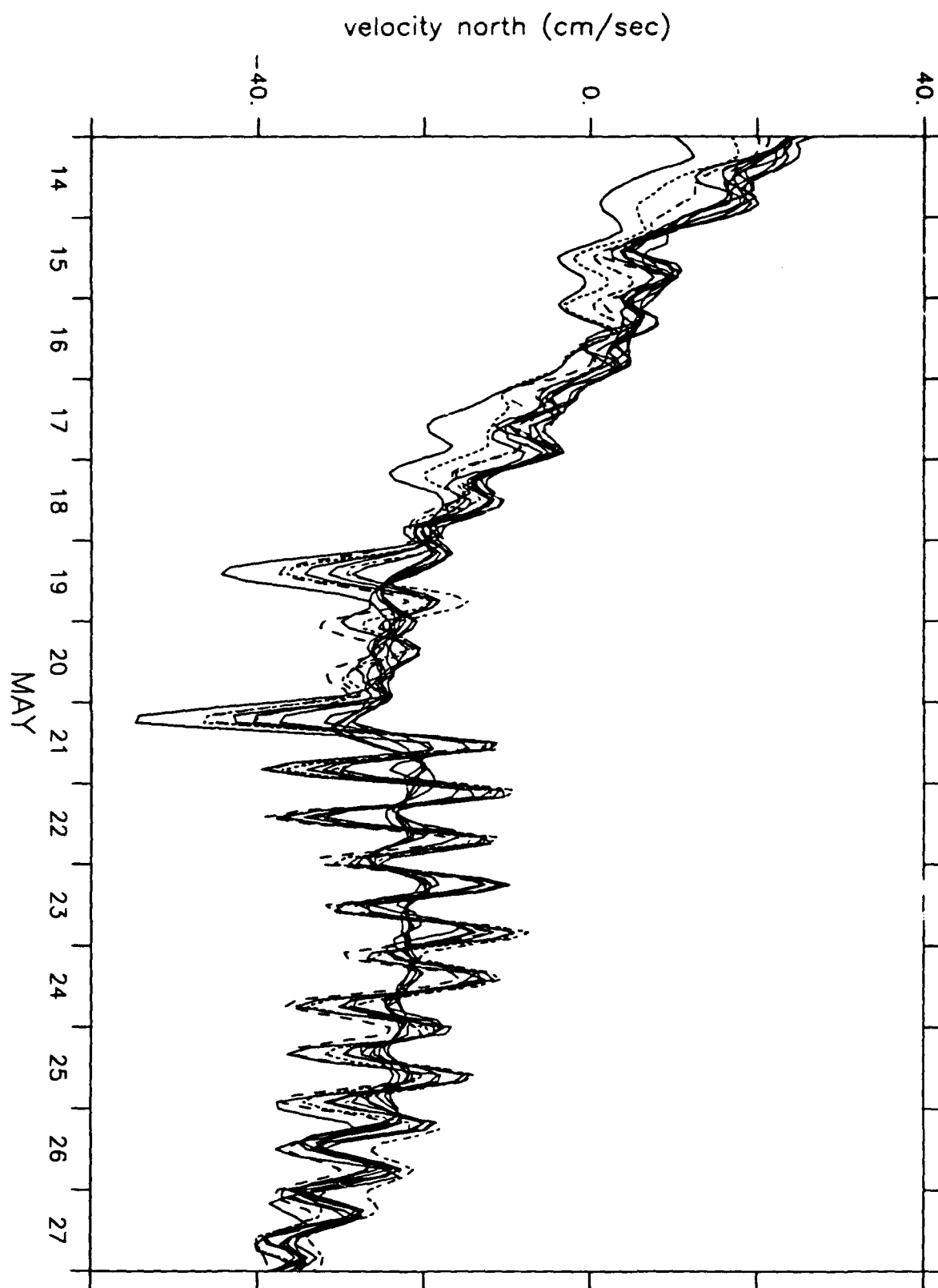


Figure 16b
Velocity time series, North component.

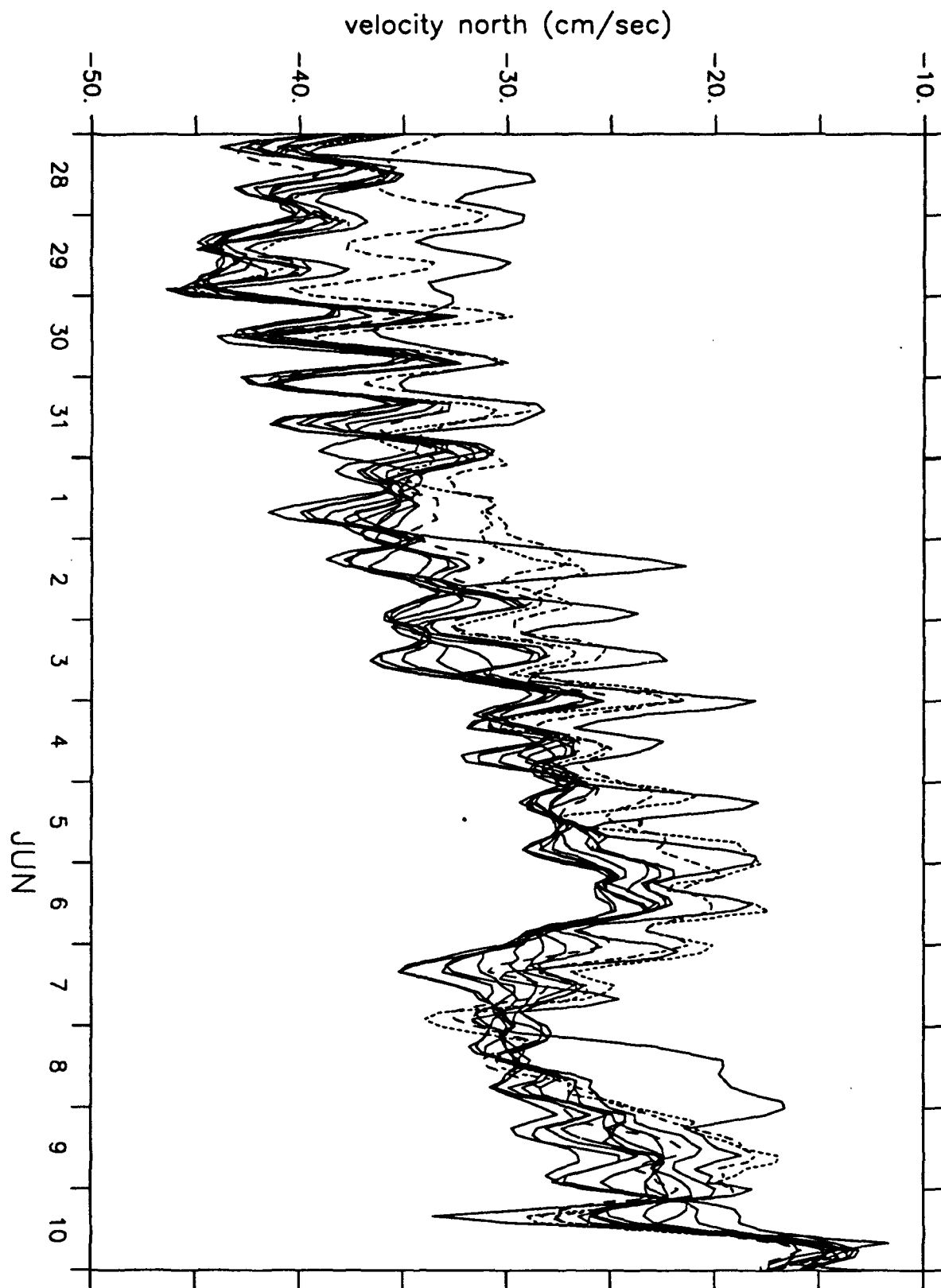


Figure 16c
Velocity time series, North component.

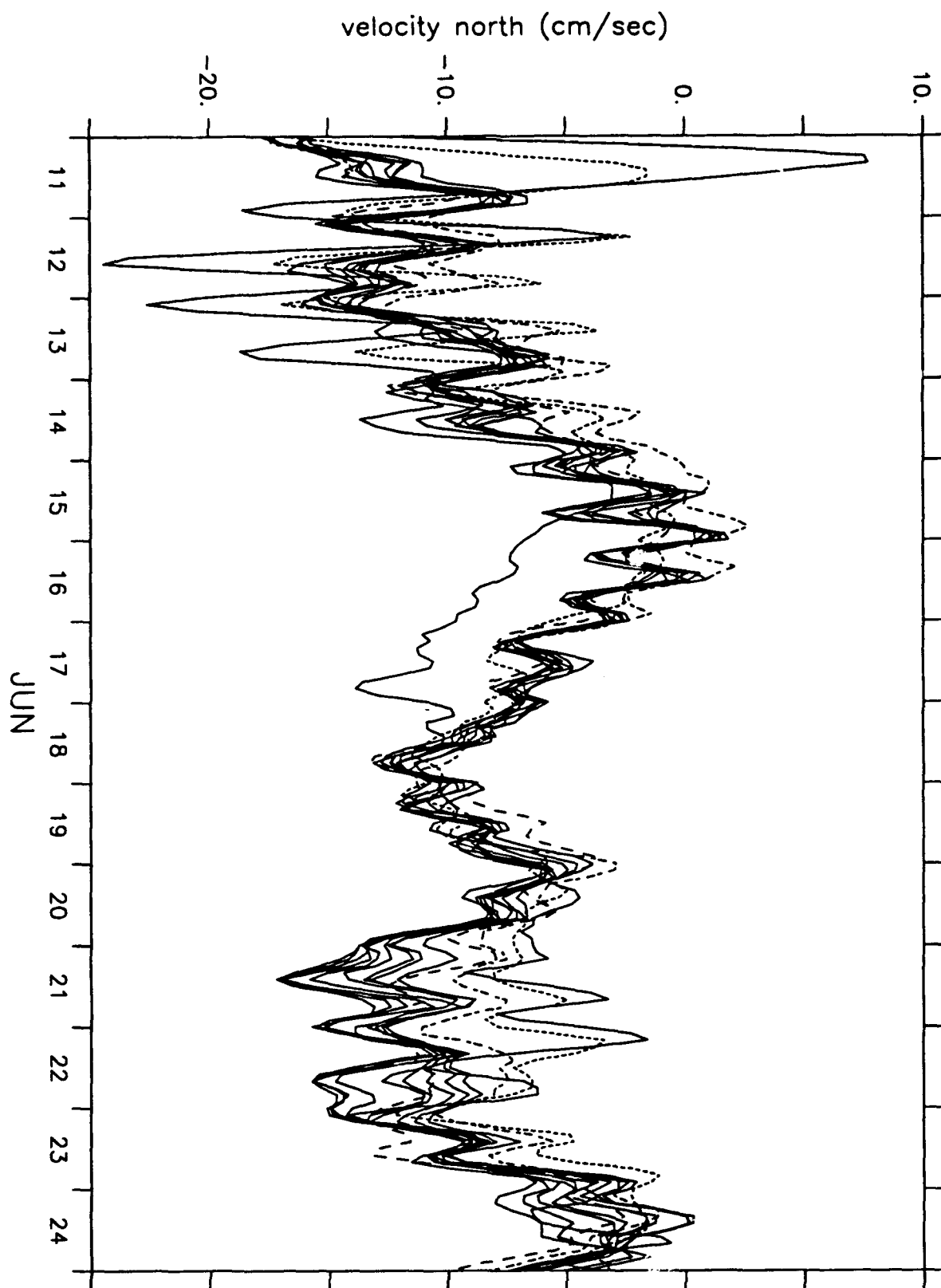


Figure 16d
Velocity time series, North component.

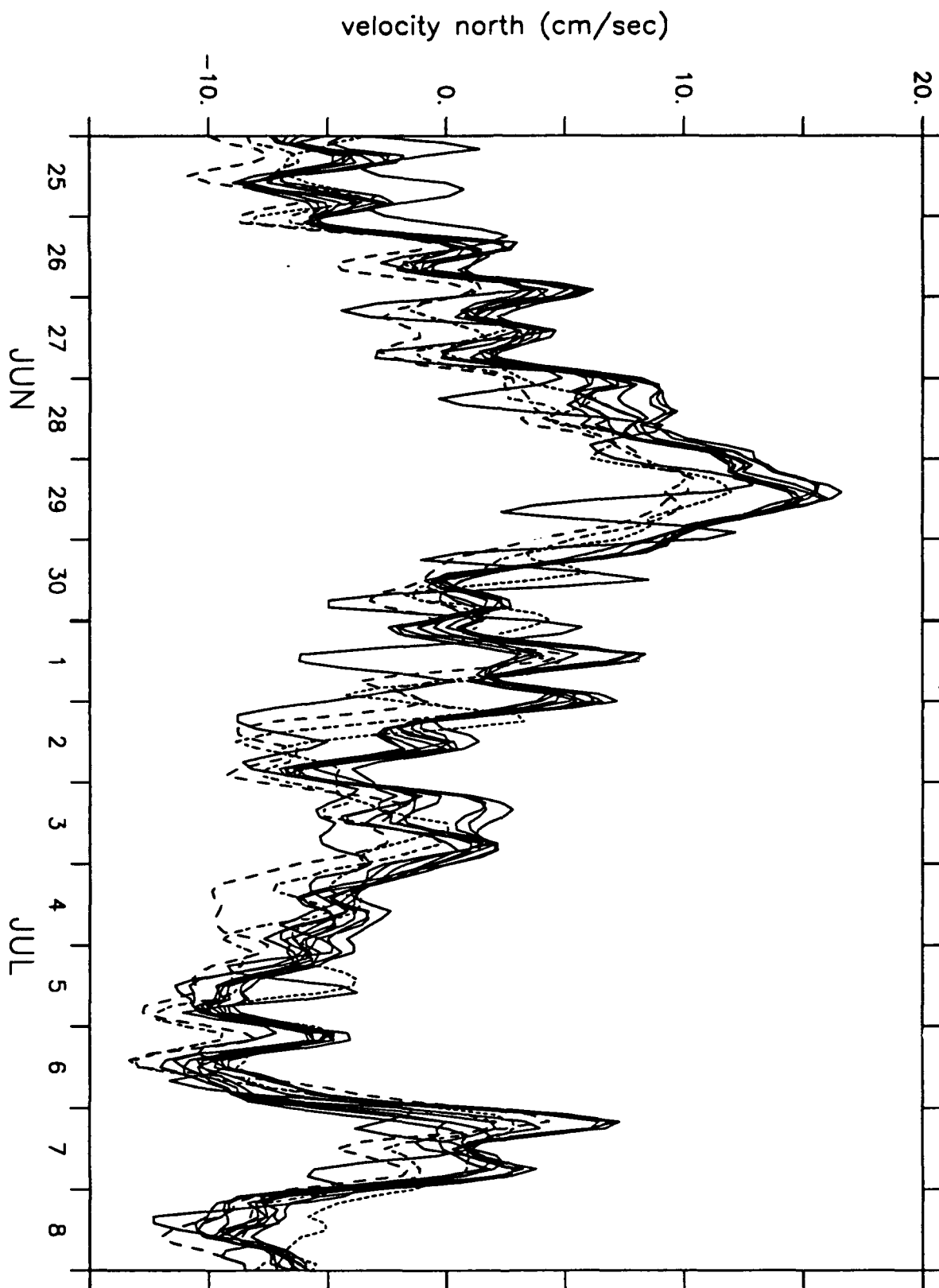


Figure 16e
Velocity time series, North component.

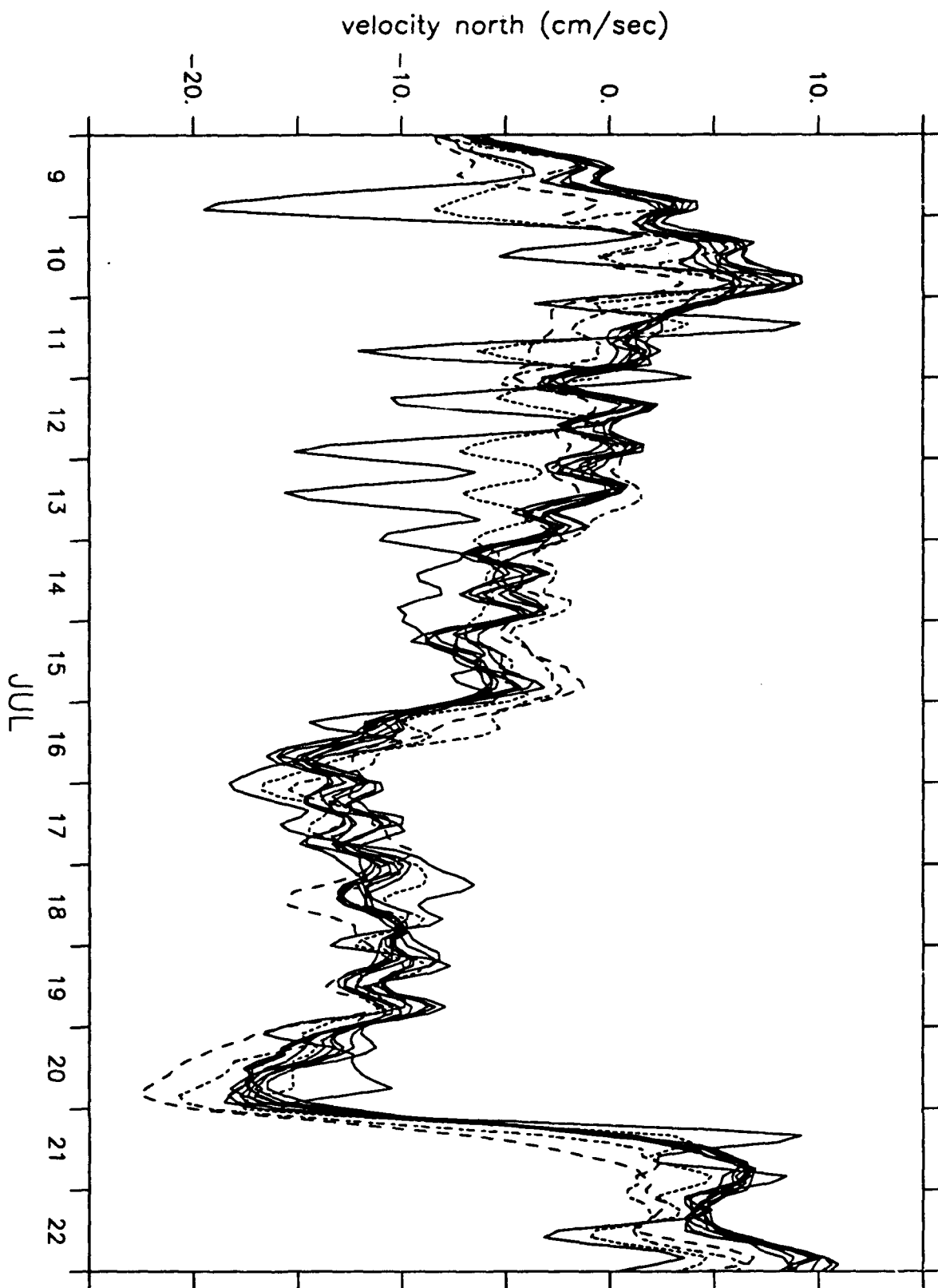


Figure 16f
Velocity time series, North component.

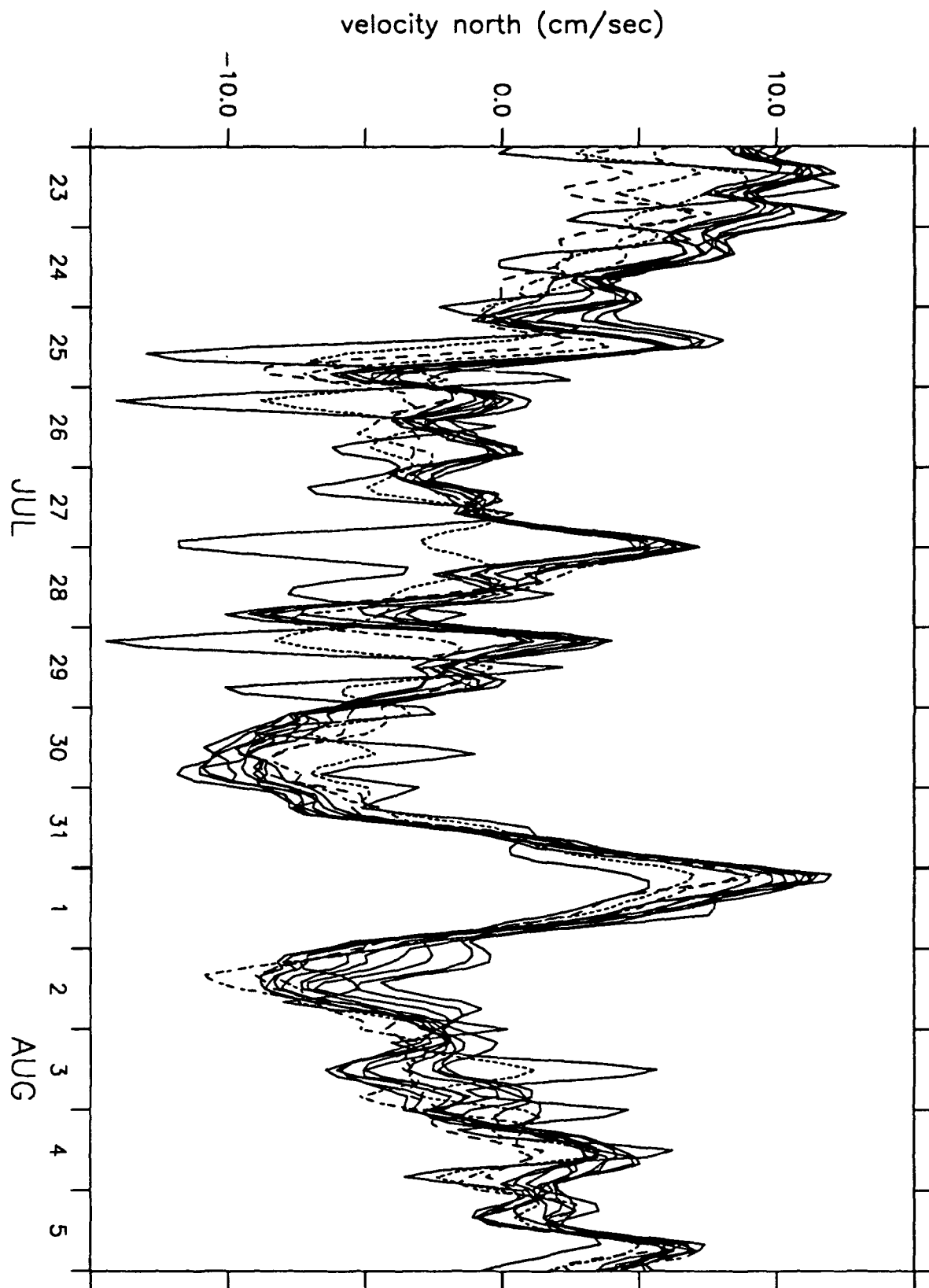


Figure 16g
Velocity time series, North component.

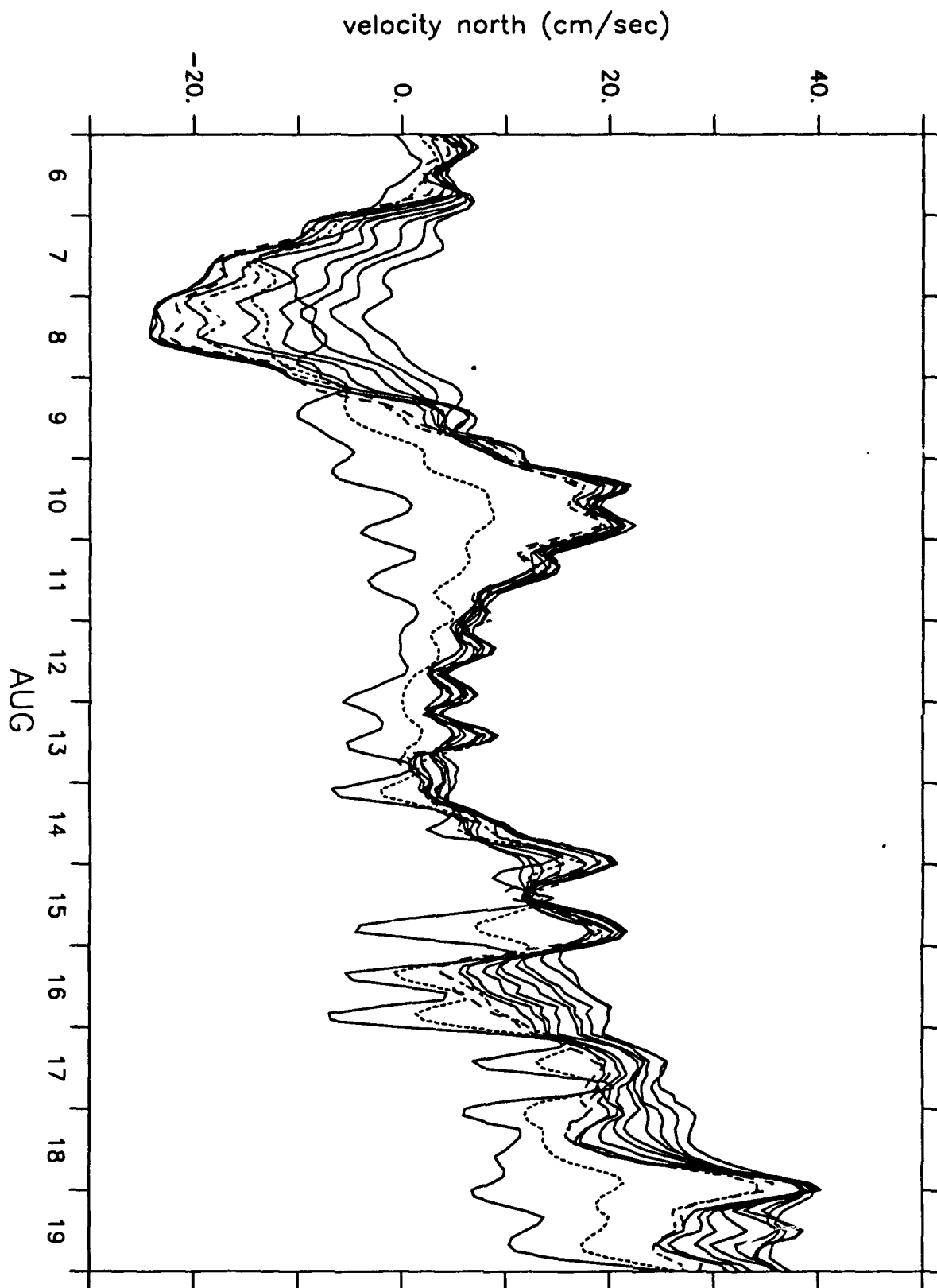


Figure 16h
Velocity time series, North component.

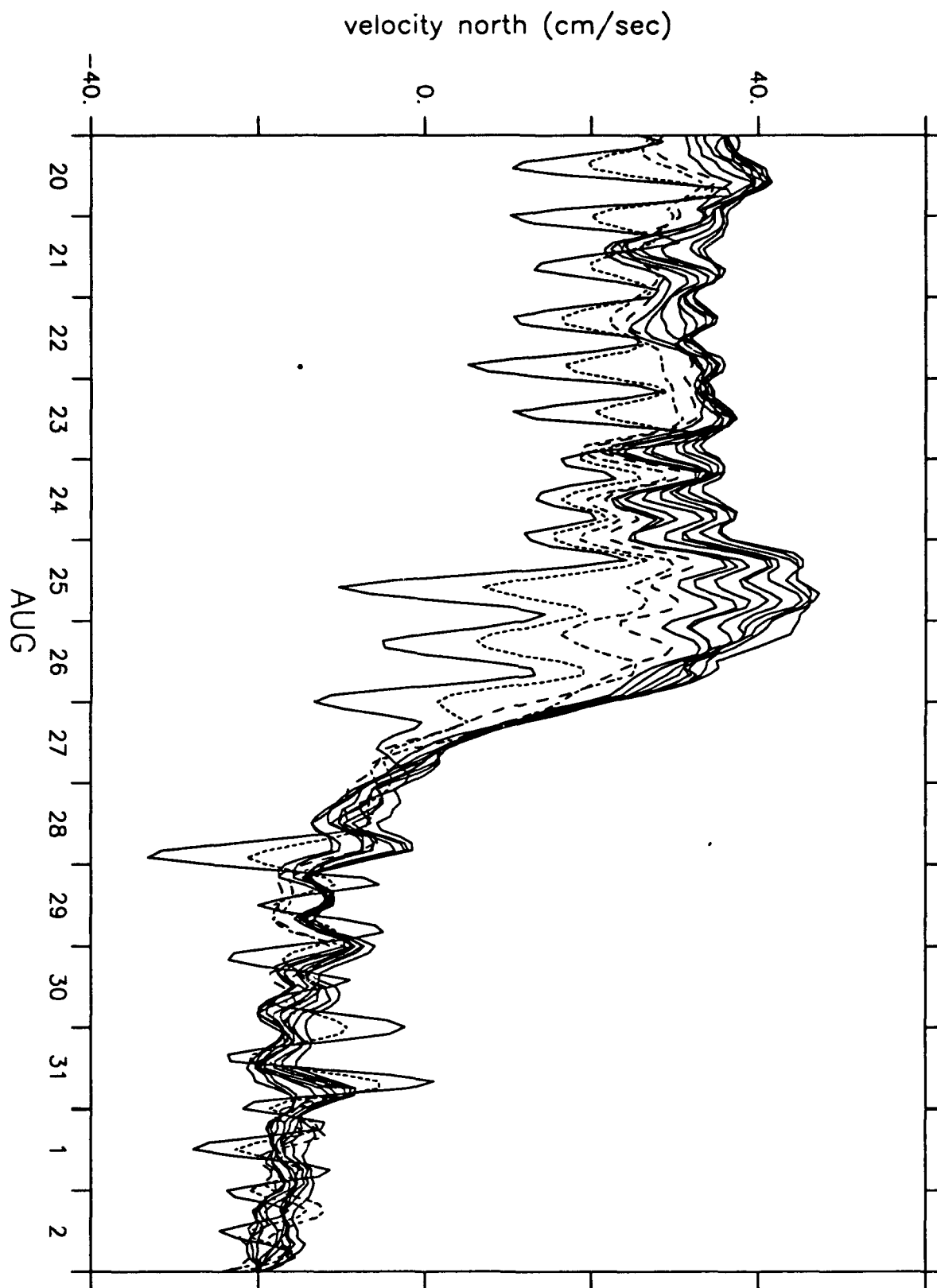


Figure 16i
Velocity time series, North component.

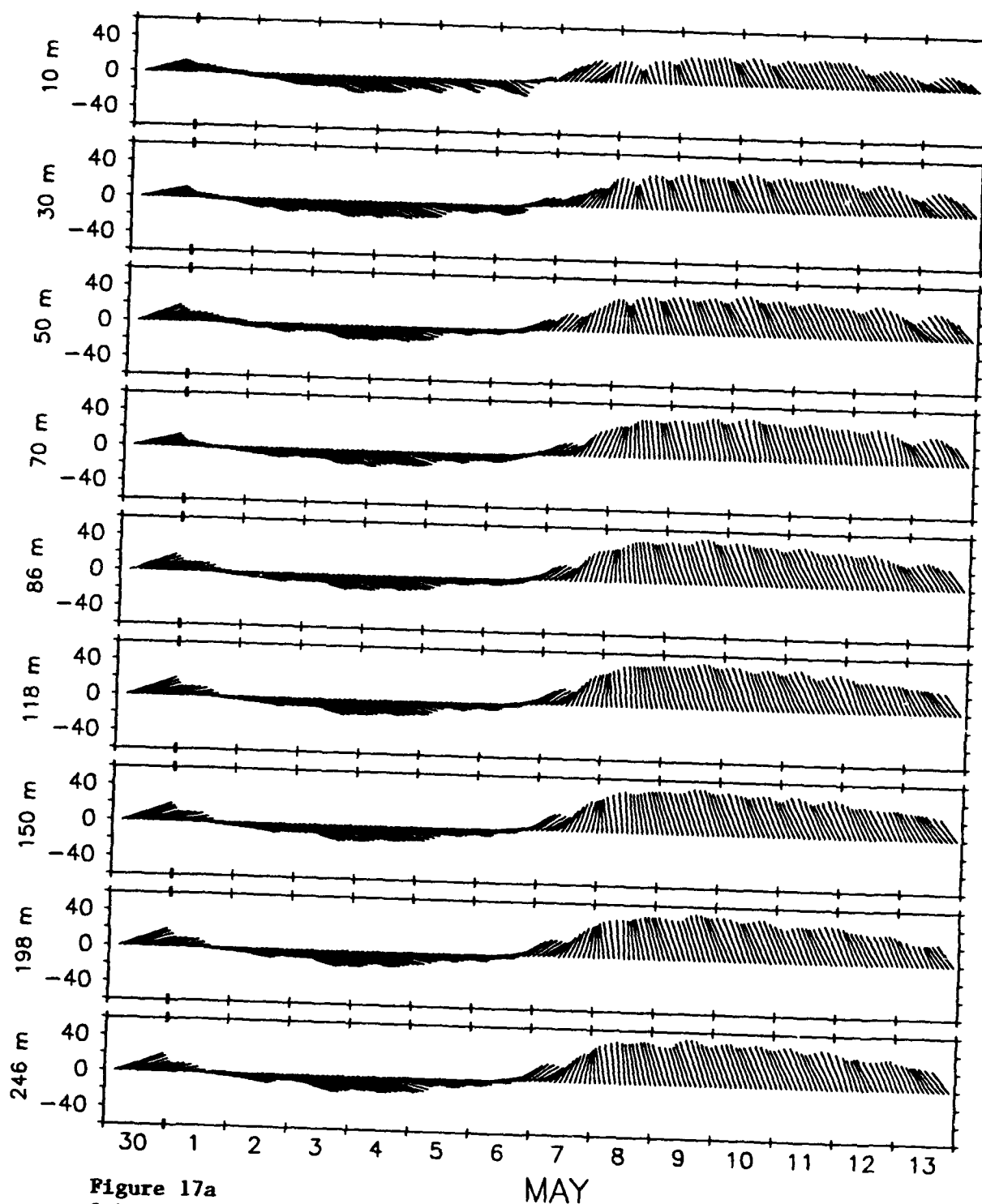


Figure 17a
Sub-surface velocity vectors at selected depths.

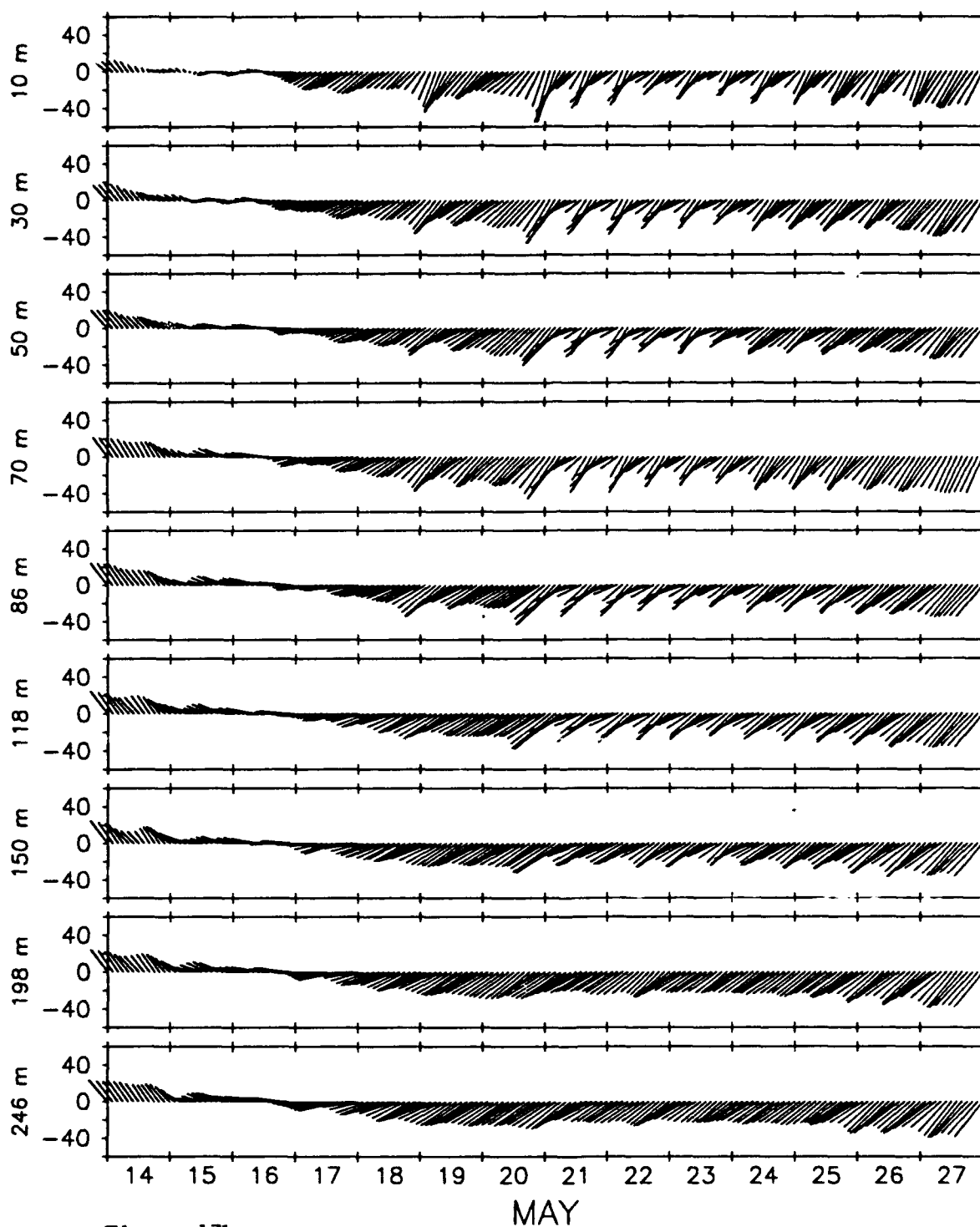


Figure 17b
Sub-surface velocity vectors at selected depths.

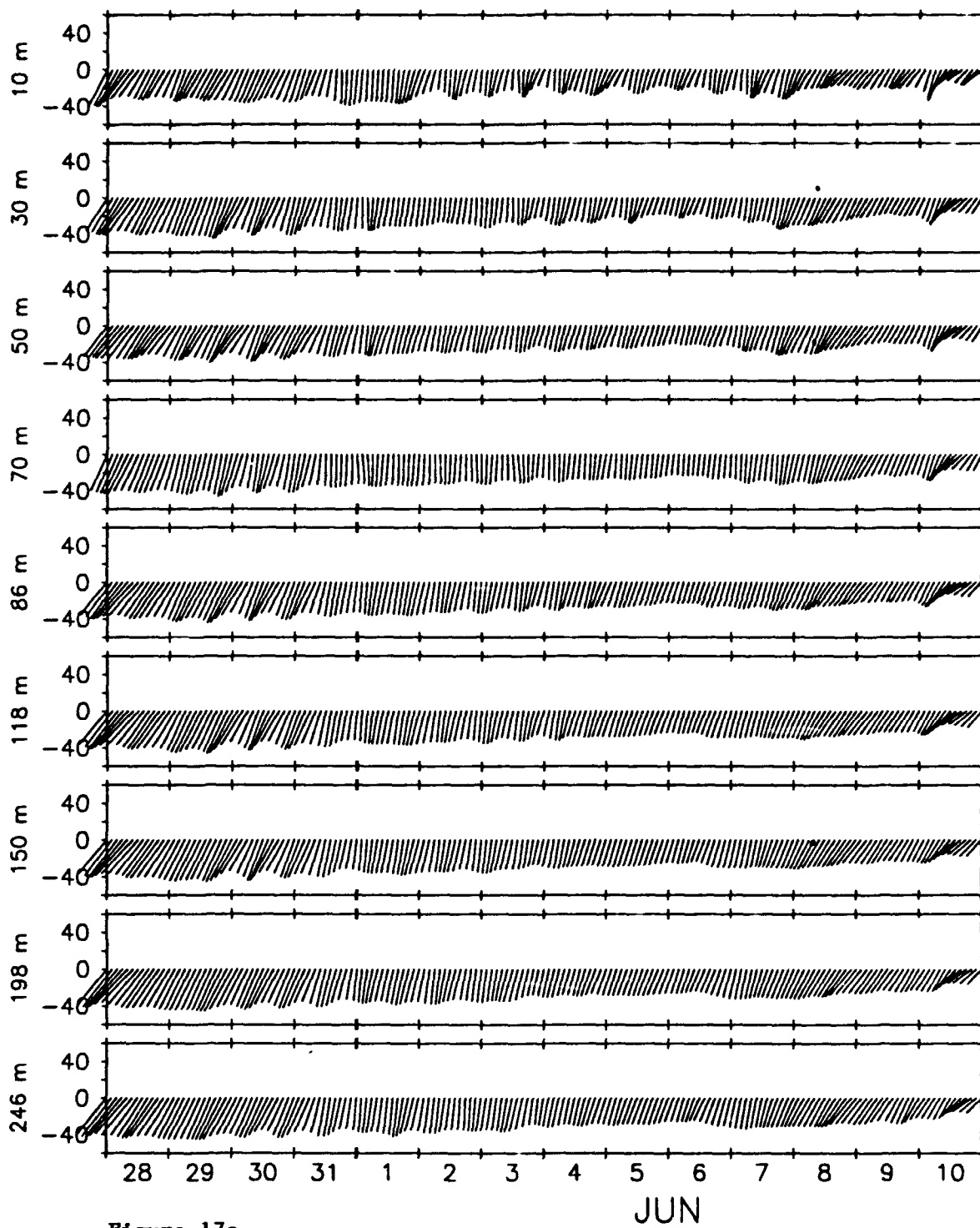


Figure 17c
Sub-surface velocity vectors at selected depths.

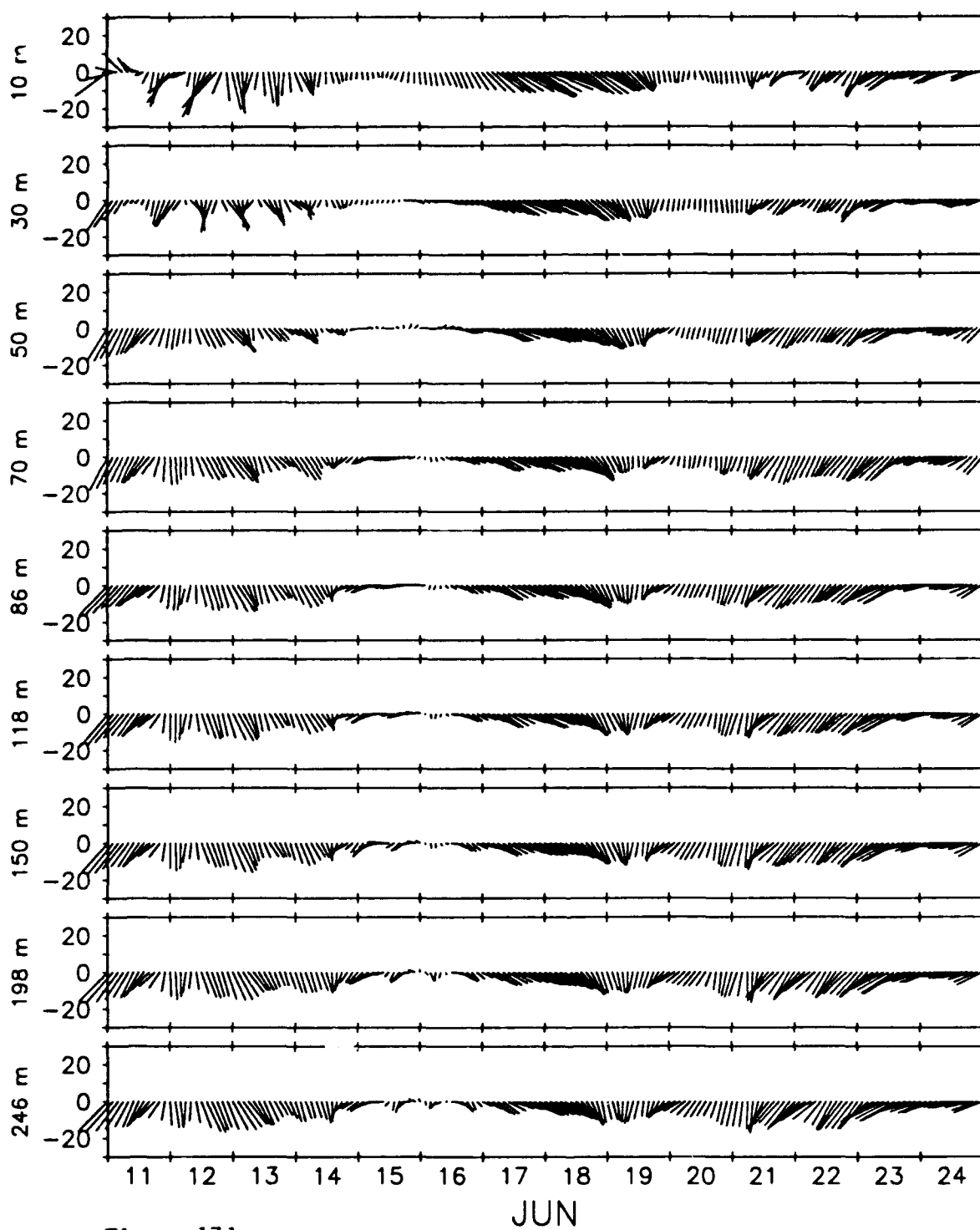


Figure 17d
Sub-surface velocity vectors at selected depths.

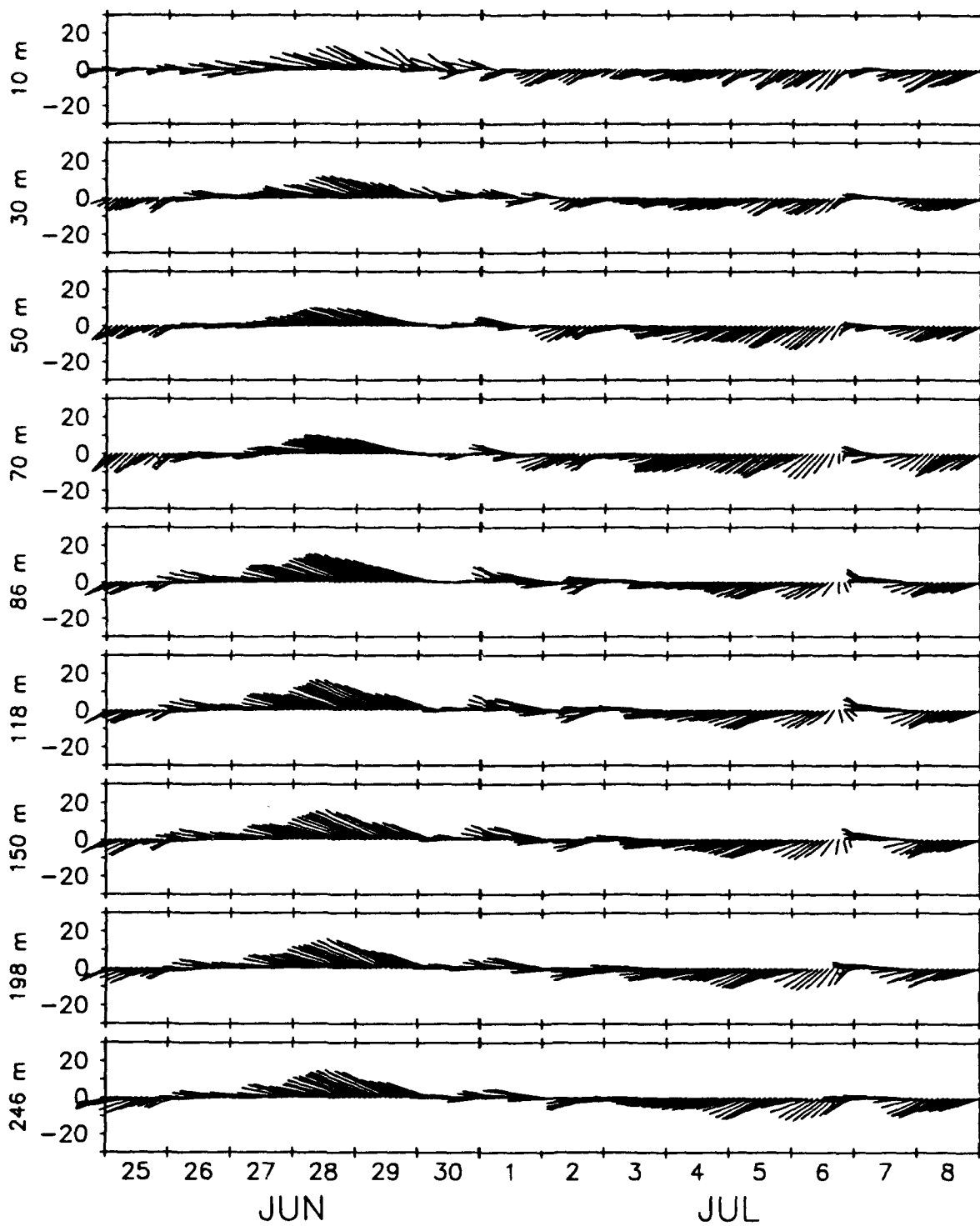


Figure 17e
Sub-surface velocity vectors at selected depths.

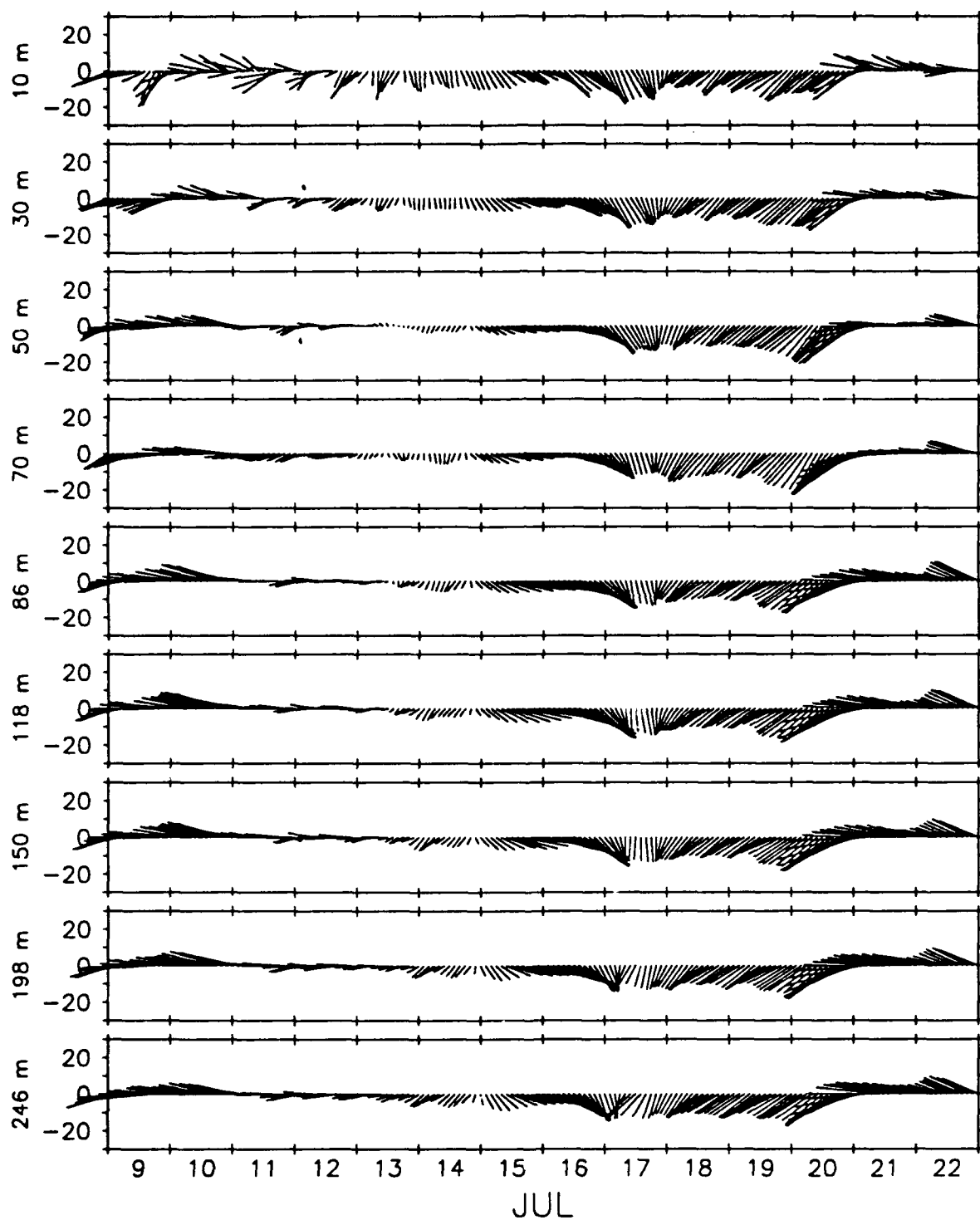


Figure 17f
Sub-surface velocity vectors at selected depths.

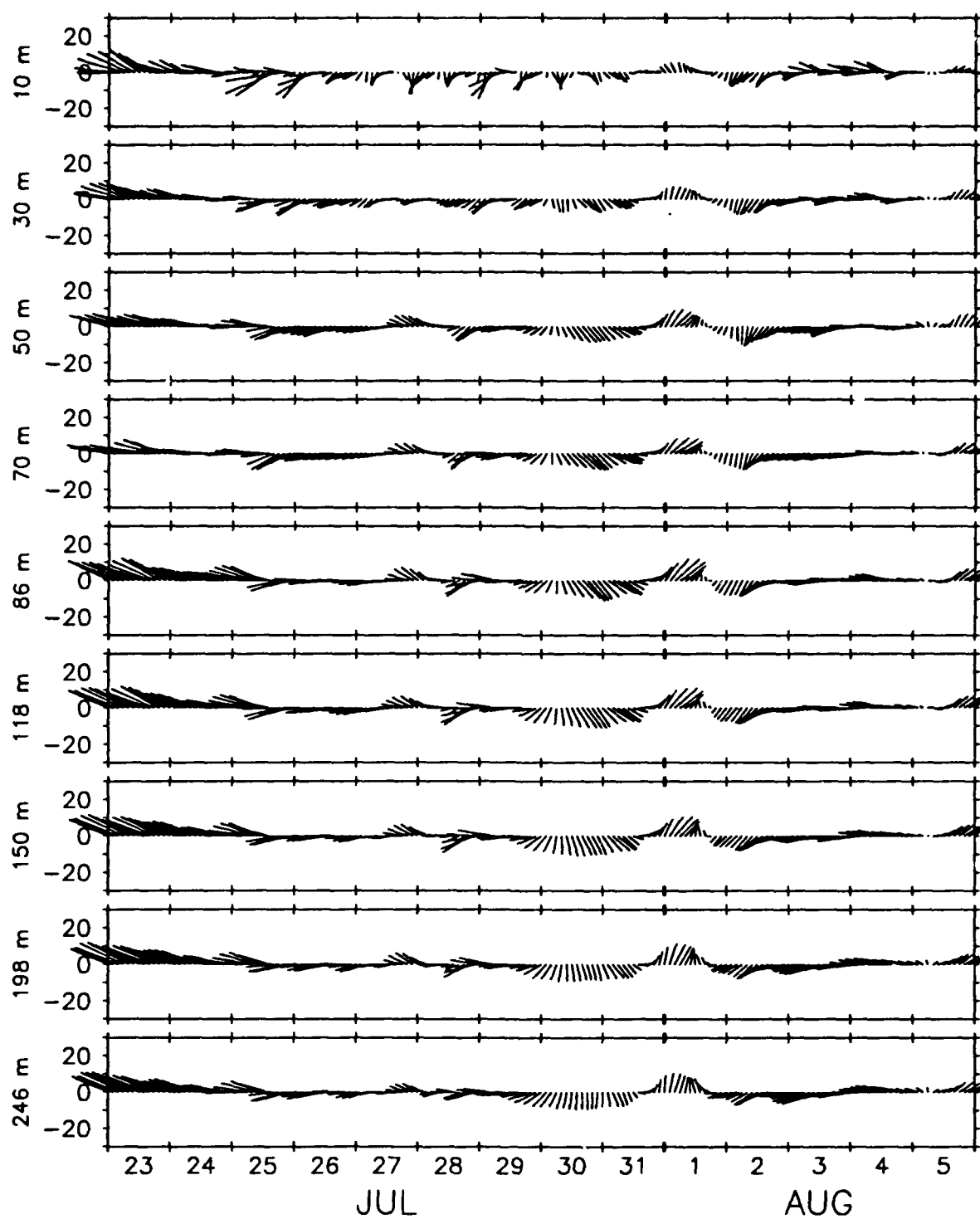


Figure 17g
Sub-surface velocity vectors at selected depths.

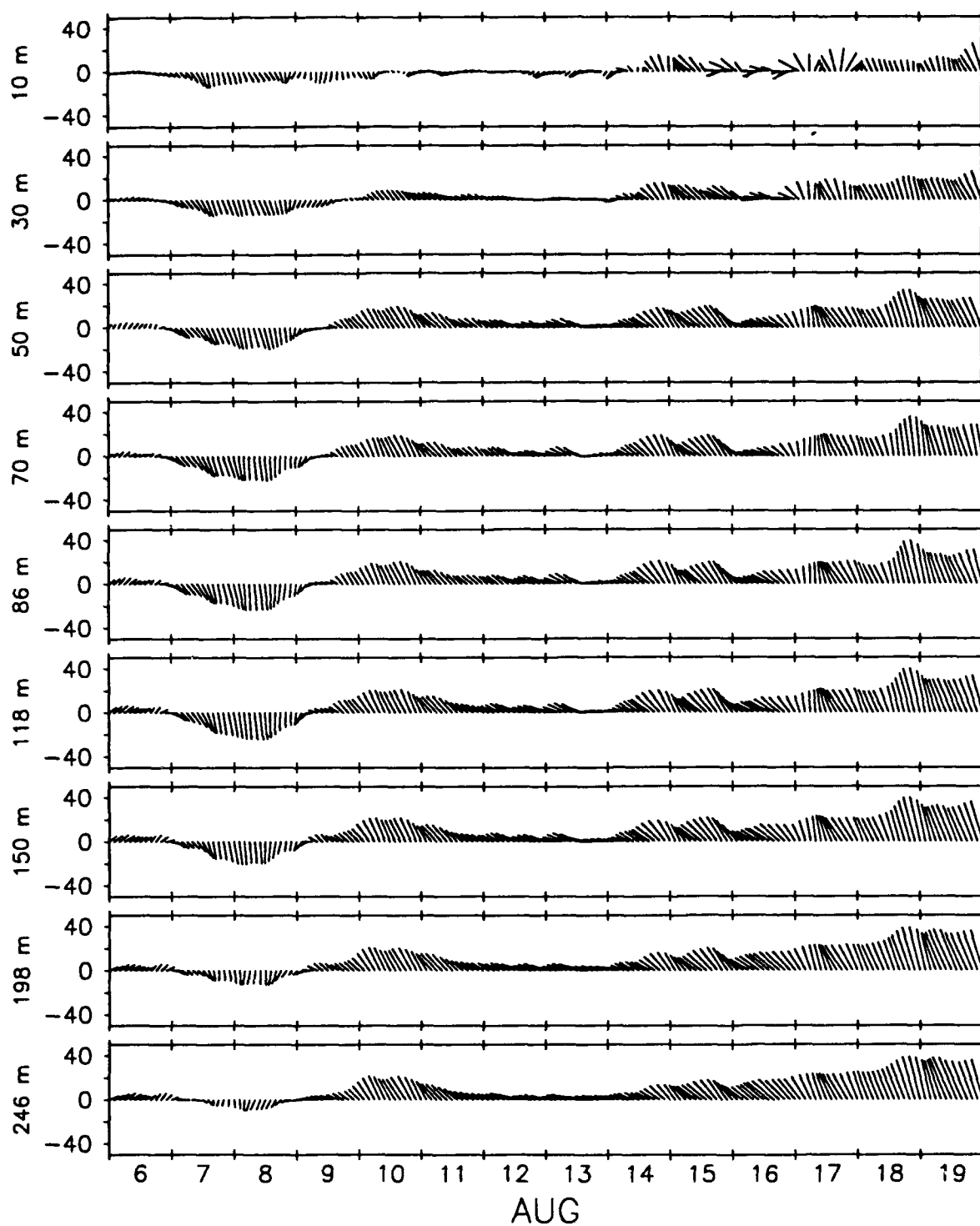


Figure 17h
Sub-surface velocity vectors at selected depths.

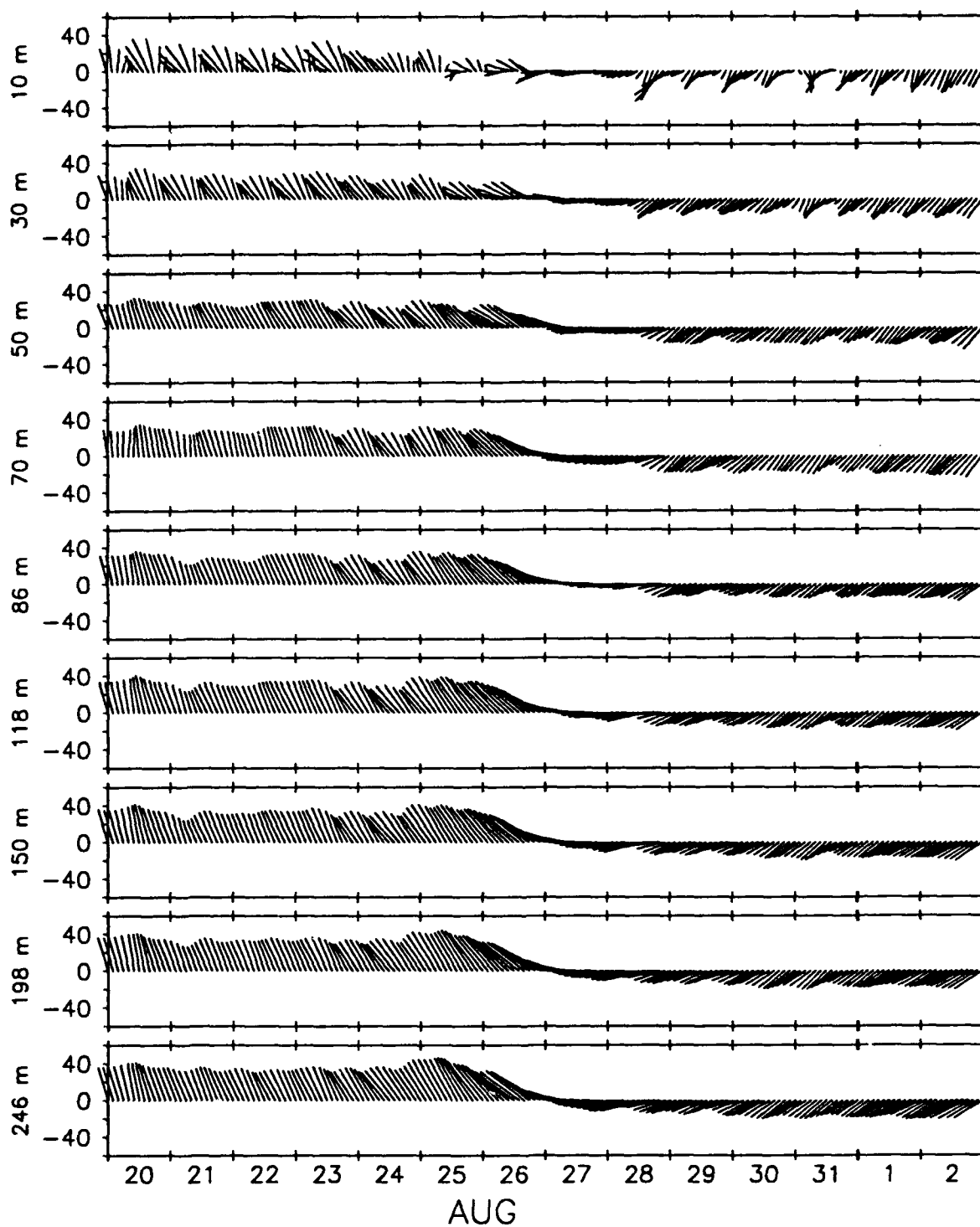


Figure 171
Sub-surface velocity vectors at selected depths.

Acknowledgments

The cooperation of M. Grosenbaugh in the 1991 mooring design study contributed to its success. The mooring was expertly fabricated at the WHOI rigging shop under the direction of D. Simoneau. Experimental logistics and cruise preparation were overseen by R. Trask. The deployment and recovery operations would not have been possible without the cooperation and assistance of the Captain and crew of the R/V ENDEAVOR. Much of the substantial effort resulting from pre and post deployment calibrations of the UOPG instrumentation was borne by R. Payne and W. Horn. C. Grant and L. Costello of WHOI assisted in the deployment and recovery operations. N. Brink handled the initial processing of the VAWR data tapes. M. Samelson handled the initial processing of the Brancker STLs and assisted in the flux calculations. M. A. Lucas assisted with the preparation of the manuscript. This work was funded by Codes 1122SS and 1123B of the Office of Naval Research under Grant Number N00014-89-J-1683.

References

- Briscoe, M. G. and R. A. Weller, 1984. Preliminary results from the Long-Term Upper-Ocean Study (LOTUS). *Dynamics of Atmospheres and Oceans*, 8, 243-265.
- Clarke, N. E., L. Eber, R. M. Laurs, J. A. Renner, and J. F. T. Saur, 1974. Heat exchange between ocean and atmosphere in the eastern North Pacific for 1961-71. NOAA Technical Report, NMFS SSRF-682, U.S. Department of Commerce, Washington, D.C.
- Dickey, T. D., J. Marra, C. Langdon, and D. A. Siegel, 1988. Preliminary results obtained from the multi-variable moored system during the Biowatt experiment in the Sargasso Sea. *Eos*, 68, 1703-1704.
- Dickey, T. D., J. Marra, T. Granata, C. Langdon, M. Hamilton, J. Wiggert, D. Siegel, and A. Bratkovich, 1991. Concurrent high resolution bio-optical and physical time series observations in the Sargasso Sea during the Spring of 1987. *Journal of Geophysical Research*, 96(C5), 8643-8663.
- Dickey, T. D., D. V. Manov, D. A. Siegel and R. A. Weller, 1993. Determination of net longwave heat flux at the air-sea interface using measurements from ship and buoy platforms. *Journal of Atmospheric and Oceanic Technology*, submitted.
- Ducklow, H. W., 1989. Joint global ocean flux study: The 1989 North Atlantic bloom experiment. *Oceanography Magazine*, 2(1), 4-7.
- Fung, I. Y., D. J. Harrison, and A. A. Lacis, 1984. On the variability of the net longwave radiation at the ocean surface. *Reviews of Geophysics and Space Physics*, 22, 177-193.
- Isemer, H. J., and L. Hasse, 1987a. The Bunker climate atlas of the North Atlantic Ocean. Volume 1: Observations. Springer-Verlag, Berlin, 218 pp.
- Isemer, H. J., and L. Hasse, 1987b. The Bunker climate atlas of the North Atlantic Ocean. Volume 2: Air-Sea Interactions. Springer-Verlag, Berlin, 252 pp.
- Kraus, E. B., 1977. Modelling and prediction of the upper layers of the ocean. Pergamon Press, Oxford, England, 325 pp.
- Lambert, R. B. and G. T. Hebenstreit, 1985. Upper ocean stratification and variability in the North Atlantic. Technical Report SIAC-84/1778, Science Applications International Corporation, McLean, Virginia, 67 pp.

- Large, W. G. and S. Pond, 1981. Open ocean momentum flux measurements in moderate to strong winds. *Journal of Physical Oceanography*, **11**, 324-336.
- Large, W. G. and S. Pond, 1982. Sensible and latent heat flux measurements over the ocean. *Journal of Physical Oceanography*, **12**, 464-482.
- Levitus, S., 1982. Climatological Atlas of the World Ocean. NOAA Professional Paper No. 13, National Oceanic and Atmospheric Administration, Rockville, Maryland, 173 + xv pp.
- List, R. J., 1984. *Smithsonian Meteorological Tables*, Smithsonian Institution Press, Washington, DC, 572 pp.
- Paulson, C. A., and J. J. Simpson, 1977. Irradiance measurements in the upper ocean. *Journal of Physical Oceanography*, **7**, 952-956.
- Price, J. F., R. A. Weller and R. Pinkel, 1986. Diurnal cycling: Observations and models of the upper ocean response to diurnal heating, cooling, and wind mixing. *Journal of Geophysical Research*, **91**(C7), 8411-8427.
- Robinson, M. K., R. A. Bauer and E. H. Schroeder, 1979. Atlas of North Atlantic-Indian Ocean monthly mean temperatures and mean salinities of the surface layer. U.S. Naval Oceanographic Office Reference Publication 18, Department of the Navy, Washington, D.C., 234 pp.
- Siegel, D. A., and T. D. Dickey, 1987. Observations of the vertical structure of the diffuse attenuation coefficient spectrum. *Deep-Sea Research*, **34**(4), 547-563.
- Weller, R. A., D. L. Rudnick, R. E. Payne, J. P. Dean, N. J. Pennington, and R. P. Trask, 1990. Measuring near-surface meteorology over the ocean from an array of surface moorings in the subtropical convergence zone. *Journal of Atmospheric and Oceanic Technology*, **7**(1), 85-103.

Appendix 1: Cruise Participants

WHOI Participants on Deployment Cruise:

George Tupper
Will Ostrom
Bryan Way
Paul Bouchard
Carleton Grant

WHOI Participants on Recovery Cruise:

Mark Grosenbaugh
George Tupper
Larry Costello
Will Ostrom
Carleton Grant

Appendix 2: Chronological Log

The UOPG scientific party arrived at the agent's in Reykjavik at 0900Z, 22 April. The shipping agent for the cruise was the Iceland Steamship Company (Eimskip), who provided very good support in general, although we did have to wait 1/2 day for our container to be delivered to our working area. The working area itself was excellent, a portion of a large warehouse, about 30 feet from where the ship was tied up. Workbenches were 4 x 8 sheets of plywood set on stacks of pallets. Power was supplied by a long extension cord and was 220 volts, 50 cycles. We had brought a step-down transformer and all equipment seemed to work fine on 110V 50 cycles. By the end of the day our container was unloaded and the electronics test stations were set up and running.

A magnetic survey was done by George Tupper outside the warehouse in an attempt to find a good location for buoy spins. Unfortunately, the magnetic variability was very strong. The magnetic heading to a visual reference point varied by 25 degrees over a distance of 30 feet. It was assumed that this variation was caused by the pilings under the dock. Since the overhead door opening was high enough to get a fully instrumented discus buoy through, We decided to do the spins indoors, sighting through the open door on a small lighthouse which appeared to be 1-2 miles away and had a bearing of 035 degrees magnetic. The magnetic variability indoors was significantly better than on the dock, with a typical variation of 2-3 degrees over a distance of 10 feet. The resulting compass variation (Figure 18) didn't come out quite as well as we would have liked, but we decided not to attempt any corrective action since the local conditions were less than ideal and the spins done at Woods Hole with the same instruments and the same buoy were good.

During pre-cruise checkout, Bryan Way found a high current drain in VAWR SN 706. He found a bad FSK Modem Controller, replaced it, and both VAWRs

were up and running. While the spins were in progress, Bryan noticed that VAWR SN 184 was outputting data through the Argos package every 3-5 seconds (should be once every 15 minutes). After the spins were completed, he found a bad O.C. controller in the Argos package. He replaced that and fixed the problem.

There were a few problems with the documentation of the buoy tension package and George spent some time making sure things were right before installing it into the buoy. The final check was to hook the tensiometer to an upright roof support and pull on it with a forklift to see that tension really was working.

At 1500Z on 26 April, the buoy was moved outside, where the air temperature was about 4°C, and the wind was estimated at 15-20 knots from the east. At 1624Z, the two sea temp thermistors were put into an ice bucket and left there overnight. The buoy was on the ship from midday 27 April til midday 29 April. Ground truth measurements were made near the buoy with hand-held standards. A chronology of important events during deployment and recovery operations and documentation of ground truth data follows.

26 April 1991

0850Z Begin buoy compass spin.

1022Z Finish spin (see Figure 17).

1029Z Chart-recorder tensiometer (SN 278) turned on.

1105Z Pulled 500 Lbs on tensiometer 278 for one minute.

1500Z Discus buoy moved from indoors to outdoors (Outside air temp = +4°C).

1624Z Both VAWR Sea Temp probes placed in bucket of ice water, remained in water overnight.

1600Z Begin pre-deployment ground truth observations.

	WSPD (m/s)	BP (mb)	RH (%)	AT (C)
1600Z (26 April)	7-10	995.4	69.0	+5.5
1800Z	5-8	993.2	75.5	+4.6
1915Z	5-8	992.4	77.4	+4.7
2248Z	1-2	989.5	78.9	+5.2
0730Z (27 April)	1-2	986.5	68.8	+6.0

28 April 1991

1230Z Continued ground truth observations, note that comparison with buoy speed will not be valid because at this time the buoy is on its side on the deck of the ENDEAVOR.

	WSPD (m/s)	BP (mb)	RH (%)	AT (C)
1230Z	—	1014.4	46.0	7.4
1630Z	—	1016.6	47.9	8.3

6 September 1991

1130Z Begin pre-recovery ground truth observations. Measurements made with hand-held sensors onboard ENDEAVOR approximately 1/4 mile downwind from buoy. Ship's sail data also recorded.

	Hand-held			Endeavor SAIL	
	Wet (C)	Dry (C)	BP (mb)	BP (mb)	RH (%)
1130Z	13.50	14.4	1036.3	1035.5	93.4
1135Z	13.45	14.7	1036.3	1035.2	93.4
1140Z	13.40	14.5	1036.2	1035.2	93.4
1145Z	13.45	14.6	1036.2	1035.2	93.3
1150Z	13.40	14.3	1036.2	1035.1	93.3
1155Z	13.40	14.3	1036.2	1035.3	93.3
1200Z	13.40	14.3	1036.2	1035.2	93.2

1250Z Acoustic Release fired.

1900Z All mooring instrumentation, wire, and hardware aboard.

7 September 91

1302Z Ice-water bag held against lower thermistor on bridle (VAWR SN 706).

1334Z Ice bag off lower thermistor, transferred to upper thermistor (VAWR SN 184).

1415Z Ice bag off upper thermistor.

18 September 91

1221:00Z Pull on bridle tensiometer with come-along

1222:00Z Loosen come-along

1223:30Z Pull on bridle tensiometer with come-along

1223:00Z Loosen Com-along

1723Z 15 Temperature loggers from MLML mooring into walk-in reefer.

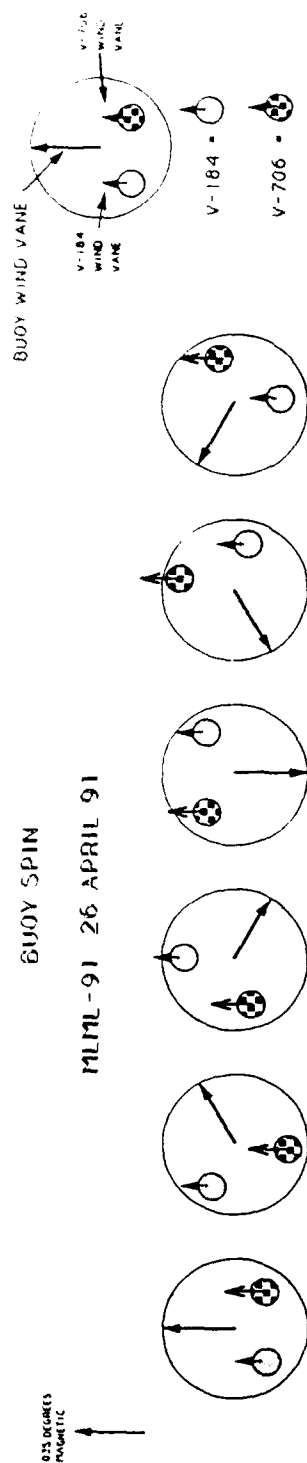
1840Z 15 Temperature loggers out of reefer, back in main lab.

22 September 91

1213:50–1218Z Two MLML engineering instruments turned vertical (before and after this period they were stored horizontally).

1227Z 12 Subduction NW Temperature loggers into walk-in Reefer.

1401Z 12 Subduction NW Temperature loggers out of walk-in, back in main lab.



BEARING = ALGEBRAIC SUM OF INSTANTANEOUS COMPASS AND VANE

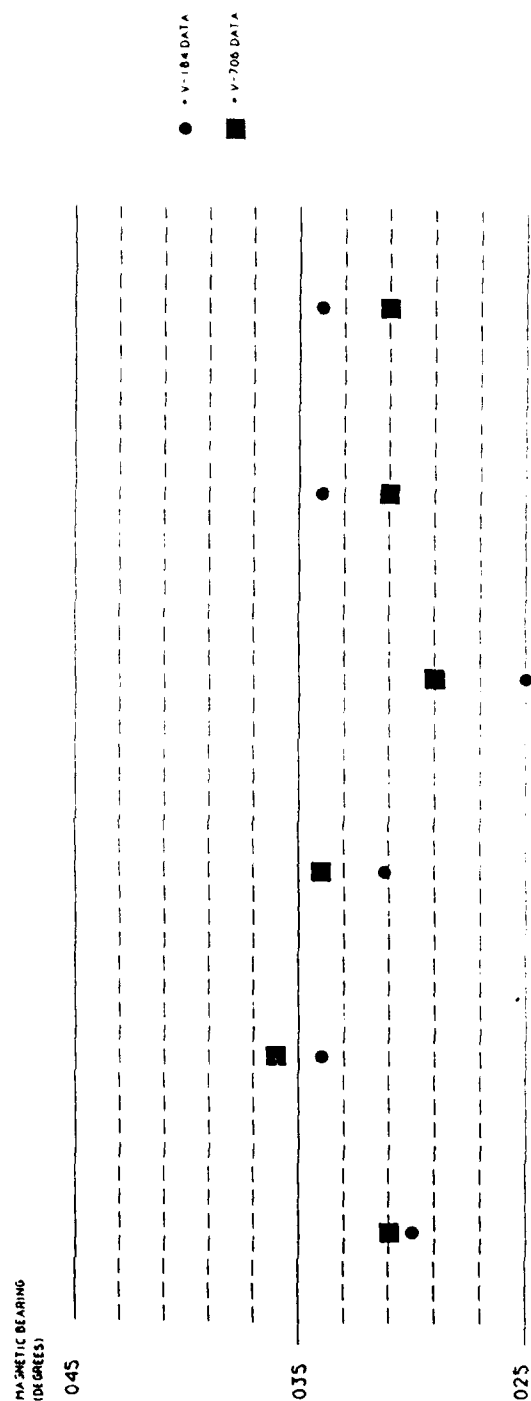


Figure 18: Data from the pre-deployment buoy spin in Reykjavik, Iceland are shown. Compass readings from the two VAWRs (SN 184 and 706) are compared to a sighting point at a bearing of 035°.

DOCUMENT LIBRARY

Distribution List for Technical Report Exchange - July 1, 1993

University of California, San Diego
SIO Library 0175C (TRC)
9500 Gilman Drive
La Jolla, CA 92093-0175

Hancock Library of Biology & Oceanography
Alan Hancock Laboratory
University of Southern California
University Park
Los Angeles, CA 90089-0371

Gifts & Exchanges
Library
Bedford Institute of Oceanography
P.O. Box 1006
Dartmouth, NS, B2Y 4A2, CANADA

Office of the International Ice Patrol
c/o Coast Guard R & D Center
Avery Point
Groton, CT 06340

NOAA/EDIS Miami Library Center
4301 Rickenbacker Causeway
Miami, FL 33149

Library
Skidaway Institute of Oceanography
P.O. Box 13687
Savannah, GA 31416

Institute of Geophysics
University of Hawaii
Library Room 252
2525 Correa Road
Honolulu, HI 96822

Marine Resources Information Center
Building E38-320
MIT
Cambridge, MA 02139

Library
Lamont-Doherty Geological Observatory
Columbia University
Palisades, NY 10964

Library
Serials Department
Oregon State University
Corvallis, OR 97331

Pell Marine Science Library
University of Rhode Island
Narragansett Bay Campus
Narragansett, RI 02882

Working Collection
Texas A&M University
Dept. of Oceanography
College Station, TX 77843

Fisheries-Oceanography Library
151 Oceanography Teaching Bldg.
University of Washington
Seattle, WA 98195

Library
R.S.M.A.S.
University of Miami
4600 Rickenbacker Causeway
Miami, FL 33149

Maury Oceanographic Library
Naval Oceanographic Office
Stennis Space Center
NSTL, MS 39522-5001

Library
Institute of Ocean Sciences
P.O. Box 6000
Sidney, B.C. V8L 4B2
CANADA

Library
Institute of Oceanographic Sciences
Deacon Laboratory
Wormley, Godalming
Surrey GU8 5UB
UNITED KINGDOM

The Librarian
CSIRO Marine Laboratories
G.P.O. Box 1538
Hobart, Tasmania
AUSTRALIA 7001

Library
Proudman Oceanographic Laboratory
Bidston Observatory
Birkenhead
Merseyside L43 7 RA
UNITED KINGDOM

IFREMER
Centre de Brest
Service Documentation - Publications
BP 70 29280 PLOUZANE
FRANCE

REPORT DOCUMENTATION PAGE	1. REPORT NO. WHOI-93-33	2.	3. Recipient's Accession No.		
4. Title and Subtitle The Marine Light - Mixed layer Experiment Cruise and Data Report R/V Endeavor Cruise EN-224, Mooring Deployment, 27 April-1 May 1991 Cruise EN-227, Mooring Recovery, 5-23 September 1991			5. Report Date May 1993		
			6.		
7. Author(s) Albert J. Plueddemann, Robert A. Weller, Thomas D. Dickey, John Marra, George H. Tupper, Bryan S. Way, William M. Ostrom, Paul R. Bouchard, Andrea L. Oien, and Nancy R. Galbraith			8. Performing Organization Rept. No. WHOI 93-33		
9. Performing Organization Name and Address The Woods Hole Oceanographic Institution Woods Hole, Massachusetts 02543			10. Project/Task/Work Unit No.		
			11. Contract(C) or Grant(G) No. (C) N00014-89-J-1683 (G)		
12. Sponsoring Organization Name and Address Office of Naval Research			13. Type of Report & Period Covered Technical Report		
			14.		
15. Supplementary Notes This report should be cited as: Woods Hole Oceanog. Inst. Tech. Rept., WHOI-93-33.					
16. Abstract (Limit: 200 words) <p>The Marine Light - Mixed Layer experiment took place in the sub-Arctic North Atlantic ocean, approximately 275 miles south of Reykjavik, Iceland. The field program included a central surface mooring to document the temporal evolution of physical, biological and optical properties. The surface mooring was deployed at approximately 59°N, 21°W on 29 April 1991 and recovered on 6 September 1991. The Upper Ocean Processes Group of the Woods Hole Oceanographic Institution was responsible for design, preparation, deployment, and recovery of the mooring. The Group's contribution to the field measurements included four different types of sensors: a meteorological observation package on the surface buoy, a string of 15 temperature sensors along the mooring line, an acoustic Doppler current profiler, and four instruments for measuring mooring tension and accelerations. The observations obtained from the mooring are sufficient to describe the air-sea fluxes and the local physical response to surface forcing. The objective in the analysis phase will be to determine the factors controlling this physical response and to work towards an understanding of the links among physical, biological, and optical processes. This report describes the deployment and recovery of the mooring, the meteorological data, and the subsurface temperature and current data.</p>					
17. Document Analysis a. Descriptors <ol style="list-style-type: none"> 1. air-sea interaction 2. upper ocean structure 3. re-stratification b. Identifiers/Open-Ended Terms c. COSATI Field/Group					
18. Availability Statement Approved for publication; distribution unlimited.		19. Security Class (This Report) UNCLASSIFIED	21. No. of Pages 124		
		20. Security Class (This Page)	22. Price		